ARCHIVES OF ACOUSTICS
1, 2, 87-108 (1976)

NOISE AND STRUCTURE OF A GAS JET AT THE CHOKED OUTFLOW FROM A PERFORATED DISK

WIKTOR M. JUNGOWSKI, WITOLD C. SELEROWICZ
Department of Aerodynamics, Warsaw Technical University (Warszawa)

With the aid of experimental and theoretical investigations the main gasodynamic and acoustic properties of a gas jet discharging from a disk have been determined, and the range of efficient operation of the disk, as an element that reduces the outflow noise, has been established. The properties of the gas jet from a disk and a nozzle were compared.

Notation

c sound speed,
A cross-sectional area,
b distance between holes of the disk,
d diameter of hole or nozzle,
f frequency,
G_* critical mass rate of flow,
k ratio of specific heats,
L length of cell, $\overline{L} = L/d$,
M Mach number,
n number of holes,
n_h number of hexagons,
SPL overall sound pressure level,
p pressure, $\overline{p}_a = p_a/p_o$, $\overline{p}_{as} = p_a/p_{os}$, $\overline{p} = p_n/p_o$,
St Strouhal number,
u gas velocity, $\overline{u} = u_n/c_o$,
α ratio of cross-sectional areas,
$\beta = \sqrt{M^2 - 1}$,
$\eta = b/d$,
θ angle of direction between the jet axis and a radius (in horizontal plane) from the front of the nozzle or disk,
ϱ mass density.

Suffixes

a ambient conditions,
d nozzle,
g conditions on the boundary jet,
n supersonic jet,
o supply conditions,
p subsonic jet,
s substitute conditions in coalesced jet,
$*$ critical conditions.

1. Introduction

The investigation of perforated disks, as elements to reduce exhaust noise [5], has prompted the authors to devote themselves particularly carefully to the patterns of flow and the noise generated at a choked outflow for a wide range of supply pressure. Various structures of the coalesced jet and various noise spectra were found to exist. As a result of the investigations some properties of the coalesced jet and their dependence on the supply pressure have been established and this, in turn, has contributed to determining the efficient ranges of operation for disks of different geometries. In addition, the properties of the coalesced gas jet discharged from a disk and those of a jet from single convergent nozzle have been compared.

2. Gas jet at the choked outflow of a convergent nozzle

To enable the comparison of a coalesced jet from a disk with a jet from a nozzle to be made, it will be advisable to sum up and to analyze the essentials of the information contained in numerous publications, as well as the conclusions that result from the investigations of a single jet.

The gas jet at a choked outflow, while expanding outside the nozzle, forms a characteristic cell structure. The structure of cells, their dimensions and the shape of the shock waves encountered, depend on the ratio of the ambient pressure to the supply pressure [12, 6]. Fig. 1 shows our own photographs of a gas jet, obtained by a schlieren method, with the aid of the light from a mercury lamp. It can be seen that, as the supply pressure increases, the length of the cells is also increased (a, b), and there then appears a Mach disk in the first cell (c) and, subsequently, in the second (d). The empirical formulae of various authors for the length of the first cell (at the nozzle) for air discharge ($k = 1.4$) are presented below in a uniform notation. Two groups of formulae are remarkable: the first is characterized by simple relations with regard to $\overline{p}_a$

$$\bar{L} = 0.89\sqrt{\frac{1}{\overline{p}_a} - 1.9}, \quad [12], \text{ p. 74}, \tag{1}$$

$$\bar{L} = 1.55\sqrt{\frac{0.528}{\overline{p}_a} - 1}, \quad \text{when } 0.528 \geqslant \overline{p}_a \geqslant 0.264, \ [6], \tag{2}$$

$$\bar{L} = 1.52\left(\frac{0.528}{\overline{p}_a}\right)^{0.437} - 0.5, \quad \text{when } \overline{p}_a < 0.264, \ [6], \text{ p. 6}, \tag{3}$$

$$\bar{L} = 1.2\sqrt{\frac{1}{\overline{p}_a} - 1.89}, \quad [11], \text{ p. 1048}, \tag{4}$$

$$\bar{L} = 0.89\left(0.1 + \frac{0.317}{\overline{p}_a}\right)\sqrt{\frac{1}{\overline{p}_a} - 1}, \quad \text{when } 0.528 \geqslant \overline{p}_a \geqslant 0.352, \ [7], \tag{5}$$

$$\bar{L} = 0.89\sqrt{\frac{1}{\bar{p}_a} - 1}, \quad \text{when } \bar{p}_a < 0.352, \quad [7], \text{ p. 234}, \tag{6}$$

and the second by linear relationships to β

$$\bar{L} = 1.1\beta, \quad [2], \text{ p. 576}, \tag{7}$$

$$\bar{L} = 1.306\beta, \quad [1], \text{ p. 216}, \tag{8}$$

where

$$\beta = \sqrt{M^2 - 1} = \sqrt{5\left(\frac{1}{(\bar{p}_a)^{2/7}} - 1\right) - 1}.$$

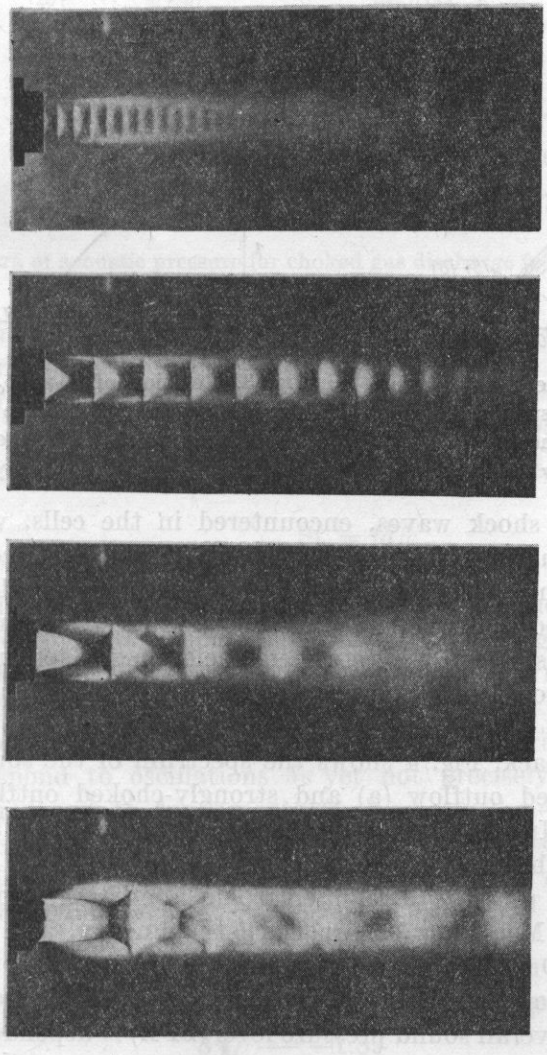

Fig. 1. Choked gas discharge from the nozzle

The results of computations made using the foregoing formulae are given in Fig. 2, where the results of the measurements of the cells' length from our own photographs are also plotted.

It can be seen that lengths of cells obtained from formulae (1), (4) and (7) differ considerably, whereas formulae (2) and (3), (5) and (6) as well as (8) differ by only a little and do not depart much from the results of measurements made by the present authors. For this reason the value of the ratio of the length of the cells over $\bar{p}_a$, obtained by measurement, has been found to be the most reliable and has provided the basis for plotting the graph $\bar{L}(\bar{p}_a)$ (Fig. 3). This, in turn, has found an application in the analysis of the supersonic gas jet formed at the outflow from the disk.

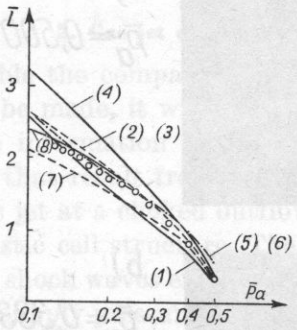

Fig. 2. Relation of the length of the first cell ($\bar{L}$) to the supply pressure ($\bar{p}_a$) of the nozzle
○ – measurements by the authors

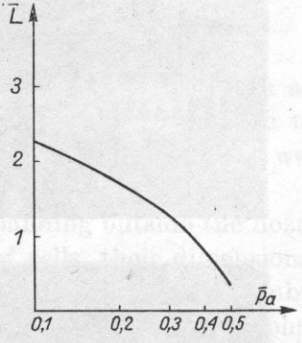

Fig. 3. Relation of $\bar{L}$ to $\bar{p}_a$ for the nozzle, according to the measurements of the authors

The interaction of shock waves, encountered in the cells, with vortices and turbulence in the unevenly expanded supersonic jet, produces additional noise, in addition to the turbulent mixing noise also generated in subsonic jets. The noise connected with the cell structure exhibits two components [2]. The former is distinguished by discrete frequencies in its spectrum and the occurrence of acoustic-flow feedback at its generation [10, 11]; it is usually called screech or whistle. The latter has a wider band with a definite peak and is produced without feedback. Fig. 4 shows the spectrum of the sound level obtained for weakly-choked outflow (a) and strongly-choked outflow (b) from the convergent nozzle. In the latter case the discrete frequency (5.4 kHz) and its first harmonic can be distinctly seen.

The overall sound pressure level increases as both the supply pressure causing an increase of Mach number on the jet boundary, and the rate of gas delivery increase. On the basis of previous results [2] and our own measurements, it has been found that for $\theta = 90°$ and within the range $0.5 < \beta < 1$ ($0.46 > \bar{p}_a > 0.31$) the overall sound pressure level (SPL) is dependent on β^4, i.e.

$$SPL[\mathrm{dB}] = \mathrm{const} + 40 \log \beta. \tag{9}$$

For $\beta > 1$, *SPL* is almost constant in level.

The generation by the jet of the above-mentioned discrete frequencies in the noise spectrum depends primarily on the ratio of the ambient pressure to the supply pressure and on conditions for the reflection of acoustic waves in the environment of the nozzle and jet [3, 4, 8, 9, 13]. The occurrence of strong discrete frequencies is connected with the decay of the discharging jet over a considerably shorter path than when they are absent (Fig. 1c).

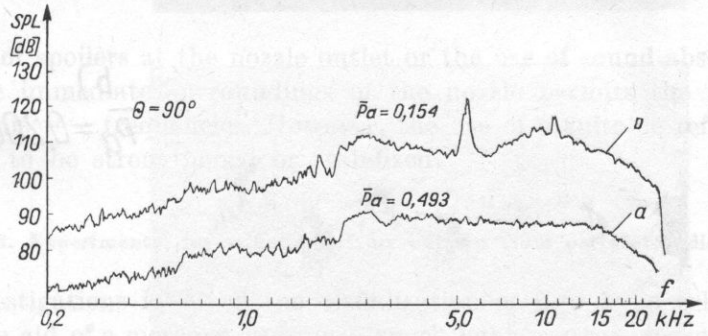

Fig. 4. Spectra of acoustic pressure for choked gas discharge from the nozzle for two values $\overline{p}_a$

Various forms of jet oscillations corresponding to different levels of supply pressure have also been described. It is possible to distinguish prevailing oscillations of an asymetric type [1, 4, 7-9, 11, 13], visible on photographs taken by schlieren (Fig. 5a) and shadow methods (Fig. 5b) using a spark light source. Fig. 6 compares Strouhal numbers evaluated from the formula

$$\mathrm{St} = fd/c_a \tag{10}$$

on the basis of the measurements of discrete frequencies stated in publications and obtained by the authors. It is possible to distinguish the band A throughout the whole range of $\overline{p}_a$ that corresponds to asymmetric oscillations, the band B within the range of higher values of $\overline{p}_a$ that correspond to oscillations of a symmetric type, and the band D within the range of lower values $\overline{p}_a$, that correspond to oscillations as yet not precisely investigated. The given values correspond to fundamental frequencies, whereas in spectra the first harmonic can frequently be observed. For comparison Strouhal numbers are also specified which have been evaluated from the empirical formulae stated in two publications:

$$\mathrm{St} = \frac{1}{3\sqrt{\frac{1}{\overline{p}_a} - 1.89}}, \quad [11], \text{ p. } 1048 \tag{11}$$

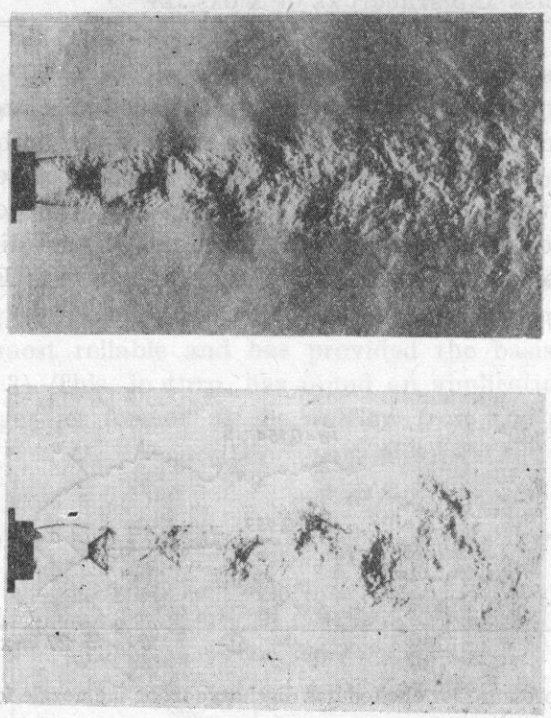

Fig. 5. Choked discharge from the nozzle-oscillations of the jet (of an asymmetric type): a) the photo made by steak trail method, b) the photo made by shadow method

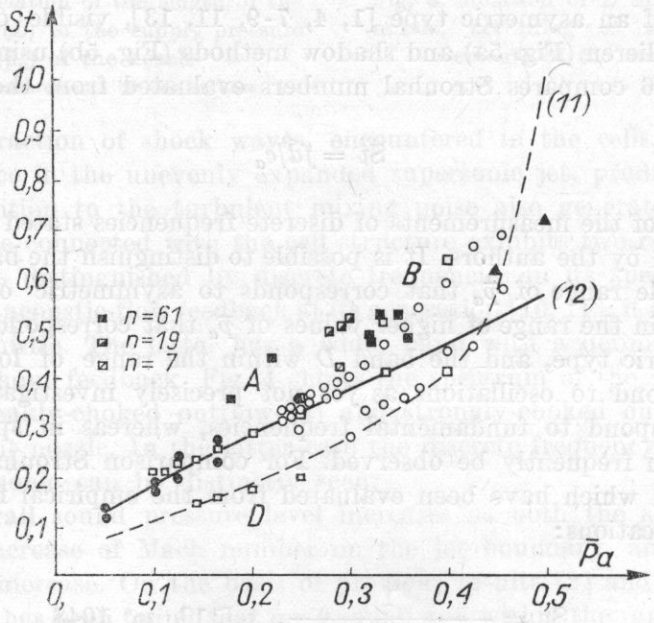

Fig. 6. Relation of Strouhal number to supply pressure ($\bar{p}_a$) for discrete frequencies in a spectrum

■ – measurements by the authors

and

$$\mathrm{St} = \frac{0.567}{\sqrt{\frac{1}{\overline{p}_a} - 1}}, \quad [7], \text{ p. } 235. \tag{12}$$

It can be seen that formula (12) is in a good agreement with the measurement results within a wide range of $\overline{p}_a$ and is associated with the band A. On the other hand, formula (11) is only partially in agreement with all three bands.

The use of spoilers at the nozzle outlet or the use of sound-absorbing materials in the immediate surroundings of the nozzle permits the removal of some of the discrete frequencies. However, the use of a suitable reflector may enable them to be strengthened or stabilized.

3. Experimental investigation of air outflow from perforated disks

The investigations involved the visualization of flow by a schlieren method with the aid of a mercury lamp or a spark light source; measurements of static and stagnation pressure by means of a Prandtl tube of small dimensions; measurements of overall sound pressure level (*SPL*) and noise spectra with the aid of apparatus from Brüel and Kjaer comprising a half-inch microphone (type 4133) with pre-amplifier (type 2616), analyser (type 2010) and level recorder (type 2307). A microphone was located at a radius of 50 cm from the nozzle outlet or the disk, and the angle θ between the radius and jet axis in a horizontal plane varied within the range 45° to 135°.

All disks were provided with holes arranged on the sides of hexagons (Fig. 20a). The total cross-section of the holes was always equal to the cross-section of the nozzle, of diameter 16 mm. The number of holes in the disks depended on the number of concentric hexagonals and can be expressed by the formula [1]

$$n = 1 + 3n_h(n_h + 1). \tag{13}$$

Disks with three numbers of holes arranged at various distances were used:

n_h	n	η					
1	7	0.5	0.645				
2	19	0.07	0.5	0.861			
4	61	0.07	0.5	0.772	1.07	1.243	1.523

Visualization of jet structures. Figs. 7 and 8 show air jets discharging from disks with equal $\eta = 0.5$, but with different numbers of holes: 61 and 19, respectively. At lower supply pressures the cell structure occurs only in the prox-

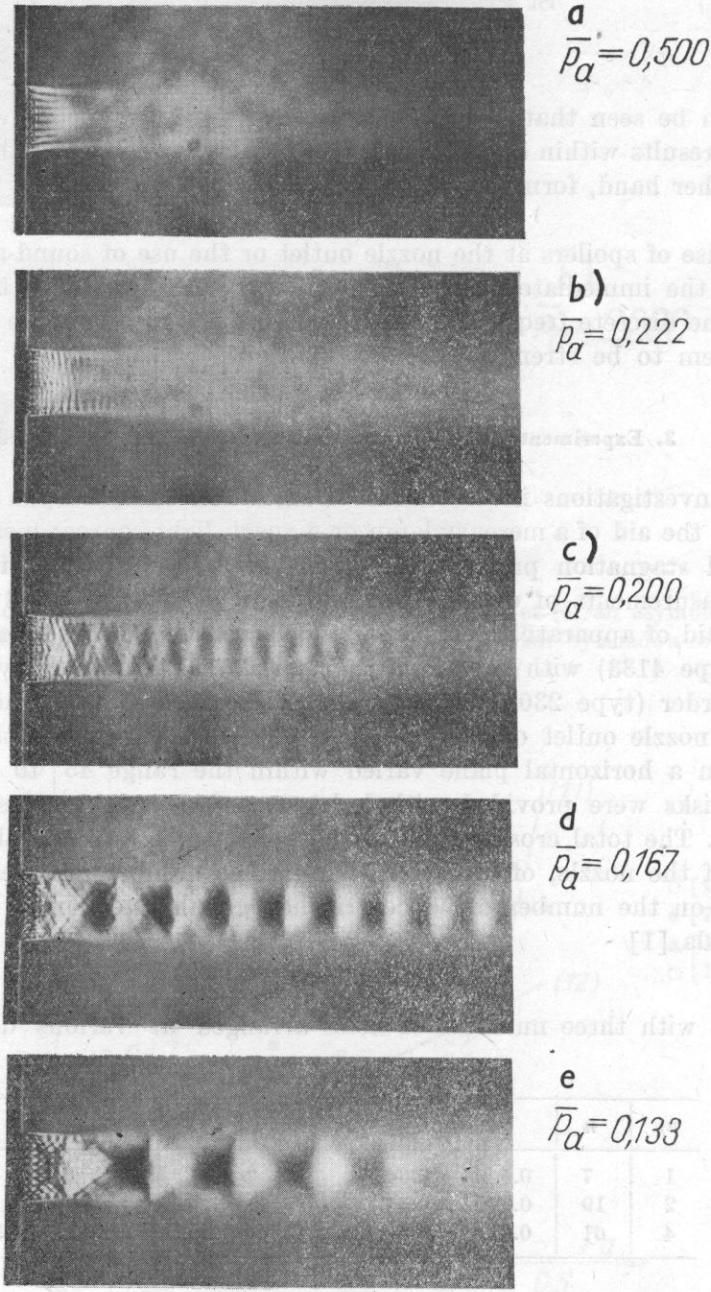

Fi .7. Choked gas discharge from a disk ($n = 61$, $\eta = 0.5$) for various supply pressures

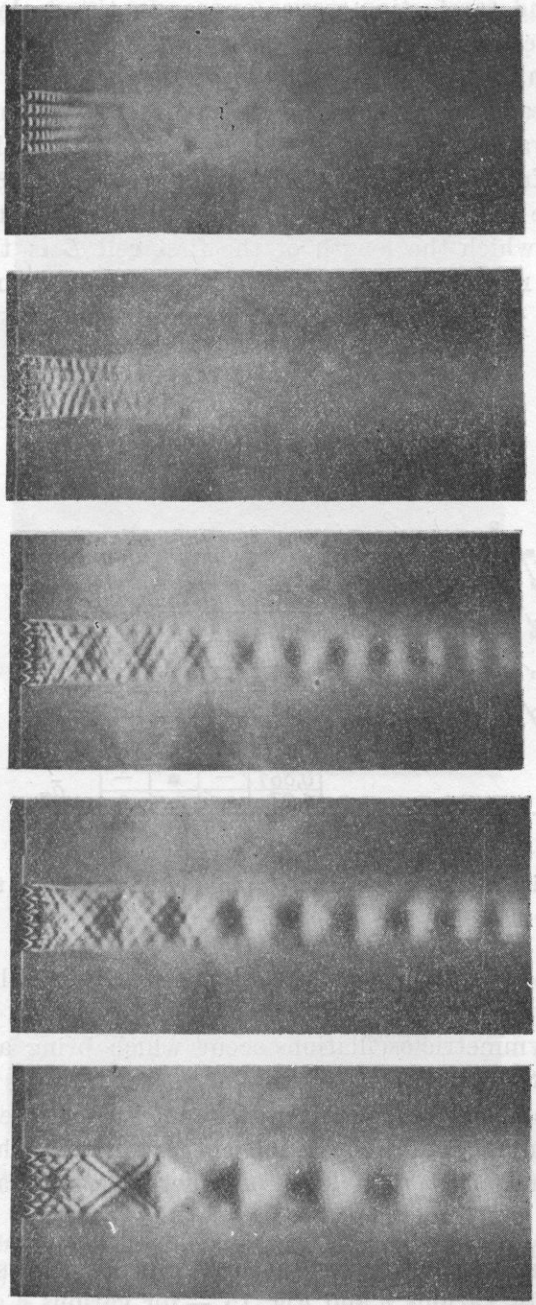

Fig. 8. Choked gas discharge from a disk ($n = 19$, $\eta = 0.5$) for various supply pressures

imity of the disk. Jets meet as subsonic ones to form a coalesced subsonic jet (a). As the pressure increases, the plane of joining of the jets moves towards the disk, while shock and rarefaction waves appear in the coalesced jet (b). With sufficiently high pressure distinct cells occur in the coalesced jet (c, d, e), which increase in length as the supply pressure rises.

On the basis of the measurement of the length of the first distinct cell of the coalesced jet and the graph shown in Fig. 3, the form of the substitute supply pressure ($\overline{p}_{as}$) as a function of real disk supply pressure ($\overline{p}_a$) is shown in Fig. 9 (the substitute disk supply pressure ($\overline{p}_{as}$) corresponds to the nozzle supply pressure ($\overline{p}_a$) at which the length of the first cell $\overline{L}$ is the same for both the disk and the nozzle). As can be seen, the growth of η at constant n and $\overline{p}_a$ causes $\overline{p}_{as}$ to increase, i.e. reduces the substitute supply pressure p_{os}.

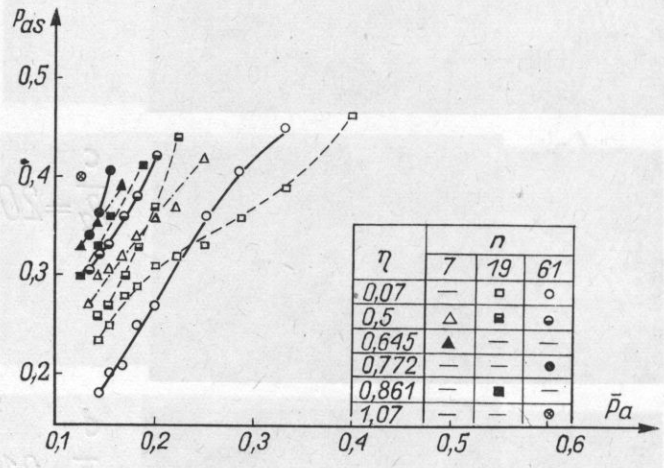

Fig. 9. Relation of the substitute supply pressure ($\overline{p}_{as}$) in a coalesced jet to the real supply pressure of the disk ($\overline{p}_a$)

Figs. 10-13 show gas jets at various supply pressures. At the lower and the higher values (a, c) the jet is stable and coherent, while at intermediate pressures (b) distinct asymmetric oscillations occur which bring about a very rapid decay of the jet. Such structures exist at various values of η and n. In the figures we can see Mach waves of high frequency which are propagating conically from the jet boundary, in the proximity of the disk. Furthermore, Fig. 13a shows acoustic disturbances of a lower frequency which are probably induced by oscillations of symmetric type.

Measurements of overall sound pressure level. Fig. 14 shows the dependence of the *SPL* on $\overline{p}_a$ for various η and Fig. 15 — for various n and angles θ. From Fig. 14 it can be seen that reduction in η at constant n causes a steep rise of *SPL* at lower supply pressures. This rise comes from the supersonic coales-

ced jet. Within a wide range of pressures the minimum level *SPL* is obtained for $\eta = 0.772$. Fig. 15 shows a reduction in *SPL*, within a wide range of pressures, as n increases with constant η. The increase of *SPL* to a level that corresponds to the *SPL* of the nozzle occurs at very similar values of the supply pressure.

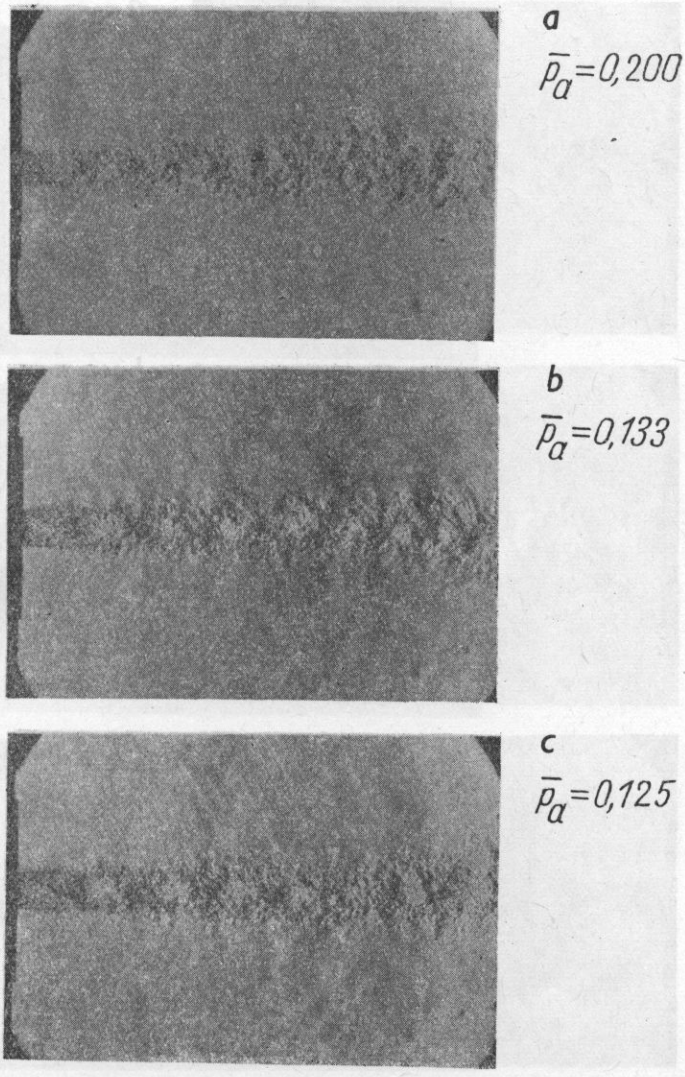

Fig. 10. Choked gas discharge from a disk ($n = 61$, $\eta = 0.07$)

The spectrum of acoustic pressure. Fig. 16 shows spectra obtained at three values of the supply pressure. The spectrum (a) corresponds to a subsonic coalesced jet, and (b) and (c) to a supersonic jet with cellular structure. The last two spectra both contain a distinct peak caused by broad-band noise

resulting from the cellular structure. Furthermore, in the spectrum (c) there occur two discrete frequencies that correspond to the noise induced by asymmetric flow oscillations with acoustic-feedback. The higher frequency is a first harmonic.

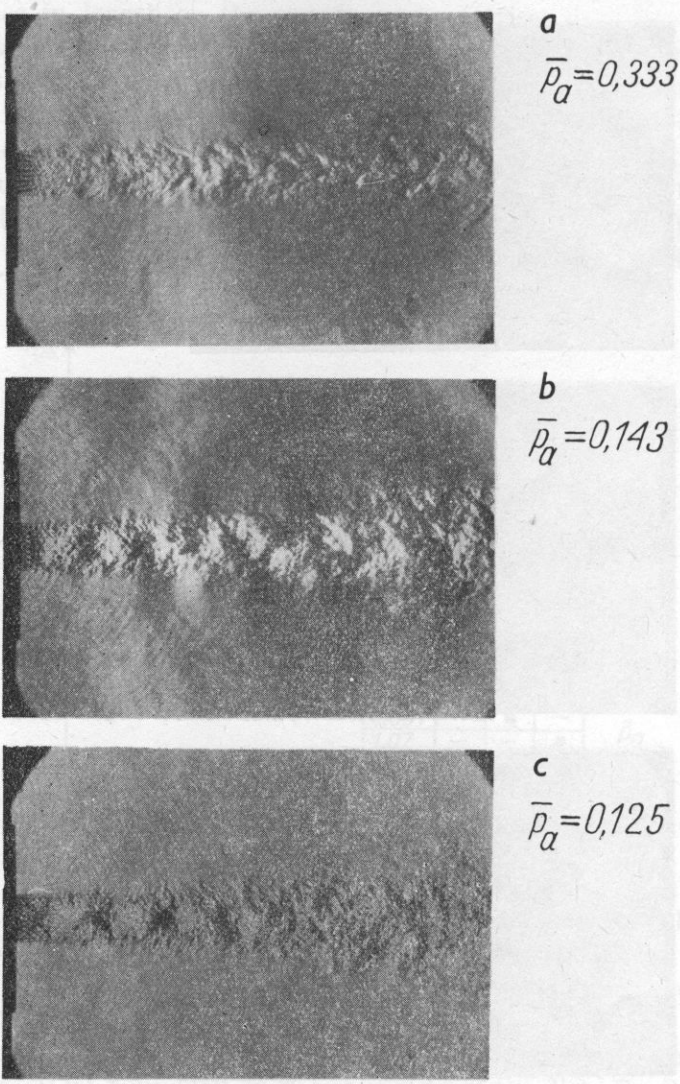

Fig. 11. Choked gas discharge from a disk ($n = 61$, $\eta = 0.5$)

Fig. 17 shows the results for the other disk. In the spectrum (c) one discrete frequency can be seen.

Fig. 18 and 19 show the effect of the angle θ on the shape of the spectrum, which, evidently, is negligible.

Measurement of stagnation and static pressures. The values of stagnations pressure as measured on the axis of the subsonic coalesced jet (in its initial cross-section) are plotted in Fig. 21a ($M_p < 1$). While measuring the static pressure at the beginning of the supersonic coalesced jet, a substantial excess

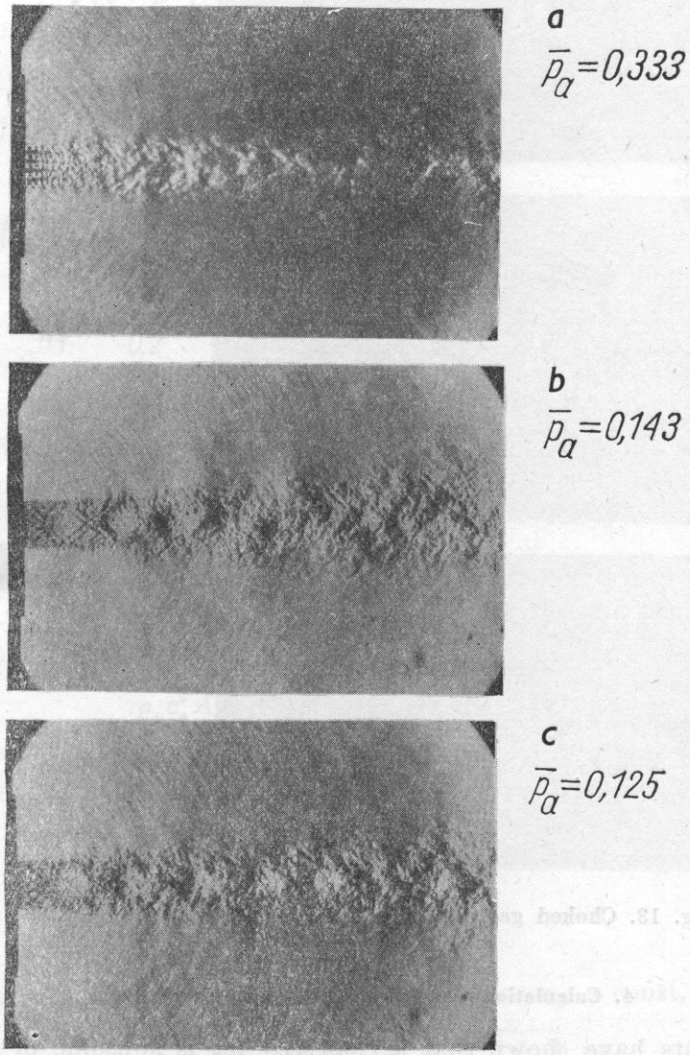

Fig. 12. Choked gas discharge from a disk ($n = 19$, $\eta = 0.5$)

pressure only a little below 1 atm at the maximum supply pressure was found to exist. The results have not been compared because they are few as a result of considerable air consumption during measurement at high supply pressures.

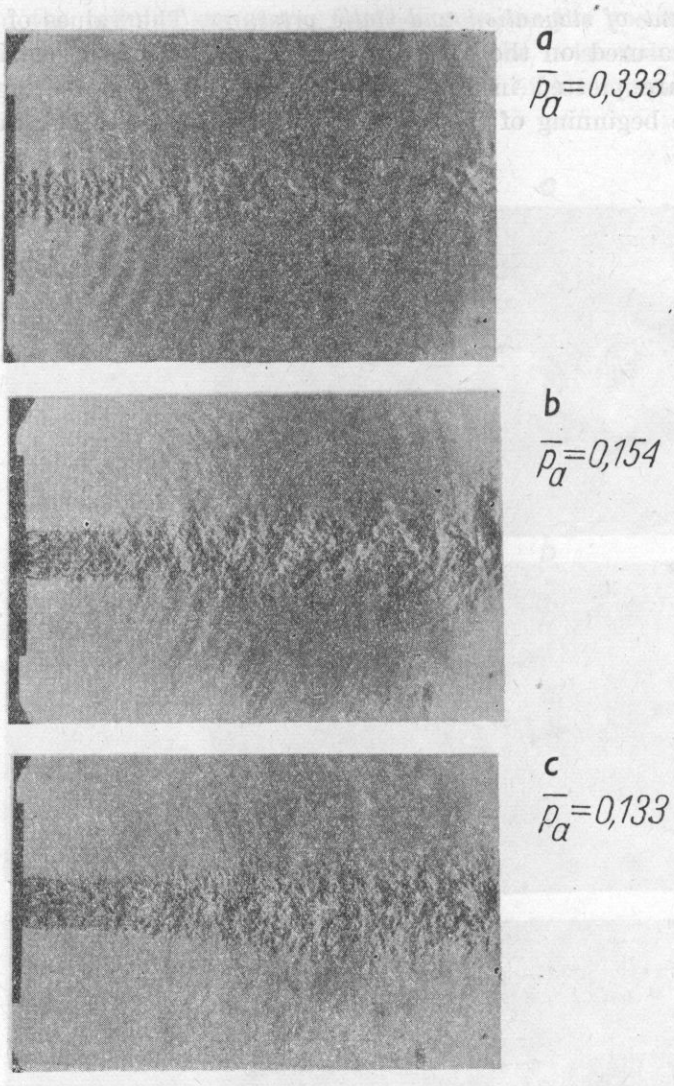

Fig. 13. Choked gas discharge from a disk ($n = 7$, $\eta = 0.5$)

4. Calculation the properties of a coalesced jet

Experiments have shown that a coalesced jet is subsonic or supersonic with cell structure depending on the range of $\bar{p}_a$, η and n. For this reason, physical models used for the calculation will be different for different jets. In both cases a simplifying assumption has been made that the gas properties at the initial cross-section of a collective jet are uniform.

Subsonic flow in a collective jet. A diagram of the structure of the flow is shown in Fig. 20b. Due to mixing of the jets discharging from a disk with

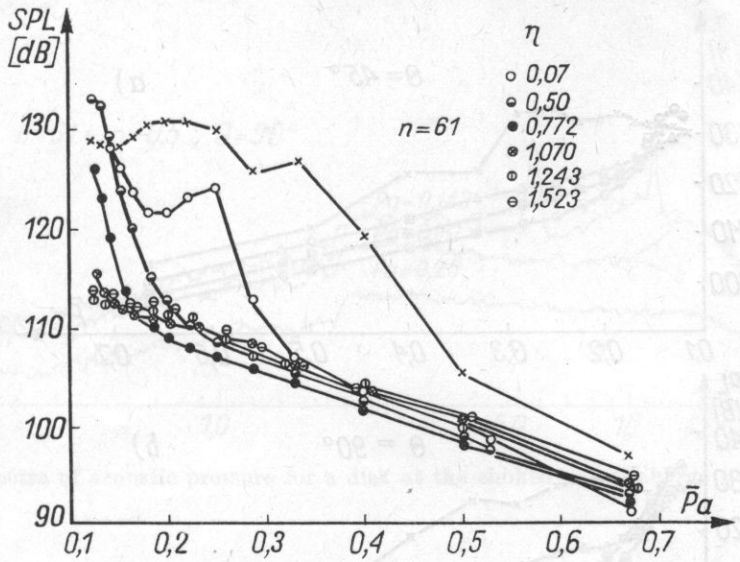

Fig. 14. Relation of *SPL* to $\bar{p}_a$ for various η ($\theta = 90°$) × – nozzle

the ambient air, subsonic portions of the jet develop around the decaying cell structure.

At a certain distance away from the disk they come into contact with each other and form a coalesced subsonic jet. Applying the principle of conservation of momentum to those jets we obtain:

$$\varrho_* c_*^2 A_* + (p_* - p_a) A_* = \varrho_p u_p^2 A_p. \tag{14}$$

After giving consideration to the equations of state of gas for single and coalesced jet, and relations

$$\alpha_p = A_*/A_p \tag{15}$$

and

$$M_p = u_p/c_p, \tag{16}$$

we determine the relation between M_p and $\bar{p}_a$, for $\alpha_p = \text{const}$, in the form

$$M_p = \sqrt{\frac{\alpha_p}{k}\left[\frac{2}{\bar{p}_a}\left(\frac{2}{k+1}\right)^{1/(k-1)} - 1\right]}. \tag{17}$$

With the aid of tables for isentropic gas flow we may find $\bar{p}_{as}(M_p)$.

It can be concluded from (17) that the problem involves a proper determination of α_p. The cross-section of the coalesced jet has been defined in two ways: as the total of the cross-sections of all of the jets with diameters

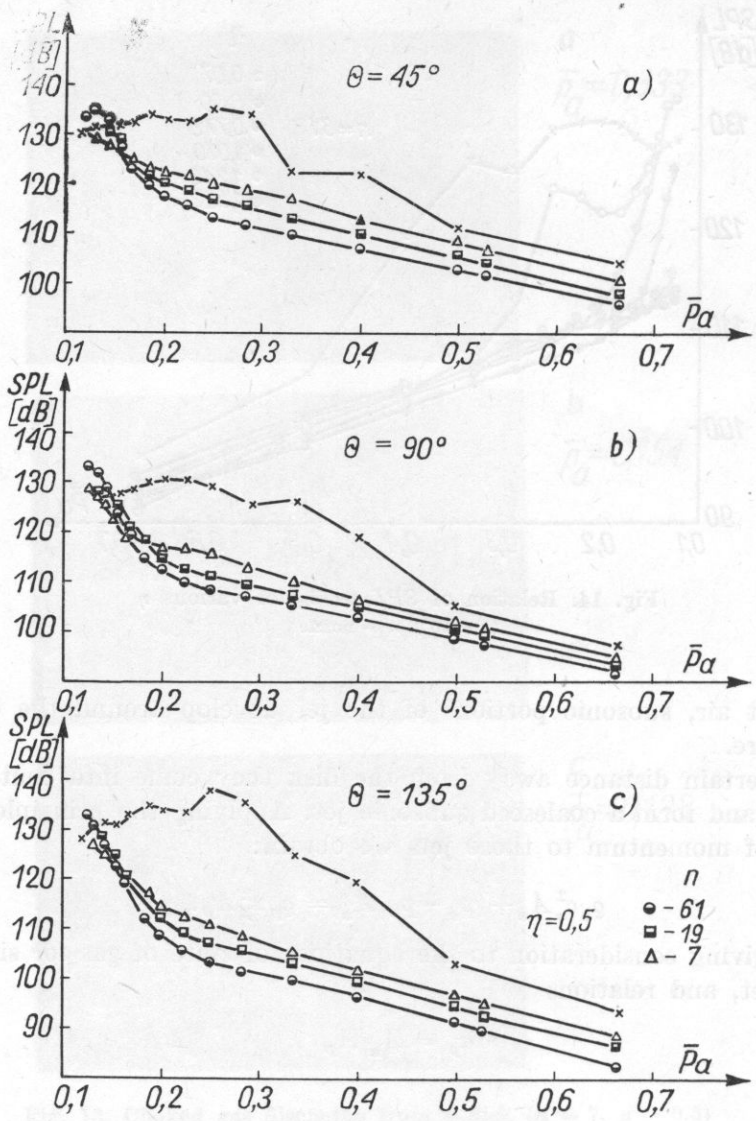

Fig. 15. Relation of *SPL* to $\overline{p}_a$ for various n and θ ($\eta = 0.5$)
× – nozzle

$d+b(A_{p1})$ or as the area (A_{p2}) bounded by dash-dot curve in Fig. 20a. Correspondingly, one obtains

$$a_{p1} = \frac{1}{(1+\eta)^2}, \tag{18}$$

$$a_{p2} = a_{p1} \frac{\pi[1+3n_h(n_h+1)]}{\frac{\pi}{6} + \frac{5}{\sqrt{3}} + 6n_h(\sqrt{3}n_h+2)}. \tag{19}$$

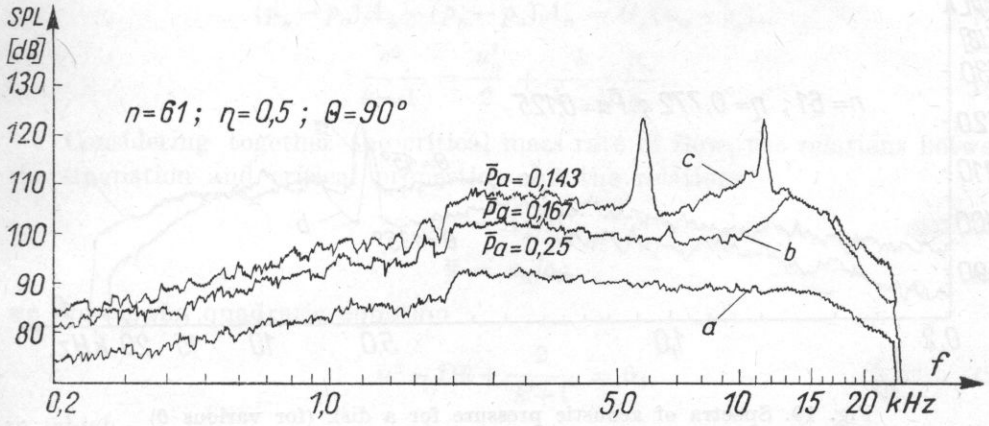

Fig. 16. Spectra of acoustic pressure for a disk at the choked gas discharge (for various $\overline{p}_v$)

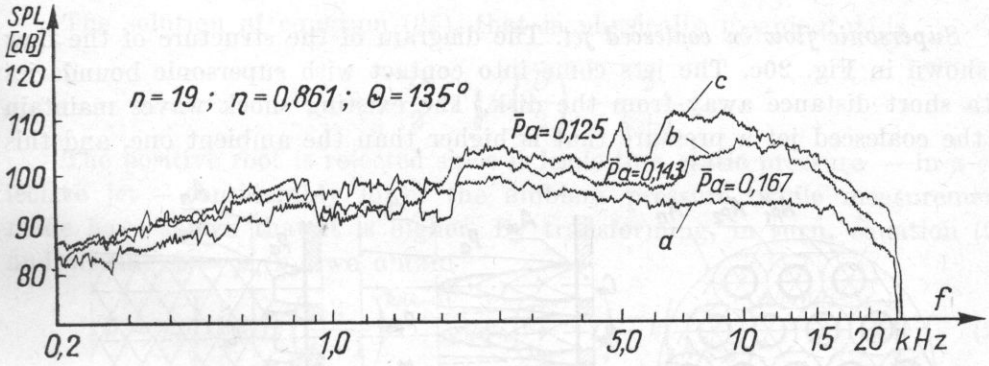

Fig. 17. Spectra of acoustic pressure for a disk (for various $\overline{p}_a$)

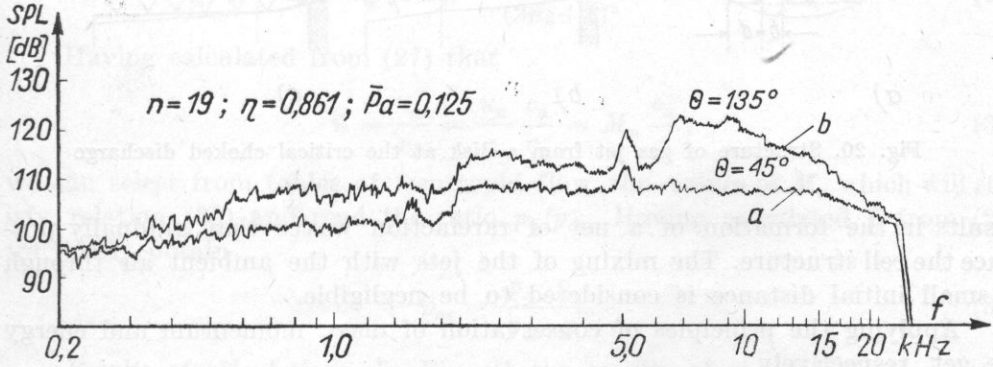

Fig. 18. Spectra of acoustic pressure for a disk (for various θ)

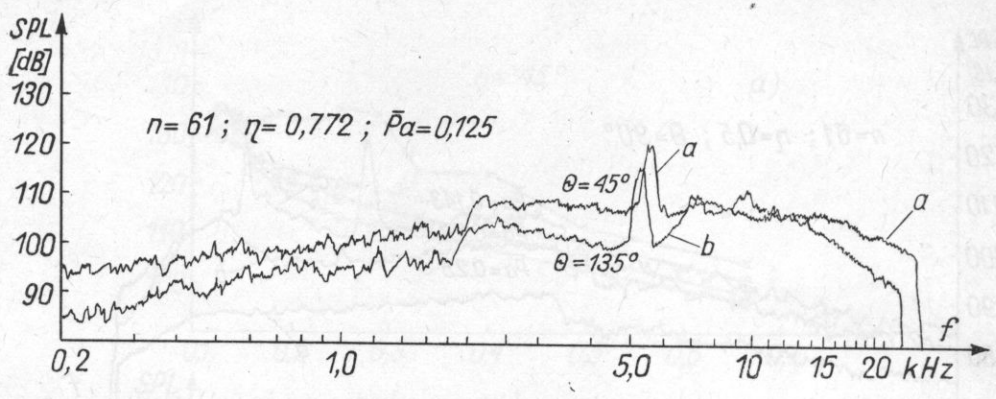

Fig. 19. Spectra of acoustic pressure for a disk (for various θ)

Thus α_{p1} depends only on the spacing of holes while α_{p2} depends also on their number.

Supersonic flow in coalesced jet. The diagram of the structure of the flow is shown in Fig. 20c. The jets come into contact with supersonic boundaries at a short distance away from the disk. The existing shock waves maintain in the coalesced jet a pressure that is higher than the ambient one, and this

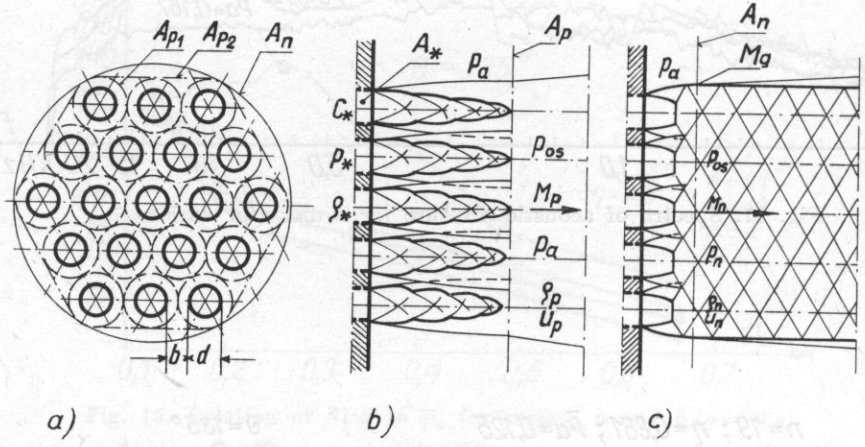

Fig. 20. Structure of gas jet from a disk at the critical choked discharge

results in the formation of a net of rarefaction waves that gradually produce the cell structure. The mixing of the jets with the ambient air through a small initial distance is considered to be negligible.

Applying the principles of conservation of mass, momentum and energy we get, respectively,

$$G_* = \varrho_n u_n A_n, \tag{20}$$

$$(p_* - p_a)A_* - (p_n - p_a)A_n = G_*(u_n - c_*), \tag{21}$$

$$\frac{c^2}{k-1} = \frac{u_n^2}{2} + \frac{k}{k-1}\frac{p_n}{\varrho_n}. \tag{22}$$

Considering together the critical mass rate of flow, the relations between the stagnation and critical properties and the relations

$$a_n = A_*/A_n, \tag{23}$$

$$\bar{u} = u_n/c_0, \tag{24}$$

we obtain the quadratic equation

$$\bar{u}^2 - D\bar{u} + \frac{2}{k+1} = 0, \tag{25}$$

in which

$$D = 2\left(\frac{2}{k+1}\right)^{1/2} + \bar{p}_a\left(\frac{1}{a_n} - 1\right)\left(\frac{2}{k+1}\right)^{(k-3)/2(k-1)}. \tag{26}$$

The solution of equation (25), that is physically meaningful, is

$$\bar{u} = \frac{D}{2} - \sqrt{\left(\frac{D}{2}\right)^2 - \frac{2}{k+1}}. \tag{27}$$

The positive root is rejected since it leads to a static pressure — in a collective jet — considerably lower the ambient pressure, while measurements made have shown that it is higher. By transforming, in turn, equation (21) and writing $\bar{p} = p_n/p_o$, we obtain

$$\bar{p} = a_n\left[(k+1)\left(\frac{2}{k+1}\right)^{k/(k-1)} + \bar{p}_a\left(\frac{1}{a_n} - 1\right) - k\left(\frac{2}{k+1}\right)^{(k+1)/2(k-1)}\bar{u}\right]. \tag{28}$$

The cross-section of the coalesced jet is defined as the circular area bounded by continuous line in Fig. 20a, which implies

$$a_n = a_{p1}\frac{1+3n_h(n_h+1)}{(2n_h+1)^2}. \tag{29}$$

Having calculated from (27) that

$$\bar{u} = \frac{u_n}{c_o} = \frac{u_n}{c_n}\frac{c_n}{c_o} = M_n\frac{c_n}{c_o}, \tag{30}$$

we can select from tables of isentropic flow the values of M_n which will satisfy relation (30) and read the ratio p_n/p_{os}. Having calculated $\bar{p}$ from (28) we finally obtain

$$\bar{p}_{as} = \frac{p_n}{p_{os}}\frac{p_a}{p}. \tag{31}$$

Results of calculations. In Fig. 21 the results of the calculations made using the above relations are denoted with continuous lines. For a subsonic

coalesced jet (a) ($M_p < 1$), the results of measurement show good agreement with the results of calculations obtained using α_{p1} for bigger η, and α_{p2} for smaller. In the case of a supersonic jet ($M_g > 1$) this agreement deteriorates, notably for $n = 19$.

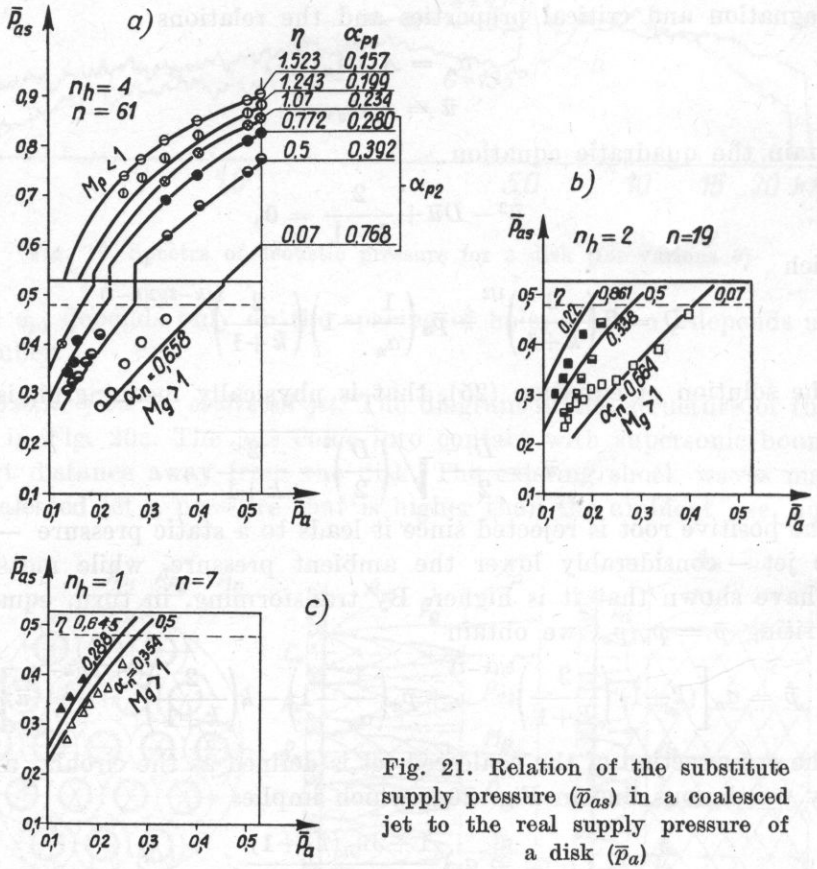

Fig. 21. Relation of the substitute supply pressure ($\bar{p}_{as}$) in a coalesced jet to the real supply pressure of a disk ($\bar{p}_a$)

The curves obtained do not join at $\bar{p}_{as} = 0.528$, i.e. when the flow in the coalesced jet is critical. In the transsonic range, measurement results are lacking but it might be supposed that they would not have been in agreement with the calculations. These facts result from the application of the two different models of flow which are correct for a subsonic or a supersonic coalesced jet.

5. Comparison of the jet from perforated disk with the jet from a nozzle

At the choked discharge of a gas from a perforated disk the collective jet can be subsonic, similar to subsonic discharge from a convergent nozzle, or supersonic, as for choked discharge. The nature of the structure of the

coalesced jet depends on the substitute supply pressure $\overline{p}_{as}$ which, in turn, is a function of $\overline{p}_a$, n and η. The collective jet exhibits all properties of the jet from a nozzle at corresponding supply pressures, i.e. when $\overline{p}_{as} = \overline{p}_{ad}$.

The *SPL* of the disk is linearly dependent on $\overline{p}_a$ since the coalesced stream is subsonic, as is the case for the disk in the range of subsonic discharge. When the cell structure appears, the *SPL* increases rapidly, as in the choked discharge from the nozzle, and can attain a level that corresponds to its maximum *SPL*.

The nature of the *SPL* spectra in corresponding supply pressure ranges is the same for the disk and nozzle. In the subsonic range the spectra are flat, while in the supersonic one they exhibit a distinct peak and discrete frequencies. Strouhal numbers calculated on the basis of discrete frequencies fall into the same range as they do for the nozzle if $\overline{p}_{as} = \overline{p}_{ad}$ (Fig. 6). Symmetric and asymmetric forms of vibrations also occur in both cases.

6. Conclusions

From the investigations carried out it can be concluded that the efficiency of a perforated disk as a means of reducing the outlet noise is limited by the supply pressure range dependence on η. Fig. 22 is a plot of values of $\overline{p}_a$ from Figs. 14 and 15 that correspond to the beginning of a steep rise of *SPL*, while the continuous line denotes the calculated values of $\overline{p}_a$ that correspond to $\overline{p}_{as} = 0.48$ (broken line in Fig. 21a), i.e. $M_g = 1.08$. The values of $\overline{p}_a$ from Fig. 21b and c, that correspond to the other number of holes, differ only insi-

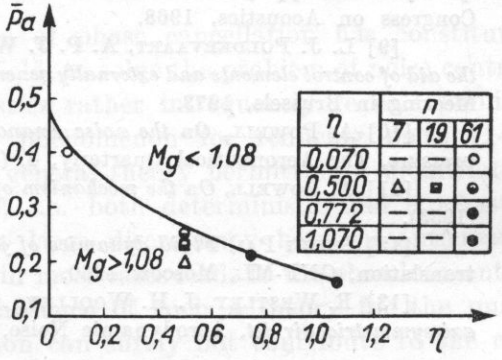

Fig. 22. $\overline{p}_a$ as a function of η for a perforated disk (corresponding to a dynamic *SPL* increase in Figs. 14 and 15)

gnificantly, as described by formula (29). It can be seen that an increase in noise occurs after the formation of the cell structure in a coalesced jet. It is, therefore, desirable that $\overline{p}_a$, for a given η, should always be within the region of efficient operation of the disk, i.e. $M_g < 1.08$. On the other hand, it was found that the lowest level *SPL* occurred when $n = 61$, corresponding to $\eta = 0.5 - 0.8$; thus, the use of higher η can be justified only when there the

the highest supply pressure occurs. It is known, that the *SPL* decreases as the number of holes in the disk [5] increases, but, at the same time, the measurements show that the supply pressure at which the *SPL* of the disk becomes equal to the *SPL* of the nozzle does not depend on the number of holes.

Thus, when using a perforated disk as a single stage element to reduce outflow noise, it is necessary to select a diameter as small as possible for holes in the disk and to choose a value of η as small as possible, but the value of $\overline{p}_a$ should always remain in the region of efficient operation of the disk.

References

[1] M. G. Davies, D. E. S. Oldfield, *Tones from a choked axisymmetric jet*, Acoustics, **12**, 4 (1962).

[2] M. J. Fisher, P. A. Lush, M. H. Bourne, *Jet noise*, Jour. of Sound and Vibr., **28** (3), 563-585 (1973).

[3] D. R. Glass, *Effects of acoustic feedback on the spread and decay of supersonic jets*, AIAA Jour., **6**, 10 (1968).

[4] A. G. Hammitt, *The oscillation and noise of an overpressure sonic jet*, JASA, **28**, 9 (1961).

(5) W. M. Jungowski, A. P. Szumowski, *Perforated disk as an element that reduces the outlet noise*, Archiwum Akustyki, **9**, 3, 339-360 (1974) (in Polish).

[6] E. S. Love, C. E. Grigsby, L. P. Lee, M. J. Woodling, *Experimental and theoretical studies of axisymmetric free jets*, NASA, TR, R-6, 1959.

[7] W. M. Mamin, A. W. Rimskij-Korsakow, *Some properties of radiation of discrete tone by supersonic air-jet*, VII Wsiesojuznaja Akusticzeskaja Konferencja po Fiziczeskoj i Techniczeskoj Akustikie, 1971, Sbornik Dokładow, Leningrad 1973 [in Russian].

[8] L. J. Poldervaart, A. T. Vink, A. P. J. Wijnands, *The photographic evidence of the feedback lopp of a two-dimensional screeching supersonic jet of air*, The 6th International Congress on Acoustics, 1968.

[9] L. J. Poldervaart, A. P. J. Wijnands, L. Bronkhorst, *Aerosonic games with the aid of control elements and externally generated pulses*, Proceedings of the AGARD specialist Meeting in Brussels, 1973.

[10] A. Powell, *On the noise emanating from a two-dimensional jet above the critical pressure*, The Aeronautical Quarterly, **4**, (1953).

[11] A. Powell, *On the mechanism of choked jet noise*, Proc. Phys. Soc., **66**, PT, 12-B (1953).

[12] Shih-i Pai, *Fluid dynamics of jets*, D. Van Nostrand Comp. Inc., 1955, Russian translation, GNF-ML, Moscow 1960.

[13] R. Westley, J. H. Woolley, *An investigation of the near noise fields of a choked axi-symmetric air jet*, Aerodynamic Noise, Proc. of AFOSR-UTIAS Symposium, 1968.

Received on 15th October 1975

ARCHIVES OF ACOUSTICS
1, 2 109-125 (1976)

GENERAL CONDITIONS OF PHASE CANCELLATION IN AN ACOUSTIC FIELD

MICHAŁ VOGT

Institute of Fundamental Technological Research (Warszawa)

The dependence of the degree of cancellation of an acoustic field, expressed by the field cancellation factor, on the correlation parameters of the signals: cancelling and cancelled is derived. Using this dependence, the necessary conditions – in terms of phase and amplitude – for the occurrence of the cancellation phenomenon at a field point are determined.

The possibility of the cancellation of larger regions of acoustic fields is investigated using such parameters as spectral characteristics of various signal classes and mutual distances of the cancelling and cancelled sources.

A classification into natural and forced cancellation is introduced and the classes of signals which can be cancelled in a natural way are determined.

The conditions for the occurrence of cancellation throughout all space are determined.

1. Introduction

For years now the phenomenon of phase cancellation has constituted a promising chance to workes in the field, to solve the problem of noise control. The literature concerned with acoustics rather infrequently reveals publications reporting trials to utilize this phenomenon for reducing noise [1-5]. At present there does not exist any general theory permitting a quantitative description for all classes of signals, i.e. both deterministic and stochastic. This may have been caused by too large discrepancy between anticipated and obtained results which, in turn, in most cases leads to the abandonment of more thorough investigations. The absence of such a theory for the quantitative conception of the phenomenon can surely not contribute to the realization of positive results as, indeed, it does not favour a proper utilization of this phenomenon in practice.

An attempt has been made in this paper to define the conditions necessary for the creation of the phenomenon of phase cancellation at a field point and to give the dependence between the degree of field cancellation and the correlation parameters of signals. The correlative approach permits to a uniform analysis of all classes of signals.

On the basis of dependence derived between the degree of field cancellation and the correlation parameters of the signals, the range of regions in which the phenomenon of cancellation occurs for various typical classes of signals has been calculated, and the classes of signals subject to natural cancellation defined. The relationship between the mutual spacing of sources, necessary for the occurrence of cancellation in a given region, and the spectral nature of the sound emitted by them has also been determined.

Consideration is merely given in the paper to the cancellation in a field, neglecting the mutual interaction of sources.

2. The field cancellation factor

Let a given source S (Fig. 1) be placed in a propagation medium and emit a signal $x(t)$. It produces in the medium a field $x(r,t)$. At any point A in this field, with the distance $|r_0|$ from the source, the wave $x_A(t)$ is only a function of time. The mean power $\langle P_{xA} \rangle$ of this wave at the point A is

$$\langle P_{xA} \rangle = \frac{1}{T} \int_0^T x_A^2(t)\,dt, \tag{1}$$

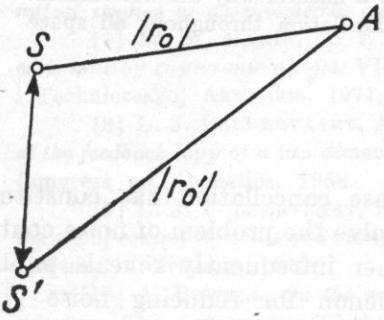

Fig. 1. Spacing of sources – cancelled S, cancelling S' – and the point A at which cancellation is required to take place

where T denotes the duration of signal.

Let another source S', which is placed in this medium at a distance d from the source S, emit a signal $y(t)$.

It produces at point A the wave $y_A(t')$ having a mean power

$$\langle P_{yA} \rangle = \frac{1}{T} \int_0^T y_A^2(t')\,dt, \tag{2}$$

where t' denotes the time calculated with regard to the coordinate system related to the source S' and is equal to

$$t' = t + \tau, \tag{3}$$

where τ is the difference of times at which signals from the sources reach the point A.

If the medium is linear, then the resulting signal $z_A(t)$ at the point A is the total of the component signals from sources S and S':

$$z_A(t) = x_A(t) + y_A(t'). \tag{4}$$

The mean power of this signal is

$$\langle P_{xyA} \rangle = \frac{1}{T} \int_0^T z_A^2(t)\, dt. \tag{5}$$

Cancellation at the point A occurs when

$$\langle P_{xyA} \rangle < \langle P_{xA} \rangle \quad \text{and/or} \quad \langle P_{xyA} \rangle < \langle P_{yA} \rangle, \tag{6}$$

depending on which field is to be cancelled.

Definition. *Phase cancellation* is a phenomenon resulting from such superposition of fields as to bring about a reduction of the signal power measured at a given point or region, compared to the signal power which would have been measured at this point or region as a result of the individual action of each component field.

In order to describe quantitatively the phenomenon of cancellation, we shall define the field cancellation factor k as the ratio of the cancelled power $\langle P_{cA} \rangle$ to the primary wave power $\langle P_{xA} \rangle$ which existed at a given point A prior to the superposition of the cancelling field:

$$k \overset{\text{df}}{=} \frac{\langle P_{cA} \rangle}{\langle P_{xA} \rangle}. \tag{7}$$

But

$$\langle P_{cA} \rangle = \langle P_{xA} \rangle - \langle P_{xyA} \rangle, \tag{8}$$

therefore

$$k = 1 - \frac{\langle P_{xyA} \rangle}{\langle P_{xA} \rangle}. \tag{9}$$

Since the mean cancelled power $\langle P_c \rangle$ cannot exceed the mean primary power $\langle P_x \rangle$, the field cancellation factor must lie between zero and unity:

$$0 < k \leqslant 1. \tag{10}$$

3. Dependence of the field cancellation factor on the correlation factor of the signals

The correlation functions for both of the signals $x(t)$ and $y(t)$ are calculated as the limit of the following integral for various values of the variable τ [6]:

$$R_{xy}(\tau) = \lim_{T\to\infty} \frac{1}{T} \int_0^T x(t)\, y(t+\tau)\, dt. \tag{11}$$

In general, the integration should extend over the whole range of $x(t)$ and $y(t)$. If the processes $x(t)$ and $y(t)$ are stationary, then their statistical properties will be the same for various samples of the processes. Thus the correlation functions of various samples will also be the same. It is then possible to calculate correlation functions of a given process for finite time intervals of width T:

$$R_{Txy}(\tau) = \frac{1}{T} \int_0^T x(t)\, y(t+\tau)\, dt. \tag{12}$$

Similarly, autocorrelation functions of component signals can be defined by

$$R_{Txx}(\tau) = \frac{1}{T} \int_0^T x(t)\, x(t+\tau)\, dt, \tag{13}$$

$$R_{Tyy}(\tau) = \frac{1}{T} \int_0^T y(t)\, y(t+\tau)\, dt. \tag{14}$$

For $\tau = 0$ the autocorrelation functions represent the mean power of the signal in the interval T:

$$R_{Txx}(0) = \frac{1}{T} \int_0^T x^2(t)\, dt = \langle P_x \rangle, \tag{15}$$

$$R_{Tyy}(0) = \frac{1}{T} \int_0^T y^2(t)\, dt = \langle P_y \rangle. \tag{16}$$

The ratio of the cross-correlation function, determined at a point of the field, to the square root of the product of values of the auto-correlation functions for the component signals at zero, is termed the *cross-correlation factor* b_τ for a time difference τ:

$$b_\tau = \frac{R_{Txy}(\tau)}{\sqrt{R_{Txx}(0) R_{Tyy}(0)}}. \tag{17}$$

The mean power of the total signal at the point A over a time T is

$$\langle P_{xyA}\rangle = \frac{1}{T}\int_0^T z_A^2(t)\,dt = \frac{1}{T}\int_0^T x_A^2(t)\,dt + \frac{1}{T}\int_0^T y_A^2(t+\tau)\,dt + \frac{2}{T}\int_0^T x(t)\,y(t+\tau)\,dt$$

$$= R_{Txx}(0) + R_{Tyy}(0) + 2R_{Txy}(\tau). \tag{18}$$

Substituting this value into formula (9) and considering condition (10), with a denoting the ratio of the cancelling signal power to the cancelled signal power,

$$a = \frac{R_{Tyy}(0)}{R_{Txx}(0)}, \tag{19}$$

we obtain the following condition for cancellation:

$$\frac{1}{2}\sqrt{a} < -b_\tau \leqslant \frac{1}{2}\frac{1+a}{\sqrt{a}}. \tag{20}$$

We also obtain the following relationship between the field cancellation factor k, the cross-correlation factor b_τ of component signals, and the ratio a of the powers of these signals:

$$k = -2b_\tau\sqrt{a} - a. \tag{21}$$

Consider first condition (20). Since a is positive, because it is the ratio of the powers of signals, both the right- and left-hand sides of inequality (20) are positive. Thus condition (20) is satisfied only if the correlation factor b_τ assumes a negative value, i.e.,

$$b_\tau < 0. \tag{22}$$

This relation is called the *phase condition.*

Let us now examine for what power ratios a the cancellation is possible and how strongly the component signals should be correlated with one another for a given power ratio a.

The right-hand side of inequality (20) represents a concave function having a minimum equal to 1 for the value $a = 1$ (Fig. 2).

From the Schwartz inequality we get a stronger condition, namely

$$|b_\tau| \leqslant 1. \tag{23}$$

Combining conditions (20) and (23), we get

$$\tfrac{1}{2}\sqrt{a} < 1, \tag{24}$$

hence the range of permissible powers for cancelling waves becomes

$$0 < R_{Tyy}(0) < 4R_{Txx}(0). \tag{25}$$

Thus the phenomenon of cancellation may occur for ratios of the power of the cancelling signal to the cancelled one within the range

$$0 < a < 4, \tag{26}$$

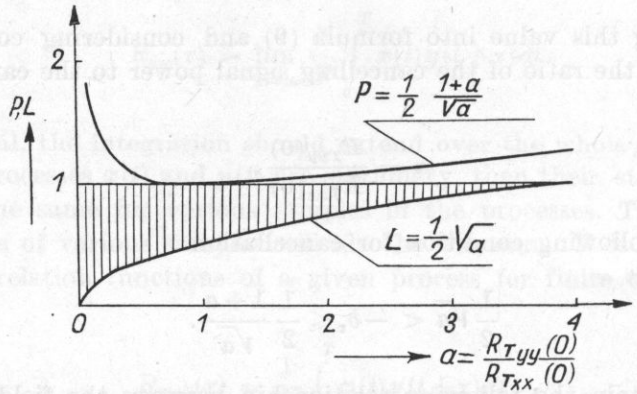

Fig. 2. A graph of the function P [which represents the right side of inequality (20)] and the function L (which represents the left-hand side of this inequality) versus the power ratio of the component signals. The shaded region determines the range of the value of the modulus of the cross-correlation factor $|b_\tau|$ necessary to obtain cancellation at a certain ratio a

while the required cross-correlation factor of both signals for given power ratio a should vary within the limits

$$\tfrac{1}{2}\sqrt{a} < -b_\tau \leqslant 1. \tag{27}$$

This condition is called the *amplitude condition.*

These relationships are shown in Fig. 2. The region of permissible values for $-b_\tau$, determined by condition (27), is shaded in Fig. 2.

Let us now analyze the mutual dependence of the degree of cancellation of a field and the degree of correlation of its component signals. To this end we present relation (21) in the form of a family of curves $k = f(a)$ for different values of the parameter b_τ(Fig. 3).

The maximum cancellation occurs for a value of the power ratio given by

$$a = b_\tau^2, \tag{28}$$

with the field cancellation factor attaining the value

$$k_{\max} = b_\tau^2. \tag{29}$$

Thus the maxima of the family of curves represented by (21) lie on the straight line

$$k_{\max} = a \quad \text{for } a \leqslant 1. \tag{30}$$

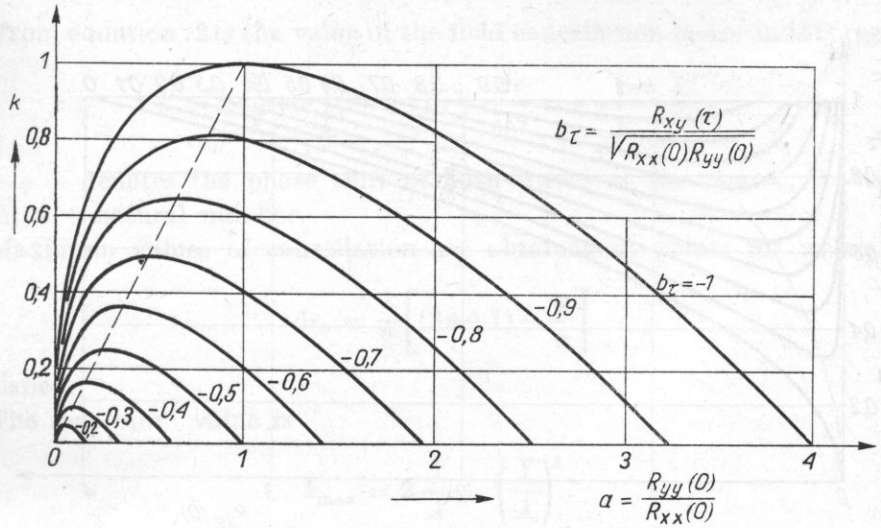

Fig. 3. Dependence of the field cancellation factor k on the power ratio a of both signals for various values of the cross-correlation factor b

Cancellation larger than any k_i is possible for signals for which the power ratio a is within the limits

$$(1-\sqrt{1-k_i})^2 < a < (1+\sqrt{1-k_i})^2, \tag{31}$$

while the modulus of the correlation factor is higher than $|b_\tau|_{\min}$, where

$$|b_\tau|_{\min} = \sqrt{k_i}. \tag{32}$$

The relations (31) and (32) are more apparent in the diagram of the required degree of correlation of the signals versus their power ratio at an assumed field cancellation factor (Fig. 4).

4. Spatial conditions for the existence of phase cancellation for monochromatic (sinusoidal) signals

Let the source S (Fig. 1) emit the wave

$$x(t) = X\sin\omega_1 t, \tag{33}$$

and the source S' the wave

$$y(t) = Y\sin(\omega_2 t+\varphi). \tag{34}$$

Let the difference of the distances from both sources to the reception point A be

$$\Delta r = \tau c, \tag{35}$$

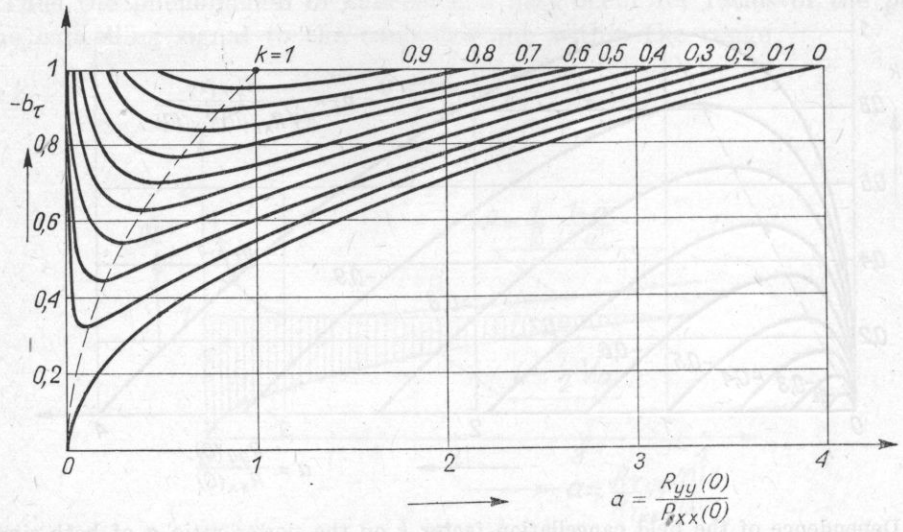

Fig. 4. Dependence of the required correlation factor b_τ on the power ratio a of both signals for an assumed field cancellation factor k

where c is the velocity of sound.

The autocorrelation functions of signals for $\tau = 0$ are:

$$R_{Txx}(0) = \frac{X^2}{2}, \qquad R_{Tyy}(0) = \frac{Y^2}{2}. \tag{36}$$

The cross-correlation function for $\omega_1 \neq \omega_2$ is equal to zero only if T is sufficiently long,

$$R_{Txy}(\tau) = 0, \tag{37}$$

so that stable cancellation cannot occur at the point A.

On the other hand, if frequencies of both signals are identical, i.e. $\omega_1 = \omega_2 = \omega$, then

$$R_{Txy}(\tau) = \frac{XY}{2}\cos(\omega\tau + \varphi), \tag{38}$$

and substituting (36) and (37) in equation (27) and considering (35) we obtain a condition for the range of the differences of distances covered by the wave and thus determine the range of the area of cancellation:

$$\left[(2n+1)\frac{\varphi}{\pi} - \frac{1}{\pi}\operatorname{arc\,cos}\frac{1}{2}\frac{Y}{X}\right]\frac{\lambda}{2}$$

$$< \Delta r < \left[(2n+1)\frac{\varphi}{\pi} + \frac{1}{\pi}\operatorname{arc\,cos}\frac{1}{2}\frac{Y}{X}\right]\frac{\lambda}{2}. \tag{39}$$

From equation (21) the value of the field cancellation factor in this region is

$$k = 2\frac{Y}{X}\cos\left[(2n+1)\pi + \frac{\Delta r}{\lambda/2}\pi + \varphi\right] - \frac{Y^2}{X^2}, \tag{40}$$

where φ — denotes the phase shift of both waves at the source, λ — wavelength, n — natural number.

Maximum values of cancellation are obtained at points for which

$$\Delta r_0 = \frac{\lambda}{2}\left[(2n+1) - \frac{\varphi}{\pi}\right] \tag{41}$$

is satisfied.

The maximum value is

$$k_{\max} = 2\frac{Y}{X} - \left(\frac{Y}{X}\right)^2. \tag{42}$$

This value can be obtained for two ratios of signal amplitudes, namely

$$\frac{Y}{X} = 1 \pm \sqrt{1 - k_{\max}}. \tag{43}$$

The dependence between these amplitude ratios is the following:

$$\left(\frac{Y}{X}\right)_1 \left(\frac{Y}{X}\right)_2 = k_{\max}. \tag{44}$$

Thus cancellation occurs for the amplitude ratios of signals in the interval $0 < Y/X < 2$, while the maximum possible value of cancellation $k_{\max} = 1$ is obtained for $Y/X = 1$.

If in equation (41) it is assumed that the phase shift of signals at the source is equal to zero, then maximum cancellation will occur at such points in space that the difference of distances from the sources is exactly an odd multiple of half wavelengths. In the proximity of these points there will also be cancellation, which will decrease with the cosine of the ratio $\Delta r/\frac{1}{2}\lambda$; symmetrically for distance differences Δr smaller and higher than Δr_0.

The limiting values of the difference Δr_g at which the cancellation finishes is determined by

$$\Delta r_g = \Delta r_0 \pm \frac{\lambda}{2\pi} \operatorname{arc\,cos} \frac{1}{2}\frac{Y}{X}. \tag{45}$$

Hence, it can be concluded that the cancellation region extends for a phase difference $\Delta\psi$ between the signals given by

$$\Delta\psi = 2 \operatorname{arc\,cos} \frac{1}{2}\frac{Y}{X}. \tag{46}$$

The relationships described in equations (42) and (46) are shown in Fig. 5, and that of equation (40) in Fig. 6. From these figures it can be seen that the question as to whether the ratio Y/X is larger or smaller than unity is not trivial. In both cases, the same values of k_{max} can be obtained, but for $Y/X < 1$

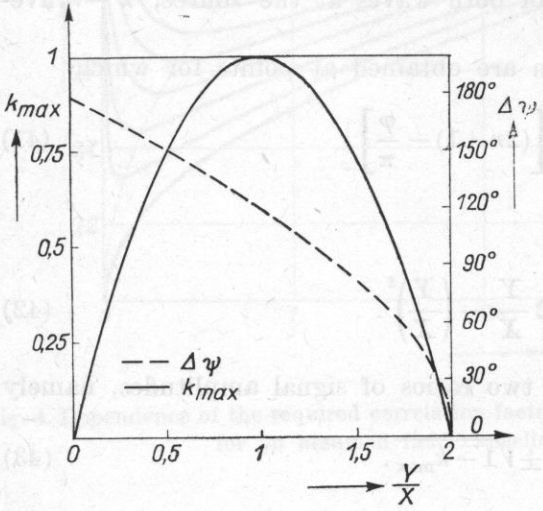

Fig. 5. Dependence of the maximum field cancellation factor k_{max} and the maximum permissible phase difference $\Delta\psi$ between signals on the amplitude ratio of the signals

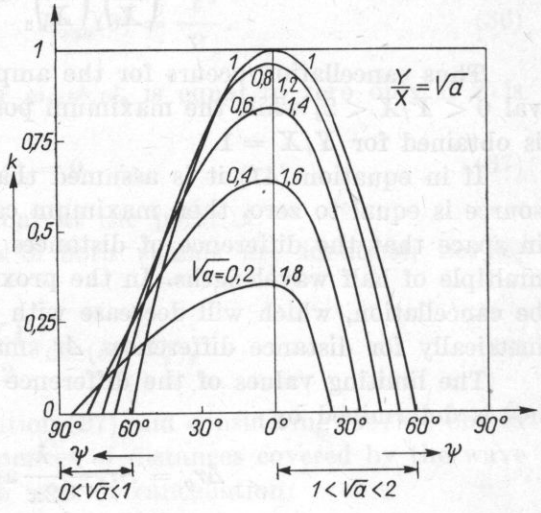

Fig. 6. Dependence of the field cancellation factor k on the phase

$$\psi = (2n+1)\pi + \frac{2\Delta r}{\lambda}\pi + \varphi$$

at various amplitude ratios of the signals

the range of phase difference $\Delta\psi$, at which the cancellation occurs, and hence the range of cancellation, is larger than in the case $Y/X > 1$. Another consequence of equation (45) is that the range of the cancellation region is proportional to the wavelength, and thus higher for lower frequencies.

5. Phase cancellation of periodic signals

Let the sources S and S' (Fig. 1) emit suitable periodic signals of the forms

$$x(t) = \sum_n^\infty X_n \sin(n\omega t), \tag{47}$$

$$y(t) = \sum_n^\infty Y_n \sin(n\omega t + \varphi_n). \tag{48}$$

We shall limit ourselves to signals of the same fundamental and harmonic frequencies, since in the case of different frequencies the cross-correlation factor is equal to zero and it is not possible to achieve stable cancellation.

The correlation functions of singals (47) and (48) for a point whose distances from the sources differ by $\Delta r = c\tau$ are

$$R_{Txx}(0) = \sum_n^\infty \frac{X_n^2}{2}, \quad R_{Tyy}(0) = \sum_n^\infty \frac{Y_n^2}{2}, \tag{49}$$

$$R_{Txy}(\tau) = \sum_n^\infty \frac{X_n Y_n}{2} \cos(n\omega\tau + \varphi_n). \tag{50}$$

A general analysis for any values of Y_n and X_n is too complicated and we will consider the simple case $X_n = Y_n$.

Substitution of functions (49) and (50) in equation (27) gives

$$\tfrac{1}{2} \sum_n^\infty X_n^2 < \sum_n^\infty X_n^2 \cos[(2m+1)]\pi + n\omega\tau + \varphi_n] \leqslant \sum_n^\infty X_n^2, \tag{51}$$

where $m = 0,1, \ldots$

The right-hand side of (51) determines complete cancellation. It occurs if

$$(2m+1)\pi + n\omega\tau + \varphi_n = 0, \tag{52}$$

i.e. if the phases φ_n are such that, for all n,

$$\varphi_n = \pi\left(2m+1-2n\frac{\tau}{T}\right) \tag{53}$$

is satisfied, where T denotes the period of the periodic signal. Let us assume that both sources emit the same signals, i.e. $\varphi_n = 0$ for all n.

To bring about a complete cancellation, all the cosines must be equal to unity, thus we obtain the condition

$$\tau = \frac{(2m+1)\pi}{2n\pi f} = \frac{\Delta r}{\lambda f}, \tag{54}$$

and hence

$$\Delta r = \frac{\lambda}{2}\frac{2m+1}{n}, \tag{55}$$

where λ is the wavelenght of the periodic signal, n – the n-th component, m – the m-th multiple of the half wavelength.

Equation (55) must be satisfied for all components, i.e.

$$\Delta r_k = \Delta r_l, \tag{56}$$

where k, l denote any two components of the periodic signal. Substituting in (55), we have

$$\frac{2m_k+1}{k} = \frac{2m_l+1}{l}, \tag{57}$$

so that

$$m_k = \frac{k}{l}m_l + \frac{k-l}{2l}. \tag{58}$$

In order to satisfy this equality, m_k should be integral for all m_l. This is the case if, assuming $k > l$,

$$\frac{k-l}{2l} = \text{integer}. \tag{59}$$

In this case the ratio k/l is also an integer, and equation (58) will be valid when this is an odd number.

From this discussion it can be concluded that complete cancellation of periodic signals is possible only for signals with only odd harmonics.

Periodic signals with only odd harmonics possess half-wave symmetry, i.e.

$$y(\theta+\pi) = -y(\theta). \tag{60}$$

This means that the part of the wave in the interval $(\pi, 2\pi)$, after being rotated about the θ axis and shifted by π, coincides exactly with that part of the wave in the interval $(0, \pi)$ (Fig. 7). Thus at points which the waves from

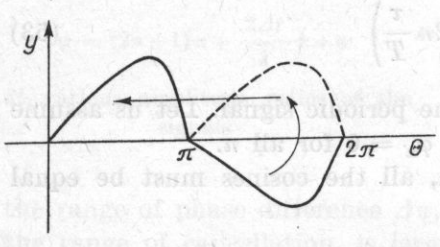

Fig. 7. A signal $y(\theta)$ exhibiting half-wave symmetry

the sources reach with a time difference $\tau = T/2$, the element of the medium is acted upon by equal and opposite forces which are completely balanced.

6. Phase cancellation for other classes of signals

Other signals do not all exhibit a natural half-wave symmetry, and for this reason it is not possible to achieve complete cancellation with them.

However, any signal (e.g. noise) may be taken, reversed artificially, and superimposed on the original signal. If the primary signal is $x(t)$, then the reversed and delayed signal is $y(t+\tau) = -x(t)$, and the cross-correlation function of these signals will be

$$R_{Txy}(\tau) = \frac{1}{T}\int_0^T x(t)\,y(t+\tau)\,dt$$

$$= \frac{1}{T}\int_0^T x(t)[-x(t)]\,dt = -R_{Txx}(0) = -R_{Tyy}(0). \qquad (61)$$

When substituting from equation (61) into equation (27), one can see that the condition for the complete cancellation is satisfied. Thus, a signal having no symmetry whatsoever can be completely cancelled by the use of its artificial reverse with respect to phase. This operation gives any signal half-wave symmetry with regard to the primary signal, since the relation between the secondary and primary signals is the following:

$$y(t+\tau) = -y(t) \qquad (62)$$

(cf. equation (60)).

It would appear advisable to classify cancellation into natural and forced, especially in view of the fact that the phenomenon of natural cancellation is observed without performing any operations on the signal. The possibility of this phenomenon occurring results from the characteristics of the signal itself, namely its half-wave symmetry. Such cancellation can therefore occur only for classes of signals which have a natural halfwave symmetry. They include monochromatic and periodic signals with only odd harmonics. All other signals can, however, be cancelled by performing on them a phase reversal operation, but because of this operation, cancellation obtained in this way will be defined as *forced cancellation.*

7. Dependence of the range of the cancellation region on the signal power density spectrum

In section 4 it has been shown that the range of the cancellation region for monochromatic signals is inversely proportional to their frequency.

Let us now consider how the range of the cancellation region depends on the power density spectrum of any signal. In the case of the superposition of two identical signals only reversed in phase and shifted by τ_A, the cross-

correlation function of both signals will be a mirror reflection of the autocorrelation function a_τ of primary signal shifted by τ_A relative to the τ axis. Since — as a result of the uncertainty relation [7] — the width of the autocorrelation function is inversely proportional to the upper frequency limit of the signal,

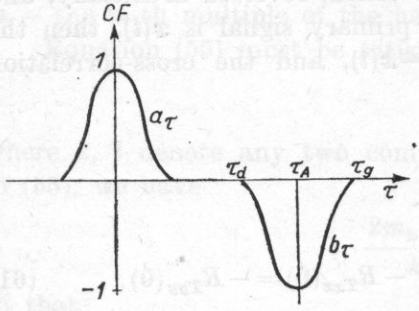

Fig. 8. a_τ — autocorrelation function of the primary signal, b_τ — cross-correlation of the primary signal with the primary signal inversed in phase and shifted by τ_A

the width of the correlation function will also be inversely proportional to this frequency in agreement with the formula

$$\tau_g - \tau_d = \frac{C}{f_g}, \tag{63}$$

where C is a constant.

Since the width of the interval $\tau_g - \tau_d$, in which the cross-correlation function assumes negative values, is decisive for the range of the cancellation region, signals whose power density spectra are shifted in the direction of low frequencies will produce larger cancellation regions.

8. Dependence of the range of the cancellation region on the source spacing

The time delay τ_A of the signals reaching point A depends on the distance d between the sources and on the position of point A relative to both sources (Fig. 9).

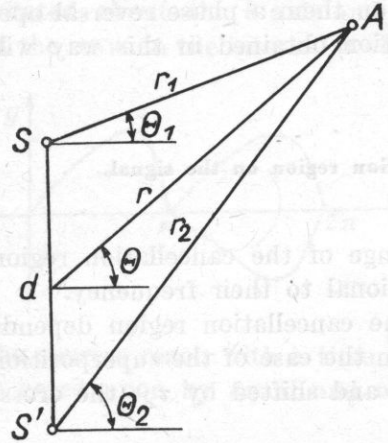

Fig. 9. The mutual spacing of the sources and of the receiving point A in a polar system

The smaller the distance d, the smaller the time delay τ_A will be and the cross-correlation curve in Fig. 8 will be shifted towards zero. If the distance d is reduced so that, for given signal, τ_d becomes negative (passes through point $\tau = 0$), the cancellation region will start from the sources themselves.

We shall now investigate the condition which the distance d between sources should satisfy to obtain cancellation throughout the whole region.

The condition for cancellation throughout the whole region is that the cross-correlation factor should be negative at every point of the region.

Such a condition is satisfied if

$$\Delta r = r_2 - r_1 = c\tau \leqslant c\tau_g \tag{64}$$

for all r_1 and r_2, where

$$r_1 = \sqrt{r^2 + \frac{d^2}{4} - rd\sin\theta}, \tag{65}$$

$$r_2 = \sqrt{r^2 + \frac{d^2}{4} + rd\sin\theta}. \tag{66}$$

Substituting (65) and (66) in to (64) we obtain the following condition for the distance d:

$$d \leqslant c\tau_g \sqrt{\frac{4r^2 - c^2\tau_g^2}{4r^2\sin^2\theta - c^2\tau_g^2}} = B. \tag{67}$$

If the cancellation is to extend to infinity, the condition

$$d \leqslant \lim_{r\to\infty} B = \frac{c\tau_g}{\sin\theta} \tag{68}$$

must also be satisfied.

If condition (68) is met, the cancellation region will extend to infinity but only within an angle $\pm\theta$. To obtain cancellation throughout the whole region, condition (68) is further limited to

$$d \leqslant c\tau_g. \tag{69}$$

Considering (63) and assuming $\tau_d = 0$ (the condition of cancellation from the sources themselves) we finally obtain

$$d \leqslant C\frac{c}{f_g}. \tag{70}$$

Thus, the higher the upper frequency limit of a signal, the closer the sources must be placed to obtain cancellation throughout the whole region.

For white noise $f_g \to \infty$ while $d \to 0$, thus the primary and secondary sources should be placed at the same point.

9. Conclusions

The investigations carried out lead to the following conclusions:

1. To obtain field cancellation at a point, a suitable value of the coefficient a, the ratio of the cancelling signal power to the cancelled one, is necessary, as it is also for such a correlation of the signals that phase condition (22) (a negative cross-correlation factor for the signals) as well as amplitude condition (27) (that the modulus of the cross-correlation factor should be higher than half square root of the ratio of the cancelling signal power to the cancelled signal power) should be met.

2. Complete cancellation occurs only if signals are entirely correlated, directed in opposition (correlation factor equal to -1), and have equal powers. This means that they are the same signals but reversed in phase.

3. The maximum feasible field cancellation factor is equal to the square of the modulus of the cross-correlation factor of the component signals. It is obtained at a precisely defined ratio of the powers of these signals which is also equal to the square of the modulus of cross-correlation factor. This implies that the maximum degree of field cancellation is obtained when the power of the cancelling signal is smaller than or equal to the power of the cancelled signal.

4. The maximum range of changes of the ratio a of the cancelling signal power to the cancelled signal power, at which cancellation can be obtained, is $0 < a < 4$. As the power ratio tends to the limit values, the degree of cancellation decreases. If the degree of cancellation is to be higher than a given value k_i, then the range of required power ratio of the signals is diminished to

$$(1-\sqrt{1-k_i})^2 < a < (1+\sqrt{1-k_i})^2.$$

5. The value of modulus of the cross-correlation factor necessary to obtain the required degree of field cancellation depends on the ratio of powers of the component signals. It is least for the condition $a = k_i$, i.e. when the power of the cancelling signal is smaller than or equal to the power of the cancelled signal.

6. The range of the cancellation regions in the case of monochromatic signals is inversely proportional to their frequency, while in the case of composite signals it is inversely proportional to their upper frequency limit.

7. To obtain complete cancellation in a certain region, the cancelled and cancelling waves should propagate along parallel tracks. This ensures the conservation of constant phase and amplitude ratios within this region throughout the whole process of cancellation. This condition determines the location of source of the cancelling signal relative to the cancelled one and relative to the region in which the primary signal is to be cancelled.

8. It appears constructive to distinguish between natural and forced cancellation. Natural cancellation occurs because of the superpositions of various phases of the same signal. It is possible only for signals having half-wave symmetry, i.e. for monochromatic and periodic signals of only odd harmonic components. Forced cancellation can involve all classes of signals. For this purpose it is necessary to use a special device for the phase inversion and time delay of a given signal.

9. An interesting class of signals classified under natural cancellation are monochromatic signals. The cancellation regions of these signals are concentrated around points whose distances from the sources differ by an odd number of half wavelengths. At these points the degree of cancellation assumes a maximum value and it gradually decreases when moving away from them. Cancellation is possible for ratios of the signal amplitudes within the limits $0 < Y/X < 2$, the closer this ratio is to unity, the closer to unity the field cancellation factor becomes.

The same degree of cancellation can be obtained for two ratios of the signal amplitudes Y/X – one smaller and one larger than unity. However, this ratio has some effect on the range of the cancellation region. If $Y/X < 1$, the range of the differences of the component signal phases at which the cancellation occurs is higher, and this results in a larger value of the range of the cancellation region.

References

[1] H. F. Olson, M. E. May, *Electronic sound absorbers*, JASA, **25**, 6, 1130-6 (1953).

[2] S. Czarnecki, *Investigations of the sound transmission properties of a medium resulting from sound wave compensation caused by other sources*, JSVib, **11**, 2, 225-233 (1970).

[3] O. Bschorr, *Lärmauslöschung durch gesteuerte Interferenz*, 7 ICA, Budapest 1971, Rep. 21N8.

[4] B. D. Tartakovsky, *Systems of active compensation of sound field for bounded structures*, 7ICA, Budapest 1971, Rep. 21V1.

[5] M. J. M. Jessel, G. A. Mangiante, *Active sound absorbers in an air duct*, JSVib, **23**, 3, 383-390 (1972).

[6] J. S. Bendat, A. G. Piersol, *Measurement and analysis of random data*, John Wiley Sons, Inc. New York 1966, p. 1-35.

[7] R. Bracewell, *Fourier transformation and its applications*, WNT, Warszawa 1968, p. 153-194 (in Polish).

Received on 9th December 1975

ARCHIVES OF ACOUSTICS
1, 2, 127-136 (1976)

PSYCHOACOUSTICAL EQUIVALENTS OF TUNING CURVES AS DETERMINED BY THE POST-STIMULATORY MASKING TECHNIQUE

ANTONI JAROSZEWSKI, ANDRZEJ RAKOWSKI

Laboratory of Musical Acoustics, Academy of Music (Warszawa)

The method and results of measurements of psychoacoustical tuning curevs covering about 6500 individual judgements are described. Three experienced music students served as subjects in the experiment. The slopes of tuning curves obtained reach 1040 to 2200 dB/oct at the characteristic frequency 1 kHz. With reference to KIANG's [7], TONNDORF's [16] and MØLLER's [10] data the importance of functions of the cochlear nucleus or the higher neurons in the perception of pitch is discussed.

1. Introduction

Since KIANG's [7] investigation of the 8th nerve bioelectrical activity which resulted in the so-called «tuning curves» determining the frequency resolving power of an ear, much effort has been spent on attempts to find their hydromechanical or psychoacoustical equivalents.

These attempts have been largely induced by a significant disproportion between the well accepted and widely published data pertaining to the excitation patterns of the basilar membrane, obtained from the direct visual examination [1, 2] or inferred from the direct masking patterns [20], and the results of investigation of bioelectrical activity or of the difference limen for frequency [11, 12].

The slopes of the basilar membrane excitation patterns, obtained by BÉKÉSY from direct observation, were small: about 20 dB/oct above the frequency of excitation and about 6 dB/oct below this frequency.

To achieve vibration amplitudes of the basilar membrane sufficiently large for direct observation with the use of an optical microscope, the sound pressure levels of about 140 dB were used in this experiment. Such pressure levels could have resulted in substantial nonlinearities.

RHODE [14] using the Mössbauer technique obtained, at 7 kHz, slopes of about 100 dB/oct and 24 dB/oct, respectively, above and below the point of maximum excitation. RHODE used Squirrel Monkeys in his experiment.

KOHLLÖFFEL's [8] investigation using laser light on Guinea Pig post-mortem samples, at the same frequency of excitation, gave slopes of about

56 dB/oct and 10 dB/oct respectively. In living animals, at 28 kHz and at a sound pressure level of about 100 dB, he was able to find slopes of 100 to 130 dB/oct above and 7 to 9 dB/oct below the point of maximum excitation.

The slopes of *tuning curves*[1]) determined by KIANG as calculated by WILSON [19] for the region above *CF* reach 200 dB/oct. WILSON also cited EVANS [3] unpublished data which show slopes reaching 200 to 500 dB/oct.

Psychoacoustical equivalents of tuning curves as determined by HOUTGAST [4] using the pulsation-threshold method, do not show the slopes to be substantially higher than 200 dB/oct above the *CF*. The slopes of psychoacoustical tuning curves determined by ZWICKER [21] using the direct masking-method and threshold tracking with Békésy's automatic audiometer, reach about 150 to 200 dB/oct for $CF = 2$ kHz. ZWICKER's data are thus comparable with those of HOUTGAST [4]. Significantly higher slopes, up to about 950 dB/oct in the range above *CF* 2 kHz and 560 dB/oct above *CF* 1 kHz have been found by VOGTEN [18] who used the poststimulatory masking method of measurement.

In the present report the results of a psychoacoustical investigation of tuning curves are presented. The experiments were run using the poststimulatory masking technique similar to that used by VOGTEN [18], but with a slightly different construction of the time paradigms of signals used. This research has been induced by the promising data, obtained in the earlier experiments pertaining to pitch shifts in the poststimulatory masking [5, 13], which indicated the existence of quite substantial values for the slopes of psycho-acoustical tuning curves at $CF = 1$ kHz, even greater than those determined by VOGTEN [18] for $CF = 2$ kHz.

2. Procedure

The attempt of this experiment was to determine the poststimulatory masking curves for short (50 ms) 1 kHz tone pulses at a 15 dB sensation level L_m masked by comparatively long tone pulses at sensation levels $L_M + L_m$ and frequencies in the vicinity of the maskee frequency. A two-alternative-forced-choice procedure was used. The stimuli were presented to the listeners according to the time paradigm given in Fig. 1. The maskee was present in the paradigm only in 50% of successive presentations and was switched in and out noiselessly in a semi-random manner.

After each presentation a listener signalled with a push-button whether he had detected the maskee in the presented paradigm, or not.

---

[1]) The term *tuning curves* refers to the dependence of the intensity of exciting tone pulses on the tone frequency, with the assumption that the nerve fibre which is in contact with the microelectrode reacts to each of the pulses with the same number of spikes. The frequency at which maximum sensitivity is observed has been called the *characteristic frequency* or *CF*.

All listeners in all sessions passed a routine 5 min. screening test before they were allowed to the experimental runs which consisted of 18 successive series lasting 2 min. each with 5 min. intervals every 6 series.

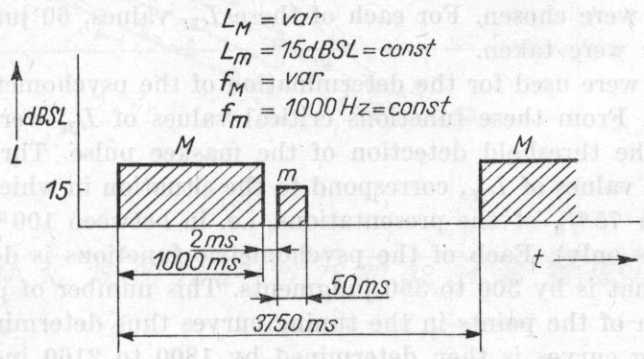

Fig. 1. Time paradigm of the stimuli used in the determination of psycho-acoustical tuning curves

The research was carried out using a three-channel analogue modulator controlled by a programmable time counter [6]. Sine signals stable to 10^{-4} per day were fed to the inputs of the modulator. The frequencies of these signals were measured with an electronic counter with an accuracy of 10^{-4}.

These sequences of stimuli, defined in the time domain to an accuracy of $\pm$ 1 ms, were presented in an anechoic chamber using a QUAD electrostatic loudspeaker and power amplifier.

In a pilot study a modification of procedure in this experiment was introduced, namely two function modules were added to the analogue modulator, to shape the initial and final transients of tone pulses. These were a linear slope function module for the masker and a Gaussian function module for the maskee. The slopes of the psycho-acoustical tuning curves obtained in these pilot measurements were comparable to those reported by VOGTEN [18].

In the final version of the experimental set-up both function modules were eliminated (switched out). To reduce to some extent the spectrum width of the signals processed, *LP* filters with cut-off frequencies of 1.25 kHz and slopes of about 300 dB/oct were used at the outputs of the analogue modulator.

Three listeners served as subjects in the experiment; two music students aged 22 and 24 with audiologically normal ears, and one listener without musical education aged 44, with a unilateral selective permanent hearing loss of about 40 dB at 4 kHz, i.e. outside the frequency region investigated.

All listeners had great experience in the psycho-acoustical measurements. One music student has been selected from a large group of candidates as highest scoring in the *DL* for frequency test.

3. Results

For each of the six masker frequencies applied in the experiment (f_M = 980, 990, 995, 1005, 1010, 1020 Hz), five or six appropriate values of masker sensation level L_M were chosen. For each of these L_M values, 60 judgments from a single listener were taken.

These data were used for the determination of the psychometric functions given in Fig. 2. From these functions critical values of L_M were found, corresponding to the threshold detection of the maskee pulse. Threshold detection, i.e. critical values of L_M, correspond to the situation in which the maskee was detected in 75% of the presentations, i.e. in between 100% (no errors) and 50% (guess only). Each of the psychometric functions is determined by 5 to 6 points, that is by 300 to 360 judgments. This number of judgments refers also to each of the points in the tuning curves thus determined. Each of the three tuning curves is then determined by 1800 to 2160 judgments.

L_M values corresponding to the threshold detection of the maskee pulses are presented in Fig. 3 for each of the listeners separately. The horizontal axis refers to the masker frequency f_M. This pattern of presentation was first proposed by SMALL [15], and then used by ZWICKER [21] for direct masking data under the name *psychoacoustical tuning curves.*

4. Discussion

In the psycho-acoustical tuning curves presented in Fig. 3, the top parts, i.e. parts adjoining the frequency of the maskee (1 kHz) are missing. In that region the measurements are particularly difficult. However, the portions of the tuning curves determined are sufficient to make some observations pertaining to the selectivity of the respective influence of the stimuli in the poststimulatory masking near the threshold level (15 dB *SL*).

A particularly significant factor in tuning curves, which makes comparison with data from other authors possible, is the slope or steepness of the curves in the proximity of the maskee frequency. Numerical values of the slopes obtained in this experiment are given in Table 1.

At frequencies, in the range from 5 to 10 Hz above the maskee frequency, the steepness of tuning curves is comparable for all listeners and amounts to between 1 and 2 dB for 1 Hz frequency deviation.

A frequency change of 0,5 Hz, which for very low sensation levels is equal to the difference limen for frequency [12], leads to a change of the masker level by 0.5 to 1 dB, i.e. a change corresponding to the value of the difference limen for loudness. This convergence does not seem to be just accidental and it can possibly support the hypothesis of MAIWALD [9]. Accordng to MAIWALD, the detection of both amplitude and frequency changes within the organ of Corti can be assigned to the same and only receptors which are sensitive

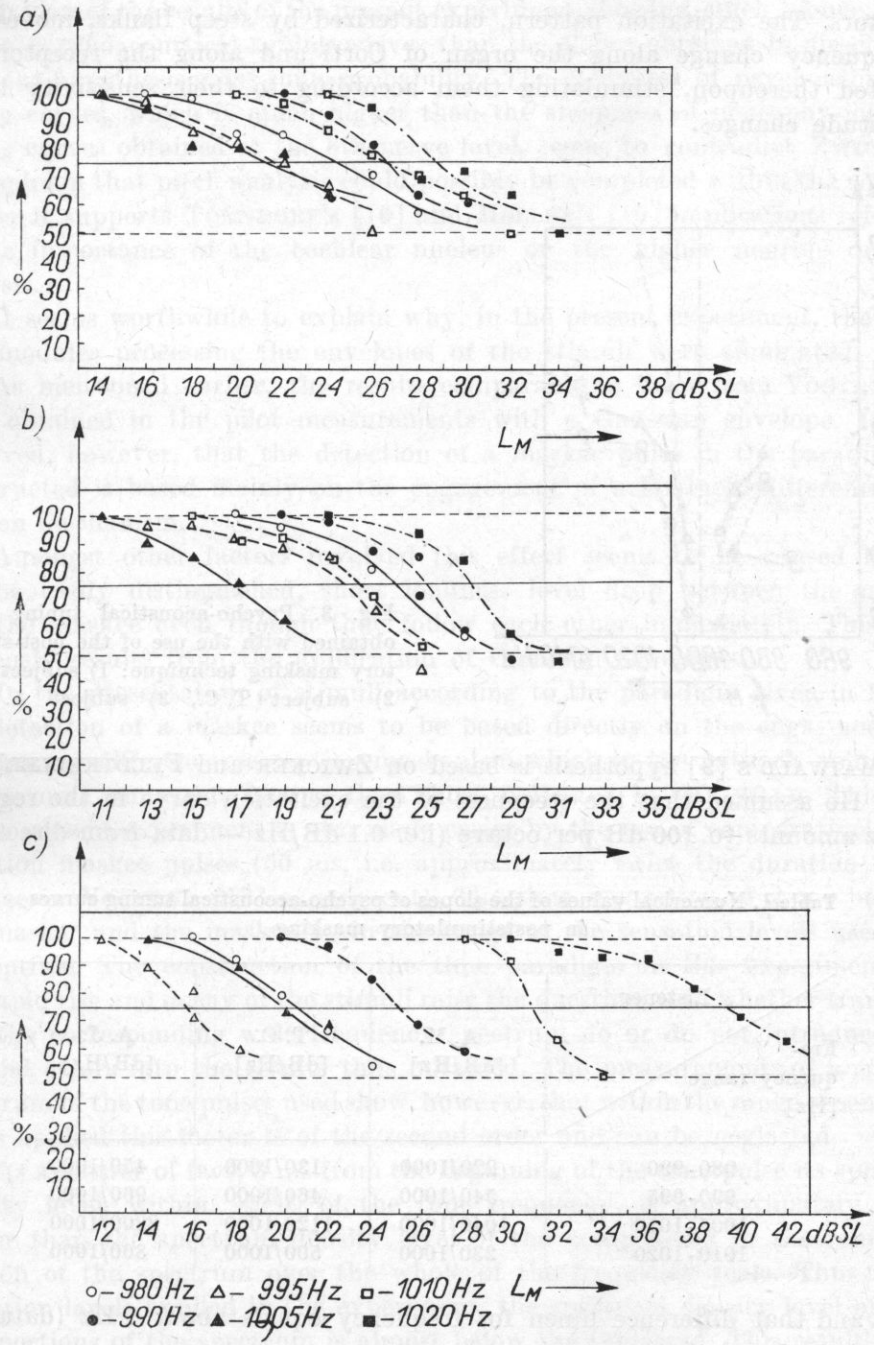

Fig. 2. Percentage of correct responses vs. masking signal level: a) subject A. M., b) subject T. C., c) subject A. J.

to the amplitude variations and operate on the principle of frequency discriminators. The excitation pattern, characterized by steep flanks, moves with a frequency change along the organ of Corti and along the receptors distributed thereupon, stimulating them according to their sensitivity to the amplitude changes.

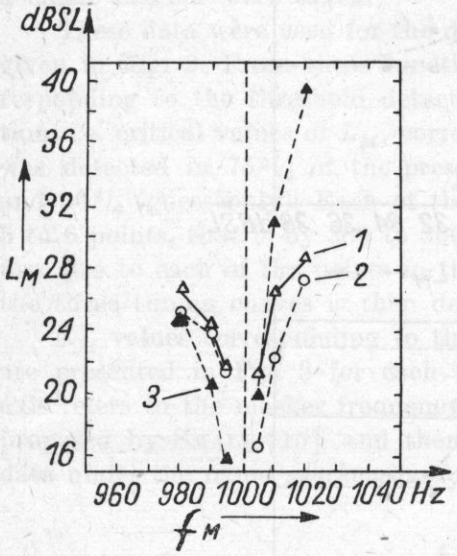

Fig. 3. Psycho-acoustical tuning curves obtained with the use of the post-stimulatory masking technique: 1) subject A. M., 2) subject T. C., 3) subject A. J.

MAIWALD'S [9] hypothesis is based on ZWICKER and FELDTKELLER'S [20] data. He assumed that the steepness of the excitation curve in the region of 1 kHz amounts to 100 dB per octave (i.e. 0.1 dB/Hz — data from direct masking) and that difference limen for frequency equals about 7 Hz (data from frequency modulation measurements).

Table 1. Numerical values of the slopes of psycho-accoustical tuning curves in poststimulatory masking

Frequency range [Hz] \ Listener	A. M. [dB/Hz]	T. C. [dB/Hz]	A. J. [dB/Hz]
980-990	220/1000	130/1000	450/1000
990-995	540/1000	460/1000	960/1000
1005-1010	1040/1000	1120/1000	2200/1000
1010-1020	230/1000	500/1000	860/1000

With the new experimental data showing that ZWICKER and FELDTKELLER'S *DL* for frequency is at least an order of magnitude higher than the

actual differential pitch threshold, MAIWALD'S hypothesis could not be accepted.

In view of the results of the present experiment showing much higher slopes of the psychoacoustical tuning curves than the slopes obtained in direct masking, the hypothesis gains some probability. The steepness of psychoacoustical tuning curves, which is much higher than the steepness of neurophysiological tuning curves obtained at the 8th nerve level, seems to contradict ZWICKER'S [21] opinion that pitch analysis could possibly be completed within the cochlea. Rather it supports TONNDORF'S [16] and MØLLER'S [10] implications referring to the importance of the cochlear nucleus or the higher neurons in this analysis.

It seems worthwhile to explain why, in the present experiment, the function modules processing the envelopes of the stimuli were eliminated.

As mentioned earlier, the results comparable to those from VOGTEN [18] were obtained in the pilot measurements with a Gaussian envelope. It was observed, however, that the detection of a maskee pulse in the paradigm so constructed is based mainly on the engagement of a loudness difference perception mechanism.

Amongst other factors involved this effect seems to be caused largely by the easily distinguished, short loudness level drop between the masker and the maskee even though they follow each other immediately. This drop obviously results from the application of Gaussian envelopes.

In the presentation of stimuli according to the paradigm given in Fig. 1, the detection of a maskee seems to be based directly on the engagement of a frequency difference perception mechanism which in the author's opinion involves more numerous factors than those indicated by MAIWALD. This task in the present experiment is also made easier by the use of comparatively long duration maskee pulses (50 ms, i.e. approximately twice the duration of the maskee in VOGTEN'S [18] experiment). The time separation of 2 ms between the masker and the maskee is, in the range of the sensation levels used, imperceptible. The construction of the time paradigm in this experiment and the rapid rise and decay of the stimuli raise the question as to whether transients and the corresponding wide frequency spectrum do or do not introduce substantial errors into the results thus obtained. The measurements of a running spectrum of the tone pulses used show, however, that within the range of sensation levels applied this factor is of the second order and can be neglected.

As a matter of fact, 3 ms from the beginning of the tone pulse its spectrum density level, within $\pm 5\%$ of the tone frequency, is approximately 20 dB higher than the spectrum density level of the components in the remaining portion of the spectrum over the whole of the frequency scale. Thus at the sensation levels applied in the experiment, the spectrum density level of these side portions of the spectrum is almost below the threshold. This results in an almost undisturbed perception of those portions of the stimuli which determine their pitch.

The value of the information contained in this report is partly limited by the fact that stimuli were presented in succession and at low sensation levels only.

However, the data obtained here, together with those of VOGTEN, show that the selectivity of hearing organ as determined by the present psychoacoustical methods (poststimulatory masking) exceeds markedly the selectivity revealed in neurophysiological experiments. It may look astonishing and the more so that some ten years ago the relation between the results of psychoacoustic experiments (simultaneous masking) and neurophysiological findings was exactly opposite.

References

[1] G. VON BÉKÉSY, *Über die Schwingungen der Schenckentrennwand beim Preparat und Ohrenmodell*, Acust. Z., 7, 173-186 (1942).

[2] G. VON BÉKÉSY, *Über die Resonanzkurve und die Abklinkzeit der verschiedenen Stellen der Schneckentrennwand*, Acust. Z., 8, 66 (1943).

[3] E. F. EVANS, Unpublished data, Dept. of Communication, University of Keele, Keele, Staffordshire, England.

[4] T. HOUTGAST, *Lateral Suppression in Hearing*, Institute for Preception TNO, Ed., Soesterberg, the Netherlands (1974).

[5] A. JAROSZEWSKI, A. RAKOWSKI, *Pitch shifts in poststimulatory masking*, Acustica, 34, 220-223 (1976).

[6] A. JAROSZEWSKI, A. RAKOWSKI, *Analogue modulator for psycho-acoustical pulse measurements*, Arch. of Acoustics **1**, 1, 25-31 (1976).

[7] N. Y. S. KIANG, T. WATANABE, E. C. THOMAS, L. F. CLARK, *Discharge patterns of single fibres in the cat's auditory* nerve, Res. Mon. No 35, M. I. T. Press, Cambridge, Mass. (1965).

[8] L. U. E. KOHLLÖFFEL, *A study of basilar membrane vibrations II and III*, Acustica, 27, 66-89 (1972).

[9] D. MAIWALD, *Ein Funktionsschema des Gehörs zur Beschreibung der Erkennbarkeit kleiner Frequenz und Amplitudenänderungen*, Acustica, 18, 81-92 (1967).

[10] A. R. MØLLER, *Coding of sounds in lower levels of auditory system*, Quart. Rev Biophys., 5, 59-155 (1972).

[11] J. O. NORDMARK, *Mechanisms of frequency discrimination*, JASA, 44, 1533-1540 (1968).

[12] A. RAKOWSKI, *Pitch discrimination at the threshold of hearing*, 7-ICA, Budapest, pap. 20 H6 (1971).

[13] A. RAKOWSKI, A. JAROSZEWSKI, *On some secondary masking effects*, Acustica, 31, 325-329 (1974).

[14] W. S. RHODE, *Observations of the vibration of the basilar membrane in squirrel monkeys using the Mössbauer technique*, JASA, 49, 1218-1231 (1971).

[15] A. M. SMALL, Jr., *Pure-tone masking*, JASA, **31**, 1619-1625 (1959).

[16] J. TONNDORF, *Cochlear mechanics and hydro-dynamics*, in *Foundations of modern auditory theory*, Tob as, J. V., Ed., Academic Press, New York-London, p. 232 (1970).

[17] J. VERSCHUURE, A. A. VAN MEETEREN, *The effect of intensity on pitch*, Acustica, 32, 33-34 (1975).

[18] L. L. M. VOGTEN, *Low-level pure tone masking and two-tone suppression*, IPO Annual Progress Report, No 9, Den Dolech 2, Eindhoven, Holland 1974.

[19] O. WILSON, *Discussion to B. M. Johnstone, K. Taylor, Mechanical aspects of cochlear function in frequency analysis and periodicity detection in hearing*, Plomp R., Smoorenburg G. F., Ed., Sijthoff, Leiden, A. W., § 970.

[20] E. ZWICKER, R. FELDTKELLER, *Das Ohr als Nachrichtenpfänger*, S. Hirzel Verlag, Stuttgart 1967.

[21] E. ZWICKER, *On a psycho-acoustical equivalent of tuning curves*, in *Facts and models in hearing*, E. ZWICKER, E. TERHARDT, Eds., Springer Verlag, 1974.

Received on 25th September 1975

ARCHIVES OF ACOUSTICS
1, 2, 137-158 (1976)

ACOUSTICAL MODELLING OF CLEFT PALATE

JANUSZ KACPROWSKI, WŁADYSŁAW MIKIEL,
ALICJA SZEWCZYK*

Institute of Fundamental Technological Research
Polish Academy of Sciences (Warszawa)

The subject of the present paper is the theoretical analysis of the influence of cleft palate upon the transmission characteristics of the vocal tract in glottal excitation. Starting with a simplified anatomical model of the human vocal system and using the graphical analysis method, we determined the pole-zero distribution of the transfer function $K(\omega)$ which describes the formant-antiformant structure of oral vowels nasalized due to the shunting effect of the nasal channel. The experimental investigations, performed with a specially designed and constructed acoustic analogue model of the speech organ in 5 : 1 dimension scale and, consequently, in 1 : 5 frequency scale, confirmed the validity of the assumptions and the results of the theoretical analysis. It was proved that the spectral analysis of oral vowels, in pathological and post-operative states of cleft palate, affords information which specifies the changes of the acoustic structure of the speech organ due to anatomical disorders. This information offers new facilities in objective phoniatric diagnostics as well as in the control of the process of medical rehabilitation in cleft palate cases, by means of acoustical methods based on the spectral analysis of the speech signal.

1. Introduction

The cleft palate (med.: *palatoschisis*) is a frequently-occurring developmental defect of the human respiratory and articulatory system which causes considerable speech disorders. The laryngological treatment consists in complicated and multistage surgical interventions, usually complemented by a long-term rehabilitation procedure. In view of the rather frequent occurrence of this defect, which averages — depending on demographic conditions — one case for several hundreds to one thousand of births, the treatment of cleft palate is a serious medical problem of considerable social as well as scientific importance. At present it constitutes one of the fundamental research trends, in jawbone and plastic surgery and in modern phoniatry.

From the physiological point of view the cleft palate consists of a discontinuity of tissue taking the form of a split in the palatal bone (med.: *os palatinum*) of the hard palate (med.: *palatum*) which separates the mouth cavity

*) At present: Central Clinical Hospital of the Medical Academy in Warszawa, Phoniatric Centre.

from the nasal one. In other cases it consists in the restraint of the motive functions or even in the atrophy of the soft palate (med: *velum*) which acts as a valve controlling the degree of coupling between the mouth cavity and the nasal cavity in the vocal system [1]. In any case, the direct effect of these pathological disorders is an anomaly in the proper cooperation of the mouth channel and the nasal channel due to the permanent and uncontrolled acoustic coupling between them, which in turn causes the forced nasalization of the originally non-nasalized speech sounds and thus distorts the correct articulation.

Since any change in the anatomical structure of the vocal tract due to cleft palate results in a measurable variation of the acoustic transmittance, which determines the pole-zero distribution of the transfer function $K(\omega)$, one may presume that the spectral analysis of the speech sounds in pathological and postoperative cases should yield essential information which could be used in objective evaluation of the actual state of cleft palate or in objective control of the rehabilitation process.

Acoustic methods of spectral analysis have recently been applied with success in clinical practice to the phoniatric diagnosis of cleft palate [8]. The subject of the present work is the theoretical analysis of the influence of the anatomical defect existing in the soft palate (med.: *palatischisis molle*) upon the transmission characteristics of the vocal tract which determine the formant structure of the speech sounds with glottal excitation, particularly oral vowels. The theoretical analysis is followed by the experimental verification of the results by means of model investigations. Finally, some conclusions are formulated which provide a method of diagnosis based upon the phonospectroscopic analysis of the speech signal segments corresponding to oral vowels nasalized due to a cleft palate.

2. Theoretical analysis

Figure 1 represents the simplified acoustic model of the human vocal system in glottal excitation and its impedance-type analogous circuit. The simplification introduced for the anatomical structure of the articulatory effectors consists of representing the pharynx cavity $P(l_p, S_p)$, the mouth cavity M (l_m, S_m) and the nasal cavity $N(l_n, S_n)$, each as a cylindrical tube of length l and constant cross-sectional area S. The system as a whole is excited by the larynx tone generator of internal impedance Z_g, producing a particle velocity v_g. The resulting particle velocity $v(0)$ of the sound wave at the observation point 0, situated at a distance d from the common plane of the mouth and noise outlets, which have radiation impedances equal to Z_{rm} and Z_{rn}, respectively, may be generally expressed in the form of the vector sum (1). Notice that the phase shifts are disregarded in view of the geometric symmetry of the radiating system, hence

$$v(0) = F_{m0}(f)\vec{v}_m + F_{n0}(f)\vec{v}_n, \tag{1}$$

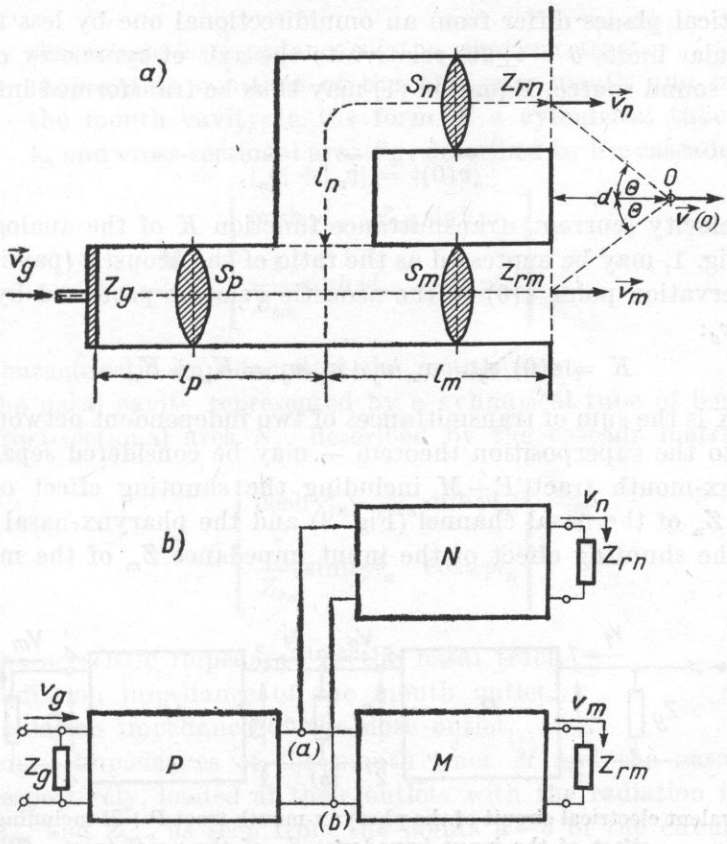

Fig. 1. Simplified acoustic model of the speech organ in glottal excitation (a) and its equivalent electrical circuit (b)

where $\vec{v}_m$ and $\vec{v}_n$ denote acoustic particle velocities of the sound waves radiated by the mouth and nose outlets, respectively, $F_{m\theta}(f)$ and $F_{n\theta}(f)$ – frequency-dependent directional radiation characteristics of the mouth and nose outlets, respectively.

Within the considered frequency range the condition $r_0/\lambda < 0.25$ is fulfilled, where r_0 stands for the radius of the mouth or nose outlet and λ denotes the wavelength. Thus both outlets may be treated as sources of spherical waves. In this connection

$$F_{m\theta}(f) = F_{n\theta}(f) \approx \text{const} = 1, \tag{2}$$

the more so since at a distance $d = 20$ cm, and with symmetrical localization of the observation point 0 with regard to mouth and nose outlets, the radiation angle $\theta = 7°$. Approximation (2) is justified by the results of FLANAGAN's [4] model investigations which showed that, for frequencies up to 5000 Hz, the directional radiation characteristics of the human head in both horizontal

and in vertical planes differ from an omnidirectional one by less than ± 1 dB within angular limits $\theta = \pm 20°$ relative to the axis of symmetry of the outlet acting as a sound source. Equation (1) may thus be transformed into the scalar form:

$$|\vec{v}(0)| = |\vec{v}_m| + |\vec{v}_n|. \tag{3}$$

The velocity (current) transmittance function K of the analogous circuit, shown in Fig. 1, may be expressed as the ratio of the acoustic (particle) velocity at the observation point $v(0)$ to the acoustic velocity produced by the larynx generator v_g:

$$K = v(0)/v_g = v_m/v_g + v_n/v_g = K_m + K_n. \tag{4}$$

Thus K is the sum of transmittances of two independent networks which — according to the superposition theorem — may be considered separately, viz.: the pharynx-mouth tract $P+M$ including the shunting effect of the input impedance Z_n of the nasal channel (Fig. 2) and the pharynx-nasal tract $P+N$ including the shunting effect of the input impedance Z_m of the mouth cavity (Fig. 3).

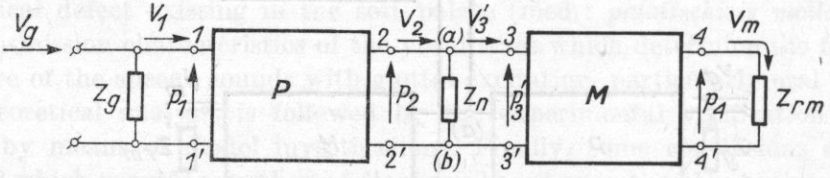

Fig. 2. Equivalent electrical circuit of the pharynx-mouth tract $P+M$ including the shunting effect of the input impedance Z_n of the nasal tract

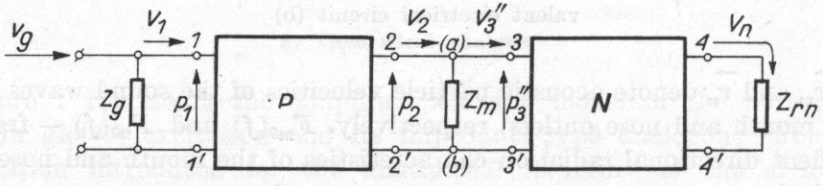

Fig. 3. Equivalent electrical circuit of the pharynx-nasal tract $P+N$ including the shunting effect of the input impedance Z_m of the mouth tract

In Figs. 2 and 3 the following symbols have been used: V_g — the volume velocity produced by the larynx generator, Z_g — the internal impedance of the larynx generator, P — the pharynx cavity in the form of a cylindrical tube of length l_p and cross-sectional area S_p, described by the cascade (chain) matrix $\mathbf{P}$,

$$\mathbf{P} = \begin{bmatrix} \cosh \gamma l_p & Z_{0p} \sinh \gamma l_p \\ \dfrac{1}{Z_{0p}} \sinh \gamma l_p & \cosh \gamma l_p \end{bmatrix},$$

where

Z_{0p} – characteristic impedance of the pharynx tract,

$\gamma = \alpha + j\beta$ – propagation constant of the pharynx, mouth and nasal tract,

M – the mouth cavity in the form of a cylindrical tube of length l_m and cross-sectional area S_m, described by the cascade matrix **M**,

$$\mathbf{M} = \begin{bmatrix} \cosh \gamma l_m & Z_{0m} \sinh \gamma l_m \\ \frac{1}{Z_{0m}} \sinh \gamma l_m & \cosh \gamma l_m \end{bmatrix},$$

Z_{0m} – characteristic impedance of the mouth tract,

N – the nasal cavity represented by a cylindrical tube of length l_n and cross-sectional area S_n, described by the cascade matrix **N**,

$$\mathbf{N} = \begin{bmatrix} \cosh \gamma l_n & Z_{0n} \sinh \gamma l_n \\ \frac{1}{Z_{0n}} \sinh \gamma l_n & \cosh \gamma l_n \end{bmatrix},$$

Z_{0n} – characteristic impedance of the nasal tract,

Z_{rm} – radiation impedance of the mouth outlet,

Z_{rn} – radiation impedance of the nose outlet,

Z_m, Z_n – input impedances of the mouth tract M and the nasal tract N, respectively, loaded at their outlets with the radiation impedances Z_{rm} and Z_{rn}, as seen from the points $a-b$ of the circuit,

$$Z_m = Z_{0m} \frac{Z_{rm} + Z_{0m} \operatorname{tgh} \gamma l_m}{Z_{0m} + Z_{rm} \operatorname{tgh} \gamma l_m},$$

$$Z_n = Z_{0n} \frac{Z_{rn} + Z_{0n} \operatorname{tgh} \gamma l_n}{Z_{0n} + Z_{rn} \operatorname{tgh} \gamma l_n},$$

V_m, V_n – volume velocities in the mouth and nose outlets, respectively,

$V_1, V_2, \ldots; p_1, p_2, \ldots$ – volume velocities and acoustic pressures at different points of the circuit.

The volume velocity (current) transmittance function K_m of the pharynx--mouth tract $P+M$ including the shunting effect of the nasal tract N, expressed as the ratio of the volume velocity in the mouth outlet V_m to the volume velocity produced by the larynx generator V_g may be represented – in agreement with the notation used in Fig. 2 – in the form of the following product:

$$K_m = \frac{V_m}{V_g} + \frac{V_m}{V_3'} \frac{V_3'}{V_2} \frac{V_2}{V_1} \frac{V_1}{V_g}. \tag{5}$$

Using the general rules and methods of linear electric network analysis and some elementary algebraic operations, one can transforme equation (5) to

$$K_m(f) = \frac{1}{\cosh\gamma l_m + \frac{Z_{rm}}{Z_{0m}}\sinh\gamma l_m}\,\frac{Z_n}{Z_n+Z_m}\times$$

$$\times\frac{1}{\cosh\gamma l_p + \frac{Z_2}{Z_{0p}}\sinh\gamma l_p}\,\frac{Z_g}{Z_g+Z_{0p}\dfrac{Z_2+Z_{0p}\operatorname{tgh}\gamma l_p}{Z_{0p}+Z_2\operatorname{tgh}\gamma l_p}} \tag{6}$$

$$= \frac{\cosh\gamma' l_m}{\cosh(\gamma+\gamma')l_m}\,\frac{Z_n}{Z_n+Z_m}\,\frac{\cosh\gamma'' l_p}{\cosh(\gamma+\gamma'')l_p}\,\frac{Z_g}{Z_g+Z_{0p}\dfrac{Z_2+Z_{0p}\operatorname{tgh}\gamma l_p}{Z_{0p}+Z_2\operatorname{tgh}\gamma l_p}},$$

where

$Z_2 = Z_nZ_m/(Z_n+Z_m)$ — equivalent impedance of the input impedances Z_m and Z_n of the mouth tract and the nasal tract, respectively, in parallel connection,

$$\gamma' l_m = \operatorname{tgh}^{-1}(Z_{rm}/Z_{0m}), \qquad \gamma'' l_p = \operatorname{tgh}^{-1}(Z_2/Z_{0p}).$$

The last substitutions express the radiation impedance Z_{rm} of the mouth tract and the load impedance Z_2 of the pharynx tract as formal modifications of the propagation constant γ of each tract.

Using the same procedure in the case of the pharynx-nasal tract $(P+N)$ in Fig. 3, one can express its volume velocity transmittance function $K_n = V_n/V_g$ in the form

$$K_n(f) = \frac{1}{\cosh\gamma l_n + \frac{Z_{rn}}{Z_{0n}}\sinh\gamma l_n}\,\frac{Z_m}{Z_m+Z_n}\times$$

$$\times\frac{1}{\cosh\gamma l_p + \frac{Z_2}{Z_{0p}}\sinh\gamma l_p}\,\frac{Z_g}{Z_g+Z_{0p}\dfrac{Z_2+Z_{0p}\operatorname{tgh}\gamma l_p}{Z_{0p}+Z_2\operatorname{tgh}\gamma l_p}}$$

$$= \frac{\cosh\gamma''' l_n}{\cosh(\gamma+\gamma''')l_n}\,\frac{Z_m}{Z_m+Z_n}\,\frac{\cosh\gamma'' l_p}{\cosh(\gamma+\gamma'')l_p}\,\frac{Z_g}{Z_g+Z_{0p}\dfrac{Z_2+Z_{0p}\operatorname{tgh}\gamma l_p}{Z_{0p}+Z_2\operatorname{tgh}\gamma l_p}}, \tag{7}$$

where, as before,

$$Z_2 = \frac{Z_mZ_n}{Z_m+Z_n}, \qquad \gamma'' l_p = \operatorname{tgh}^{-1}(Z_2/Z_{0p})$$

and, consequently,

$\gamma''' l_p = \operatorname{tgh}^{-1}(Z_{rn}/Z_{0n})$ — corrected propagation constant of the nasal tract including its radiation impedance Z_{rn}.

The transmittance functions of both channels, i.e., $K_m(f)$ of the pharynx--mouth tract and $K_n(f)$ of the pharynx-nasal tract, are complicated when account is taken of mutual shunting effects. The determination of the pole-zero distributions by means of equations (6) and (7) is thus a rather difficult mathematical task, particularly because most acoustic parameters that occur in these equations are compound. For example, the radiation impedances Z_r of the mouth and nose outlets, even when approximated by the most simple model in the form of a circular piston in an infinite plane baffle, are described be the expression of the type [7],

$$Z_r = \frac{\varrho c}{S}\left[\left(1-\frac{J_1(2\beta r)}{\beta r}\right)+j\left(\frac{K_1(2\beta r)}{2(\beta r)^2}\right)\right], \tag{8}$$

where $\beta = \omega/c = 2\pi/\lambda$, r is the piston radius, $S = \pi r^2$ — the piston area, $J_1(x)$ — first order Bessel function of the first kind, $K_1(x)$ — first order Struve function and ϱc — specific acoustic impedance of the medium. For frequencies such that the condition $\beta r \ll 1$ is fulfilled, the radiation impedance (8) may be approximated as

$$Z_r \approx \frac{\varrho c}{S}\left[\frac{(\beta r)^2}{2}+j\frac{8}{3\pi}(\beta r)\right]. \tag{8a}$$

An equally compound form is displayed by the internal impedance $Z_g = R_g + j\omega M$, whose dominant real or resistive component $R_g \gg \omega M_g$ is a function of the geometrical dimensions of the orifice of the vocal cords, i.e. its length l, width w and depth d, as well as of the volume velocity flow V_g through the orifice [2],

$$R_g(t) \approx \frac{12\mu d}{lw^3(t)}+0.875\frac{\varrho V_g(t)}{2[lw(t)]^2}, \tag{9}$$

where μ is the viscosity coefficient of the medium, i.e. the air flowing through the orifice.

Furthermore, the lossy or dissipative parameters of the vocal tract, i.e. the acoustic viscous resistance per unit length $R_a(f)$ and the acoustic conductance per unit length $G_a(f)$ due to heat conduction losses, are, in general, frequency dependent. Consequently, the real component α of the propagation constant $\gamma = \alpha + j\beta$ of the vocal tract cannot be considered to be a constant and frequency independent quantity, since

$$\alpha = \alpha_R + \alpha_G \approx \frac{R_a}{2}\sqrt{C_a/L_a}+\frac{G_a}{2}\sqrt{L_a/C_a} = f(\omega). \tag{10}$$

For the above-mentioned reasons the determination of the pole-zero distribution of the transmittance functions $K_m(f)$, formula (6), and $K_n(f)$, formula (7), in the complex frequency plane $s = \sigma + j\omega$ can be achieved only by numeri-

cal methods using computer technique. Such a procedure, although possible and sometimes used, proved to be neither necessary nor purposeful, if – as in this case – the task consists of calculating only the characteristic frequencies of the vocal tract which describe the spectral structure of vowel sounds including the effect of nasalization due to the cleft palate. For this purpose it is more convenient to introduce further, rationally motivated, simplifications of the acoustic structure of the anatomical model of the human vocal system in Fig. 1, and to transform its equivalent electrical circuit into a shape suitable for functional analysis. These simplifications are based on the following assumptions:

(a) The acoustic tubes which simulate the pharynx (P), mouth (M) and nasal (N) tracts and, consequently, the corresponding electrical four-poles, are considered as nondissipative (lossless) systems: $R_a \approx 0$, $G_a \approx 0$. In this case the attenuation constant α in (10) equals zero, the propagation constant $\gamma = j\beta$ is an imaginary quantity, whereas the characteristic impedance Z_0 of the considered acoustic tube having the cross-sectional area S is a real quantity: $Z_0 = \varrho c/S$.

(b) The radiation impedances of the mouth and nose outlets are considered as being equal to zero: $Z_{rm} = Z_{rn} = 0$. Consequently, the output terminals of the four-poles M and N in the corresponding equivalent electrical circuits are short-circuited.

(c) The larynx source is considered as a constant current generator, with an internal impedance $Z_g = \infty$, which delivers to the vocal tract a constant volume velocity, i.e. $V_g = \text{const}$ and is indepedent of the load impedance, in this case the input impedance Z_{in} of the vocal tract; this assumption is fully motivated since $|Z_g| \gg |Z_{in}|$.

The simplifying assumption (a) has negligible influence upon the accuracy of the pole frequency values of the transmittance functions, particularly those of the pharynx-mouth tract function whose attenuation constant $\alpha = \alpha_R + \alpha_G$, formula (10), is rather small, being of the order $5 \cdot 10^{-4}$ at $f = 500$ Hz, and increases with the square root of frequency [3, 5]. The influence of the radiation impedance Z_{rm} on the formant frequencies of the pharynx-mouth tract (simplifying assumption (b)) has been investigated using a theoretical model in the form of a cylindrical tube of length $l = 17$ cm and cross-sectional area $S = 5$ cm^2. It can be shown (cf. e.g. [5], p. 61–63) that loading the outlet of the tube with the radiation impedance Z_r, formula (8a), increases its effective length by $\Delta l' = 8r/3\pi$, where r is the orifice radius. It thus lowers the first and second formant frequencies from the values $F_1 = 500$ Hz and $F_2 = 1500$ Hz, calculated for $Z = 0$, to $F_1 = 470$ Hz and $F_2 = 1410$ Hz, respectively, it is by only about 6%. Using the same theoretical model of the vocal tract one can show that the condition $|Z_g| \gg |Z_{in}|$, supporting the simplifying assumption (c), is fulfilled for a broad frequency range, except in the vicinity of the first formant F_1, where $|Z_{in}|$ reaches its maximum value $|Z_{in}|_{\max} \approx 80 \cdot 10^5$ MKS acoustic ohms, and then decreases with further increase of frequency to the asymptotic

value $|Z_{in}| = |Z_r| \approx 8 \cdot 10^5$ MKS acoustic ohms, which is equal to the output radiation impedance. Substitution, for the internal impedance $Z_g = \infty$ of the larynx generator, of the finite value $Z_g = R_g + j\omega M_g = (91 + j\omega\, 6.8 \cdot 10^{-3}) \cdot 10^5$ MKS acoustic ohms, which corresponds to the average geometrical dimensions of the vocal cords orifice of an adult male ($l = 18$ mm, $w = 0.28$ mm, $d = 3$ mm) at mean subglottal pressure $P_s = 8$ cm H_2O, increases the first and second formant frequencies from the theoretical values $F_1 = 500$ Hz and $F_2 = 1500$ Hz, calculated for $Z_g = \infty$, by about $1.4\,\%$ and $1.0\,\%$, respectively, due to the apparent shortening of the effective length $l = 17$ cm of the tube by the value $\Delta l'' = M_g Z_0 c |Z_g|^{-2}$, where

$Z_0 = \varrho c / S$ — characteristic impedance of the tube,

$Z_g = \sqrt{(R_g^2 + \omega^2 M_g^2)}$ — modulus of the larynx generator's impedance,

c — sound velocity in air.

Having introduced the simplifying assumptions (a), (b) and (c), we can represent the equivalent circuits of the pharynx-mouth tract $P + M$ (Fig. 2) and of the pharynx-nasal tract $P + N$ (Fig. 3) in the forms shown in Figs. 4a and 4b.

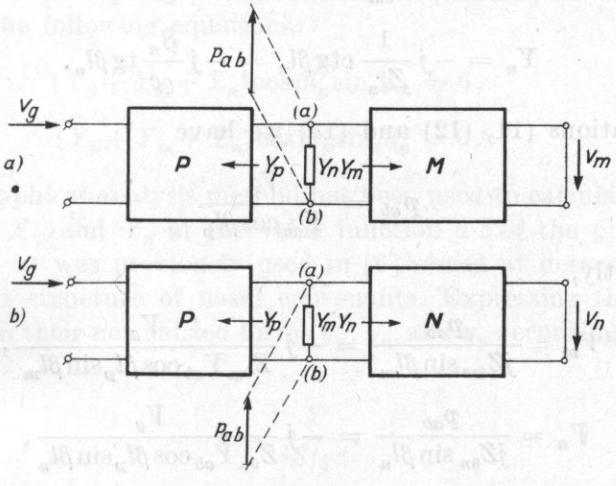

Fig. 4. Simplified equivalent electrical circuits of (a) the pharynx-mouth tract $P + M$ and (b) of the pharynx-nasal tract $P + N$

The velocity or current transmittance functions $K_m = V_m / V_g$ and $K_n = V_n / V_g$ of both tracts can now be determined by elementary methods based on well-known rules of the general theory of linear electric networks adapted to acoustic systems. According to NORTON's theorem, the acoustic pressure (or electric voltage) p_{ab} at the points a-b of the circuti may be expressed as

$$P_{ab} = \frac{V_z}{Y_{ab}}, \tag{11}$$

where

$$V_z = \frac{V_g}{\cos \beta l_p} \tag{12}$$

is the output volume velocity (or output current) of the four-pole P, provided the points a-b are short-circuited, and

$$Y_{ab} = Y_p + Y_m + Y_n \tag{13}$$

is the acoustic admittance of the system, measured between the points a-b, and is equal to the sum of the input admittances of the four-poles P, M and N as seen from the terminals a-b. In view of the previously introduced simplifications we get:

$$Y_p = j \frac{1}{Z_{0p}} \operatorname{tg} \beta l_p = j \frac{S_p}{\varrho c} \operatorname{tg} \gamma l_p, \tag{14a}$$

$$Y_m = -j \frac{1}{Z_{0m}} \operatorname{ctg} \beta l_m = -j \frac{S_m}{\varrho c} \operatorname{tg} \beta l_m, \tag{14b}$$

$$Y_n = -j \frac{1}{Z_{0n}} \operatorname{ctg} \beta l_n = -j \frac{S_n}{\varrho c} \operatorname{tg} \beta l_n. \tag{14c}$$

From equations (11, (12) and (13) we have

$$p_{ab} = \frac{V_g}{Y_{ab} \cos \beta l_p} \tag{15}$$

and, consequently,

$$V_m = \frac{p_{ab}}{j Z_{0m} \sin \beta l_m} = -j \frac{V_g}{Z_{0m} Y_{ab} \cos \beta l_p \sin \beta l_m}, \tag{16}$$

$$V_n = \frac{p_{ab}}{j Z_{0n} \sin \beta l_n} = -j \frac{V_g}{Z_{0n} Y_{ab} \cos \beta l_p \sin \beta l_n}, \tag{17}$$

whence, finally,

$$K_m = \frac{V_m}{V_g} = -j Y_{0m} [Y_{ab} \cos \beta l_p \sin \beta l_m]^{-1}, \tag{18}$$

$$K_n = \frac{V_n}{V_g} = -j Y_{0n} [Y_{ab} \cos \beta l_p \sin \beta l_n]^{-1}, \tag{19}$$

where $Y_{0m} = Z_{0m}^{-1}$ and $Y_{0n} = Z_{0n}^{-1}$.

Identical results could be obtained from the general expressions for K_m in formula (6) and K_n in formula (7) after introducing the approximations

$$\gamma = \alpha + j\beta \approx j\beta, \quad Z_{rm} = Z_{rn} \approx 0, \quad Z_g = \infty,$$

which result from the simplifying assumptions (a), (b) and (c). In point of fact, equation (6) for K_m may be rewritten as follows:

$$K_m \approx \frac{1}{\cos\beta l_m}\,\frac{Y_m}{Y_m+Y_n}\,\frac{1}{\cos\beta l_p + j\,\dfrac{1}{Z_{0p}}\,\dfrac{1}{(Y_n+Y_m)}\sin\beta l_p}$$

$$= \frac{1}{\cos\beta l_m}\,\frac{Y_m}{Y_m+Y_n}\,\frac{1/\cos\beta l_p}{1+\dfrac{Y_p}{Y_n+Y_m}} = -j\,\frac{Y_{0m}\operatorname{ctg}\beta l_m}{\cos\beta l_m\cos\beta l_p\,Y_{ab}} \tag{18a}$$

$$= -jY_{0m}[Y_{ab}\cos\beta l_p\sin\beta l_m]^{-1}.$$

Similarly, from equation (7), after identical transformations, we get

$$K_n \approx -jY_{0n}[Y_{ab}\cos\beta l_p\sin\beta l_n]^{-1}. \tag{19a}$$

The poles of the transmittance functions K_m, formula (18), and K_n, formula (19), of the pharynx-mouth tract and of the pharynx-nasal tract, respectively, which correspond to the formant frequencies, can be obtained by the solution of the following equations:

$$(Y_p+Y_m+Y_n)\cos\beta l_p\sin\beta l_m = 0, \tag{20}$$

$$(Y_p+Y_m+Y_n)\cos\beta l_p\sin\beta l_n = 0. \tag{21}$$

The same graphical analysis method has been used to calculate the network admittances Y_p, Y_m and Y_n at the velar junction a-b of the pharynx, mouth and nasal tracts, as was previously used in [6] aimed at determining the formant-antiformant structure of nasal consonants. Expressing the admittances Y_p, Y_m and Y_n in their normalized forms y_p, y_m and y_n according to the general rule

$$y = \frac{Y}{jS/\varrho c}, \tag{22}$$

and assuming equality of cross-sectional areas of all tracts ($S_p = S_m = S_n$), one can rewrite equations (20) and (21) in purely trigonometrical forms,

$$-\cos\beta(l_p+l_m) = \operatorname{ctg}\beta l_n\cos\beta l_p\sin\beta l_m, \tag{23}$$

$$-\cos\beta(l_p+l_n) = \operatorname{ctg}\beta l_m\cos\beta l_p\sin\beta l_n, \tag{24}$$

which are convenient for graphical analysis. The solutions are shown in Figs. 5 and 6 for the typical case where $l_p = 8.5$ cm, $l_m = 8.5$ cm and $l_n = 12.5$ cm, corresponding to the average geometrical dimensions of the vocal tract of an adult male. The sound velocity in air is taken to be $c = 350$ m/s (moist air at human body temperature, $t = 37°$C).

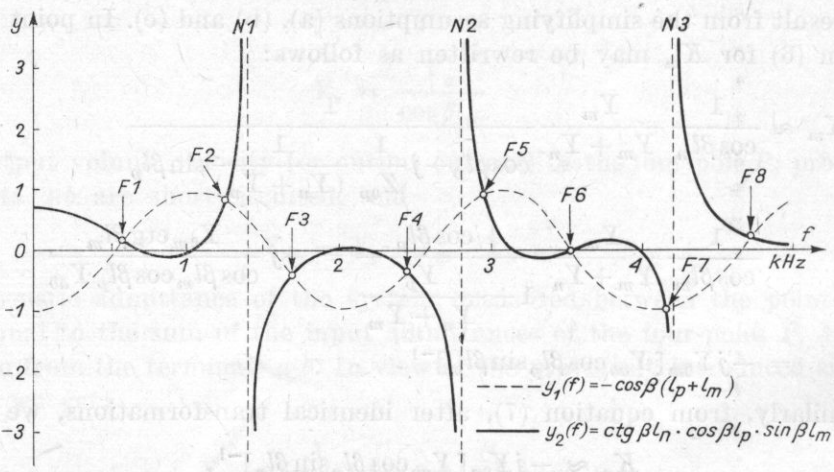

Fig. 5. Determination of the poles FX and zeros NX ($X = 1, 2, 3, \ldots$) of the transmittance function K_m (18) of the pharynx-mouth tract by graphical analysis of (23)

The intersection points of the characteristics

$$y_1(f) = -\cos\beta(l_p + l_m) \quad \text{and} \quad y_2(f) = \operatorname{ctg}\beta l_n \cos\beta l_p \sin\beta l_m$$

in Fig. 5, as well as the intersection points of the characteristics

$$y_3(f) = -\cos\beta(l_p + l_n) \quad \text{and} \quad y_4(f) = \operatorname{ctg}\beta l_m \cos\beta l_p \sin\beta l_n$$

in Fig. 6 correspond to the pole frequencies of the transmittance functions K_m (18) of the pharynx-mouth tract and K_n (19) of the pharynx-nasal tract, respectively, whereas the discontinuity points of the functions $y_2(f) = \pm\infty$

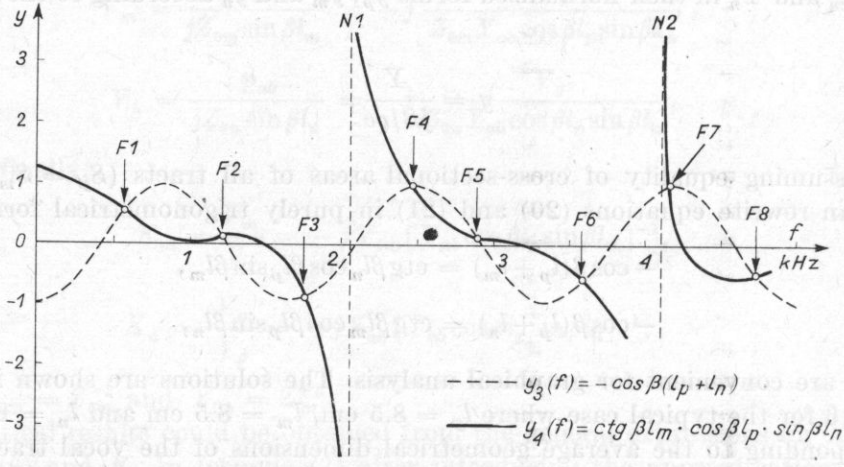

Fig. 6. Determination of the poles FX and zeros NX ($X = 1, 2, 3, \ldots$) of the transmittance function K_n (19) of the pharynx-nasal tract by graphical analysis of (24)

and $y_4(f) = \pm\infty$ determine the zeros of the respective transmittances. The curve $y_1(f) = -\cos\beta(l_p+l_m)$ describes the trivial case of the neutral vowel Э pronounced without any nasalization (no cleft palate: $Y_n = 0$). The intersection points of this curve with the abscissa, that is the points where $y_1(f) = 0$, define the classical formant frequencies

$$F_{(2n+1)} = (2n+1)\cdot\frac{c}{4l} \approx (2n+1)\cdot 515 \text{ Hz}$$

from the general condition

$$\beta l = (2n+1)\cdot\frac{\pi}{2}$$

for $n = 0, 1, 2, \ldots$, where $l = l_p+l_m = 17$ cm. The curve $y_1(f)$ may thus be considered as the reference characteristic corresponding to the articulation of the neutral oral vowel Э in physiologically normal conditions (no cleft palate).

Tables 1 and 2 contain the frequency values of the poles F_x and zeros N_x ($x = 1, 2, 3, \ldots$) of the transmittance functions K_m and K_n describing the pharynx-mouth tract (Fig. 4a) and the pharynx-nasal tract (Fig. 4b), respectively. The pole-zero frequencies were determined by graphical solution of equations (23) and (24) in Figs. 5 and 6.

Table 1. Frequency values of poles F_x and zeros N_x in the transmittance function K_m of the pharynx-mouth tract in Fig. 4a, determined by the graphical method from (23) for $l_p = l_m = 8.5$ cm, $l_n = 12.5$ cm, $c = 350$ m/s

F_x, N_x	F_1	F_2	N_1	F_3	F_4	N_2	F_5	F_6	F_7	N_3	F_8
Hz	575	1250	1400	1700	2450	2800	2960	3520	4150	4200	4720

From the viewpoint of phoniatric diagnostics the most interesting case in the pathological and postoperative states of cleft palate is the general case, when both tracts: the pharynx-mouth and the pharynx-nasal ones, are active simultaneously and shunt one another. In agreement with the previously applied superposition theorem, this case may be considered analytically as the result of summation of the transmittance characteristics (18) and (19), each of which describes a separate channel including the shunting effect of another one.

Table 2. Frequency values of poles F_x and zeros N_x in the transmittance function K_n of the pharynx-nasal tract in Fig. 4b, determined by graphical method from (24) for $l_p = l_m = 8.5$ cm, $l_n = 12.5$ cm, $c = 350$ m/s

F_x, N_x	F_1	F_2	F_3	N_1	F_4	F_5	F_6	N_2	F_7	F_8
Hz	575	1220	1760	2050	2450	2900	3580	4100	4150	4740

The analytical procedure may be interpreted in physical terms as the sum of the acoustic pressures produced at the observation point by the sound waves radiated by the mouth and nose outlets. It is assumed that the point at which the resulting sound pressure is measured lies on the axis of symmetry of the radiating system, and is far enough from both outlets.

It follows that the spectral characteristic of steady-state speech sounds, measured in real conditions, should contain — in principle — all formants and antiformants caused by the nasalization effect and which correspond to the pole-zero distributions of the transmittance functions K_m and K_n of both tracts, as listed in Tables 1 and 2. The theoretical pole-zero distribution of the resulting transmittance function $|K| = |K_m| + |K_n|$ of the complete vocal system, involving both the mouth and the nasal tract, is presented in Table 3.

Table 3. Frequency values of poles F_x and zeros N_x in the transmittance function $K = K_m + K_n$ of the vocal mouth-nasal tract, determined by graphical method in the theoretical case of articulation of the neutral vowel Э, including the nasalization effect due to cleft palate (*palatoschisis molle*), for $l_p = l_m = 8.5$ cm, $l_n = 12.5$ cm, $c = 350$ m/s

F_x, N_x	F_1	F_2	N_1	F_3	N_2	F_4	N_3	F_5	F_6	N_4	F_7
Hz	575	1235	1400	1730	2050	2450	2800	2930	3550	4150	4730

Fig. 7 shows the hypothetical transmittance characteristic $K = f(f)$, which represents the formant-antiformant structure of the neutral vowel Э being nasalized due to the cleft palate effect.

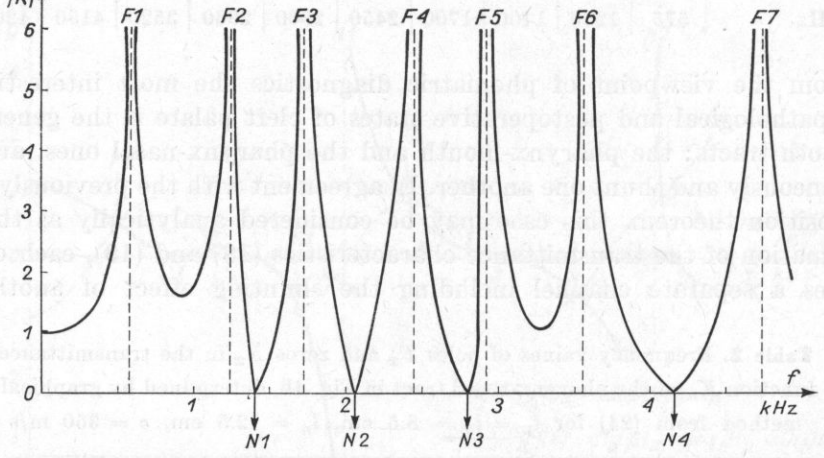

Fig. 7. Distribution of the poles FX an zeros NX ($X = 1, 2, 3, \ldots$) of the hypothetical transmittance function $|K| = |K_m| + |K_n|$ of the vocal mouth-nasal tract, including the mutual effects of both tracts: the mouth channel and the nasal channel

It seems very likely, however, that the speech spectrum envelope measured in real conditions may differ considerably from the theoretical one, due to the mutual cancellation of poles and zeros of both transmittance functions $K_m(f)$ and $K_n(f)$, which are located near one another in the frequency scale.

3. Methodology of experimental investigations

The results of the theoretical analysis have been verified by an experimental investigation performed in a physical system simulating the geometric structure of the anatomical model of the vocal tract (Fig. 1a) in the dimensional scale of 5:1, that is in the frequency scale of 1:5. The choice of the scale factor $k = 5$ was inspired by both metrological and constructional reasons: the lowered frequency range proved to be well adjusted for the electroacoustic parameters of the available measuring equipment, whereas the enlargement of model's geometry improved the accuracy of the system's design and performance.

A simplified schematic diagram of the physical model is shown in Fig. 8. The larynx source *LS* is simulated by a dynamic moving coil loudspeaker, type GDN 16/10, equipped with an acoustic feedback system controlling the

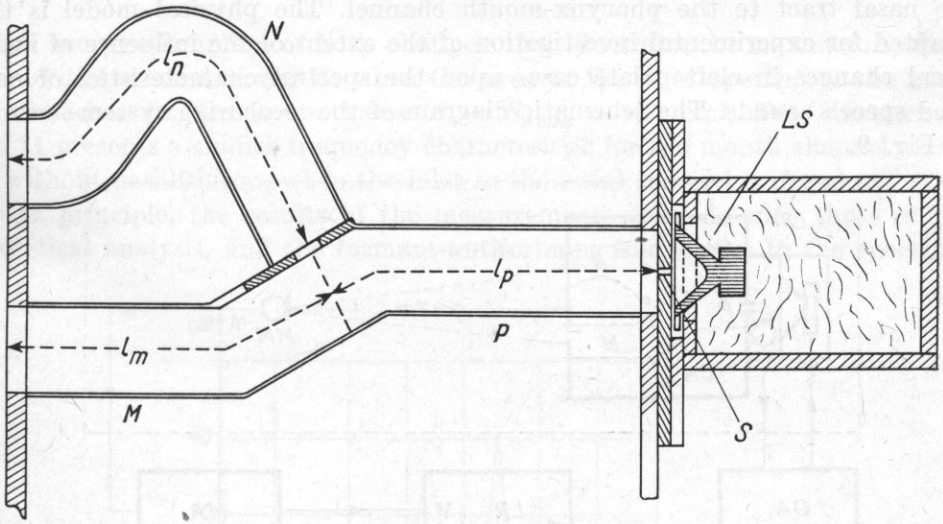

Fig. 8. Simplified schematic diagram of the experimental acoustic model of the speech organ in larynx excitation

LS – larynx source, *S* – slit simulating the vocal cord orifice, *P* – pharynx tract, *M* – mouth tract, *N* – nasal tract

sound pressure level in front of the membrane (p = const). The loudspeaker is installed in a closed and acoustically damped enclosure, whose volume approximates the average volume of the human trachea and bronchi. The larynx source is coupled with the inlet of the pharynx channel *P* through the narrow rectangular slit *S*, whose dimensions ($90 \times 5 \times 15$ mm) correspond to the average

dimensions of the human glottis (length $l = 18$ mm, width $w = 1$ mm, depth $d = 3$ mm) when taking into account the scale factor 5 : 1. The model of the vocal tract itself has the form of a bifurcated system of acoustic tubes of constant cross-sectional area $S = 125\ \text{cm}^2$ and lengths $l_p = 42.5$ cm, $l_m = 42.5$ cm, $l_n = 62.5$ cm, which simulate the pharynx (P), mouth (M) and nasal (N) tract, respectively. The areas of the outlet openings of the mouth and nasal tract are equal to $S_m = 125\ \text{cm}^2$ and $S_n = 50\ \text{cm}^2$, respectively, corresponding to 5 cm² and 2 cm² of the natural scale. Since the model is made of hard and smooth materials (textolite, plexiglas), the acoustic tubes may be considered to be lossless, at least in the frequency range of interest, i.e. up to 1000 Hz.

The human head is simulated by the wooden cubic box whose edge equals 82 cm. The outlet openings of the mouth and nostrils are located vertically in the front wall of the model and the distance between their centres is equal to 22.5 cm, i.e. 4.5 cm in the natural scale. The measuring point 0 lies on the axis of symmetry of the model, at a distance $d = 100$ cm from the plane of the outlet openings. Thus, in real conditions, the measuring microphone should be placed at a distance $d' = 20$ cm in front of the patient's head.

Facilities have been provided for varying the area of the orifice coupling the nasal tract to the pharynx-mouth channel. The physical model is thus adapted for experimental investigation of the extent of the influence of anatomical changes in cleft palate cases upon the spectral characteristics of nasalized speech sounds. The schematic diagram of the measuring system is shown in Fig. 9.

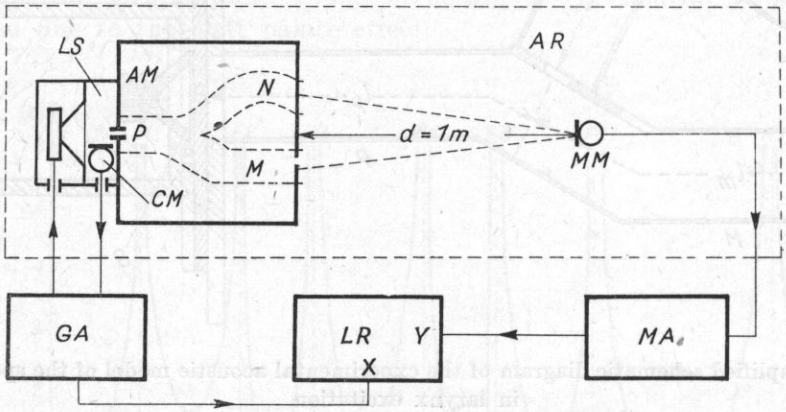

Fig. 9. Schematic diagram of the measuring circuit

AR – anechoic room, *AM* – acoustic model of the speech organ, *P* – pharynx tract, *M* – mouth tract, *N* – nasal tract, *LS* – larynx source, *CM* – control microphone, *MM* – measuring microphone, *MA* – microphone amplifier, *GA* – acoustic generator, *LR* – logarithmic level recorder

4. Results of experiments

Fig. 10 presents the frequency characteristic of the acoustic pressure produced at the measuring point by sound waves radiated from the outlets of both channels: the mouth tract and the nasal tract. The curve corresponds

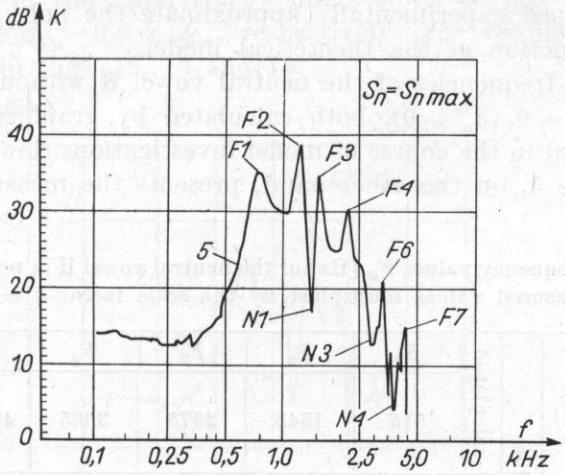

Fig. 10. Radiation frequency characteristic of both model channels: the mouth and nasal tract with full nasalization, corresponding to the maximal inlet area of the nasal channel of $S_n = S_{n\max}$. The frequency scale has been multiplied by 5

to full acoustic coupling of both channels and illustrates the maximal nasalization of the neutral vowel Ы, when the area of the inlet opening of the nasal tract reaches its maximum value $S_n = S_{n\max} = 125$ cm². For comparison, Fig. 11 presents a similar frequency characteristic for the mouth channel alone, i.e. without nasalization, when the inlet to the nasal channel is closed ($S_n = 0$).

In principle, the results of the measurements coincide with those of the theoretical analysis, and the formant-antiformant frequencies in the spectrum

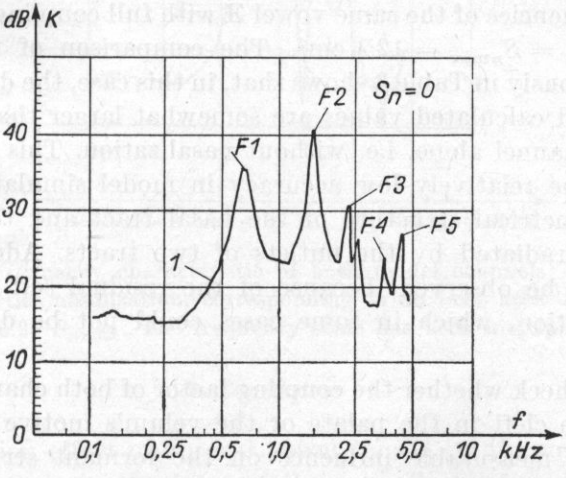

Fig. 11. Radiation frequency characteristic of the model mouth channel without nasalization ($S_n = 0$). The frequency scale has been multiplied by 5

envelope determined experimentally approximate the poles and zeros of the transmittance function of the theoretical model.

The formant frequencies of the neutral vowel ə without nasalization (no cleft palate: $Y_n = 0$, $S_n = 0$), both calculated by graphical method (upper row) and measured in the course of model investigations (lower row), are listed in Table 4. Table 5, on the other hand, presents the measured formant and

Table 4. Formant frequency values F_x [Hz] of the neutral vowel ə in purely oral articulation (measured values multiplied by the scale factor $k = 5$)

Formant frequencies F_x	Values	F_1	F_2	F_3	F_4	F_5
	calculated	515	1545	2575	3605	4635
	measured	625	1500	2400	3500	4600

Table 5. Measured frequency values of formants F_x and antiformants N_x at full acoustic coupling of both model channels: the mouth and the nasal tract, $S_n = S_{n\max}$ (measured values multiplied by the scale factor $k = 5$)

F_x, N_x	F_1	F_2	N_1	F_3	N_2	F_4	N_3	F_5	F_6	N_4	F_7
Hz	700	1250	1400	1700	–	2300	2900	–	3500	4200	4500

antiformant frequencies of the same vowel ə with full coupling of both channels, that is when $S_n = S_{n\max} = 125$ cm². The comparison of these values with those listed previously in Table 3 shows that, in this case, the differences between the measured and calculated values are somewhat larger than those occurring for the mouth channel alone, i.e. without nasalization. This fact may be attributed both to the relatively low accuracy in model simulation of the rather complicated geometrical structure of the nasal tract and to the interference of sound waves radiated by the outlets of two tracts. Additional distorting effects may also be observed, because of the residual self resonances of the model's construction, which in some cases could not be damped effectively enough.

In order to check whether the coupling factor of both channels, representing the extent of the cleft in the palate or the velum's motive capability, exerts an essential and measurable influence on the formant structure of an oral vowel, additional measurements of spectral characteristics of the neutral vowel ə have been performed at a few different values of the coupling factor, corre-

sponding to areas of the nasal tract's inlets equal to $S_n = 0.125\ S_{n\max}$, $S_n = 0.25\ S_{n\max}$, and $S_n = 0.5\ S_{n\max}$, respectively. The results of the measurements are shown in Figs. 12, 13 and 14.

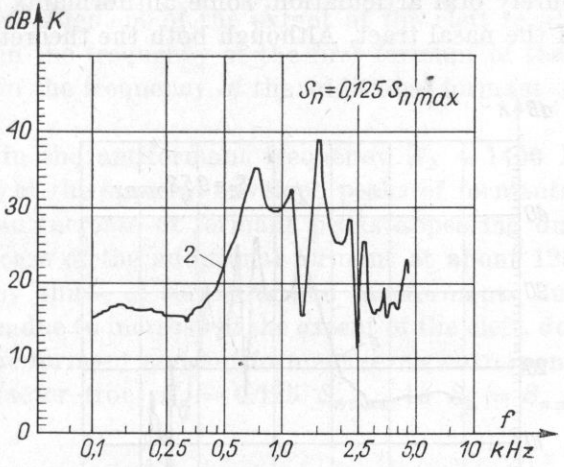

Fig. 12. Radiation frequency characteristic of both model channels: the mouth and the nasal tract with partial nasalization, corresponding to an inlet area of the nasal channel of $S_n = 0.125\ S_{n\max}$. The frequency scale has been multiplied by 5

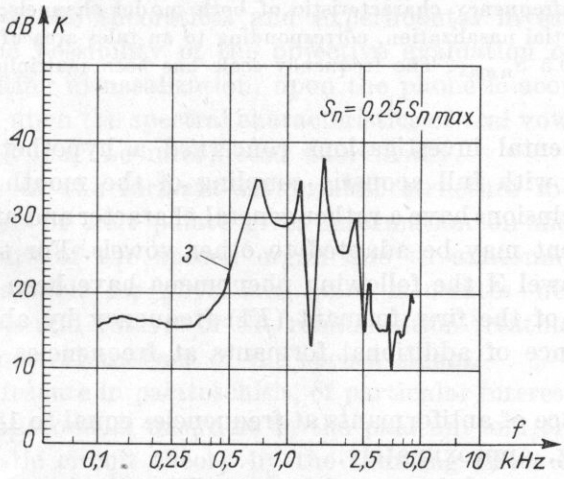

Fig. 13. Radiation frequency characteristic of both model channels: the mouth and the nasal tract with partial nasalization, corresponding to an inlet area of the nasal channel of $S_n = 0.25\ S_{n\max}$. The frequency scale has been multiplied by 5

5. Conclusions

The nasalization effect of an oral vowel caused by the velum's cleft (*palatoschisis molle*) appears in the form of theoretically predicted and experimentally verified modifications of its spectral characteristics. These modifications

consist, generally, in the deformation of the spectral envelope and in the enrichment of the vowel's formant structure. Besides additional formants, which do not exist in purely oral articulation, some antiformants appear due to the shunting effect of the nasal tract. Although both the theoretical considerations

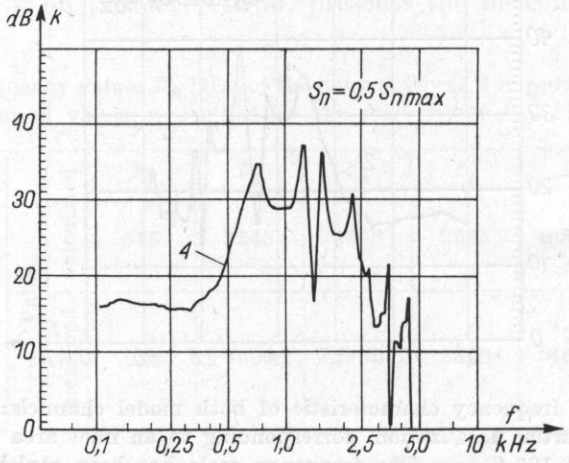

Fig. 14. Radiation frequency characteristic of both model channels: the mouth and the nasal tract with partial nasalization, corresponding to an inlet area of the nasal channel of $S_n = 0.5\ S_{n\max}$. The frequency scale has been multiplied by 5

and the experimental investigations concerned a hypothetical model of the neutral vowel Ə with full acoustic coupling of the mouth and nasal tracts, the resulting conclusions have a rather general character and after similar methodological treatment may be adapted to other vowels. For the particular case of the neutral vowel Ə the following phenomena have been observed:

(a) Increase of the first formant ($F1$) frequency by about 12%.

(b) Appearance of additional formants at frequencies equal to 1250 Hz and 1700 Hz.

(c) Appearance of antiformants at frequencies equal to 1400 Hz, 2800-2900 Hz and 4200 Hz, approximately.

(d) Disappearance of the second formant $F2$ at the frequency $F_2 = 1500$ Hz due to the appearance of a zero in the vocal tract's transmittance function at a frequency $N_1 = 1400$ Hz.

At the same time a slight lowering of the peaks of the spectrum envelope and a corresponding broadening of the bandwidths in the formants $F1$ and $F2$ of the nasalized vowel become quite visible. This phenomenon, which was also observed in the case of nasal consonants (cf. e.g. [6]), has not been interpreted analytically in view of the fact that losses in the vocal tract were *a priori* neglected.

Comparison of the spectral characteristics of the neutral vowel ə at various degrees of nasalization, realized in model investigations by a gradual increase in the inlet area of the nasal tract (cf. Figs. 12, 13 and 14), permit preliminary conclusions that enlargement of the extent of the cleft results in:

(a) Increase in the frequency of the first formant of the neutral vowel ə.

(b) Increase in the frequency of the additional formant occurring at about 1250 Hz.

(c) Increase in the antiformant frequency $N_1 \approx 1400$ Hz.

(d) Lowering of the spectral envelope peaks of formants originating from the oral vowel and increase of formant peaks appearing due to nasalization, especially in the case of the additional formant at about 1250 Hz.

The frequency shifts of formants and antiformants due to the increase of nasalization, i.e. due to increase in the extent of the cleft, do not exceed 10%. The changes of the formant and antiformant levels corresponding to variations of the coupling factor from $S_n = 0.125\ S_{n\max}$ to $S_n = S_{n\max}$ lie within the limits of 5 dB.

6. Final remarks

The results of the theoretical and experimental investigations reported above confirm the possibility of the objective evaluation of the influence of cleft palate, resulting in nasalization, upon the phonetic-acoustical parameters and, particularly, upon the spectral characteristics of oral vowels. This influence is measurable and may be interpreted analytically.

The analysis of the formant-antiformant structure in pathological and postoperative cases of cleft palate gives information on modifications of the acoustical structure of the speech organ due to anatomical disorders. The information is valuable for physicians since it creates new possibilities in objective diagnosis and control of the rehabilitation treatment of cleft palate by means of a spectral analysis of the speech signal.

An essential feature in palatoschisis, of particular interest to the physician, is the extent of anatomical disorders in the palatum and/or velum, expressed in terms of acoustic circuit theory by the shunting effect of the nasal tract. The detailed quantitative investigations of this phenomenon were not the subject of the present work. The results of preliminary experiments proved, however, that objective acoustic methods for phoniatric diagnosis of cleft palate cases may be applied as well to qualitative as to quantitative evaluations of the extent of pathological disorders. Theoretical and experimental research, aimed at these applications, has been recently initiated in the Department of Cybernetics Acoustics of the Institute of Fundamental Technological Research, Polish Academy of Sciences, in close cooperation with the Phoniatric Centre of the Central Clinical Hospital of the Medical Academy in Warsaw.

References

[1] J. BARDACH, *Clefts of the upper lip and of the palatum*, PZWL, Warszawa 1967 (in Polish).

[2] J. W. VAN DEN BERG, J. T. ZANTEMA, P. DOORNENBAL Jr., *On the air resistance and the Bernouilli effect of the human larynx*, JASA, **29**, 5, 626-631 (1957).

[3] G. FANT, *Acoustic theory of speech production*, Mouton and Co., s-Gravenhage 1960.

[4] J. L. FLANAGAN, *Analog measurements of sound radiation from the mouth*, JASA, **32**, 12, 1613-1620 (1960).

[5] J. L. FLANAGAN, *Speech analysis, synthesis and perception*, Springer Verlag, Berlin-Heildelberg-New York, 2nd edition, 1972.

[6] J. KACPROWSKI, *Synthesis of Polish nasal consonants in resonance formant circuits*, Rozprawy Elektrotechniczne, **9**, 3, 439-465 (1963) (in Polish).

[7] P. M. MORSE, *Vibration and sound*, McGraw-Hill Book Co., New York 1948.

[8] W. TŁUCHOWSKI, W. MIKIEL, A. KOMOROWSKA, E. WIDLICKA, *An approach to the correlation of bioelectric and phonospectroscopic investigations in different types of cleft palate operations in children*, Otolaryngologia Polska, **8**, 6a, 70-77 (1974) (in Polish).

Received on 23th September 1975

ARCHIVES OF ACOUSTICS
1, 2, 159-169 (1976)

DIFFRACTION OF LIGHT BY ACOUSTIC WAVES IN CRYSTALS

ZYGMUNT KLESZCZEWSKI, MARIAN WOJEWODA

Institute of Physics, Silesian Technical University (Gliwice)

Diffraction of light by acoustic waves at high frequencies, i.e. Bragg diffraction, is discussed, and the possibility of investigating the acoustic and acousto-optical properties of crystals using this method is presented. The measuring systems used, measurements of the propagation velocities and absorption coefficients of acoustic waves, and the photoelastic constants for crystals of melt quartz, TiO_2, CaF_2, Bi_{12}, GeO_{20}, and $LiNbO_3$ are presented.

1. Introduction

Investigation of the diffraction of light by acoustic waves is an important method of defining the acoustic and acousto-optical properties of solids [1, 2, 4, 7]. It is possible, however, using this method, to determine the velocity of wave propagation and thus also the corresponding elastic constants. Knowledge of these constants is necessary to evaluate the practicability of using crystals in many fields, for instance in field modulation. When investigating the diffraction of light by acoustic waves, two cases [4, 7] are usually considered:

1) Raman-Nath diffraction, observed at frequencies for which the relationship $\Lambda^2/\lambda > l$ is satisfied (where Λ and λ represent the acoustical and optical wavelengths, and l the width of the acoustic beam);

2) Bragg diffraction, observed at higher frequencies for which the relationship $\Lambda^2/\lambda < l$ is satisfied.

In this paper we shall be dealing with the latter case.

Invoking the principles of conservation of momentum and conservation of energy for a photon-phonon collision, one may write

$$\boldsymbol{k}_2 = \boldsymbol{k}_1 \pm \boldsymbol{q}, \tag{1a}$$

$$\omega_2 = \omega_1 \pm \Omega, \tag{1b}$$

where $\boldsymbol{k}_1$, $\boldsymbol{k}_2$, and $\boldsymbol{q}$ represent wave vectors of the incident light, scattered light and acoustic waves, respectively.

Since $\omega_1 \cong \omega_2 \gg \Omega$, it can be assumed that the lengths of the wave vectors $\boldsymbol{k}_1$ and $\boldsymbol{k}_2$ are changed because of the different values of optical refraction index in the directions of the incident and scattered light, k.e. $\boldsymbol{k}_1 = \boldsymbol{k}_0 n_1$ and

$k_2 = k_0 n_2$, where k_0 is the wave vector of the light wave in a vacuum, while n_1 and n_2 are values of the optical refraction index in the directions of the incident and scattered waves.

With this assumption, and using formulae (1a), (1b) and Fig. 1, it is possible to obtain expressions for the angle of incidence θ_1 and diffraction θ_2 of light,

$$\sin\theta_1 = \frac{\lambda_0 \nu}{2n_1 v}\left[1+\left(\frac{v}{\lambda_0 \nu}\right)^2 (n_1^2 - n_2^2)\right], \tag{2a}$$

$$\sin\theta_2 = \frac{\lambda_0 \nu}{2n_2 v}\left[1-\left(\frac{v}{\lambda_0 \nu}\right)^2 (n_1^2 - n_2^2)\right], \tag{2b}$$

where λ_0 denotes the wavelength of light in a vacuum, and ν and v the frequency and velocity of acoustic wave propagation, respectively.

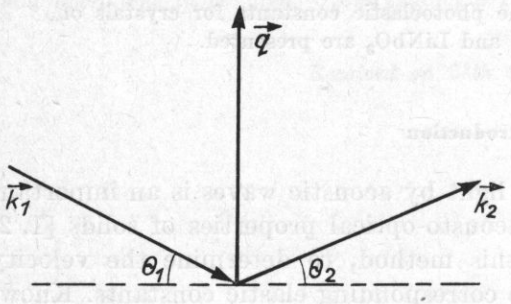

Fig. 1. Wave vector diagram for photon-phonon scattering

If $n_1 = n_2 = n$, i.e. if the medium is optically isotropic, then

$$\sin\theta_1 = \sin\theta_2 = \frac{\lambda_0 \nu}{2nv}. \tag{3}$$

In the general case it is necessary to know the coefficients of diffraction n_1 and n_2 of the angles θ_1 and θ_2, i.e. one must know the surface of wave vectors in a given crystal. This problem is very interesting and has been discussed in papers [5, 6].

Henceforth we can dispense with a detailed knowledge of the Bragg diffraction geometry. It can be seen from formulae (2a) and (2b) that it is possible to determine the velocity of wave propagation in a given direction by measurement of angles θ_1 and θ_2. On the other hand, by making a measurement of the intensity of diffracted light it is possible to determine, for a given crystal, the photoelastic constants and the absorption coefficient of acoustic waves. It is known [4] that the ratio of the intensity of the light diffracted by the acoustic wave to the intensity of incident light is

$$\eta = \frac{I}{I_0} = \frac{\pi^2 n^6 p_{ij}^2 l^2 P_a}{2\lambda_0^2 \varrho v^3}, \tag{4}$$

where I_0 denotes the intensity of incident light, I — the intensity of diffracted light, P_a — the intensity of the acoustic beam, ϱ — the density of medium, and p_{ij} — the photoelastic constants.

Measurements of the photoelastic constants using formula (4) are usually made in relation to some reference substance. The method of measurements is shown in Fig. 2. The reference substance (preferably melt quartz) is glued

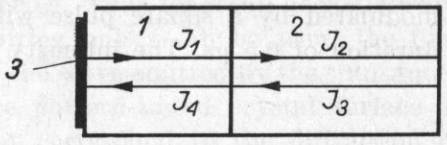

Fig. 2. Method of measurement of photoelastic constants using one transducer
1 — specimen, *2* — investigated pattern, *3* — transducer

with the substance to be tested. The acoustic wave is induced from the reference substance side. If the measurement of the intensity of diffracted light of the incident and reflected waves (I_1 and I_4) is made on the crystal-air boundary for the reference substance as well as for the tested substance (I_2 and I_3), then

$$\left(\frac{I_2 I_3}{I_1 I_4}\right)^{1/2} = \begin{cases} \dfrac{n^6 p^2/\varrho v^3}{n^6 p^2/\varrho v^3} & \begin{matrix}\text{tested substance,}\\ \text{reference substance.}\end{matrix} \end{cases} \tag{5}$$

It is also possible to make measurements of photoelastic constants by inducing to the acoustic wave both from the side of the reference substance and from the side of the substance to be tested [3]. This method should be followed when intensive absorption of acoustic wave occurs in the medium.

As can be seen from formula (4), the intensity of diffracted light is proportional to the intensity of the acoustic beam. It is thus possible to determine the attenuation coefficient of acoustic waves. If we make measurements of the intensity of light diffracted by the acoustic wave at two distances from the transducer x_1 and x_2, the absorption coefficient can be determined from the formula

$$\alpha\left[\frac{\text{dB}}{\text{cm}}\right] = \frac{8.686}{2(x_2 - x_1)} \ln \frac{I(x_1)}{I(x_2)}, \tag{6}$$

where $I(x_1)$ and $I(x_2)$ represent the intensities of diffracted light correspondingly to distances x_1 and x_2 from the transducer.

This measurement can be made for continuous and pulsed waves. In the former case, the crystal is moved in the direction of the acoustic wave and the intensity of the diffracted light measured for two positions of the crystal. While in the latter case, the crystal remains immobilized while the measurements are taken of the intensity of the light resulting from the acoustic wave, which has been reflected repeatedly from the faces of the crystals (see e.g. Fig. 9a). The method is particularly useful in cases where the absorption of the acoustic wave is insignificant, but it requires the use of crystals with precisely parallel faces.

2. Measuring system

The measuring system for investigating the diffraction of light by acoustic waves is shown in Fig. 3. The light source is a 10 mW He-Ne laser, and the source of acoustic waves is a transducer of lithium iodate operating at a fundamental frequency 200 MHz or a thin layer transducer of CdS, operating within the frequency range from 700 to 1300 MHz. The acoustic wave was modulated by a square pulse with a repetition rate of 10 kHz and a pulse duration of 0.5 μs. The intensity of the acoustic wave was about 0.1 W/cm^2.

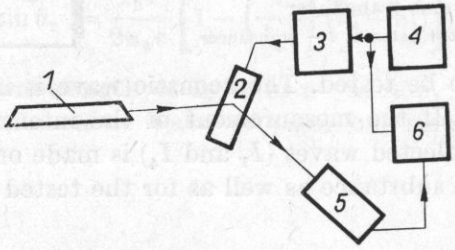

Fig. 3. Diagram of the experimental design used in the investigation of the light diffraction by acoustical waves

1 – laser He–Ne, *2* – cristall, *3* – h. f. generator, *4* – modulator, *5* – photomultipler, *6* – oscyloscope

The transducer of lithium iodate was glued to the melt quartz to be used as a reference substance. The light scattered as a result of dispersion was recorded by the photomultiplier M12FQC51 from which the signal was transmitted to the oscilloscope. The pulses obtained are shown schematically in Figs. 4 and 5.

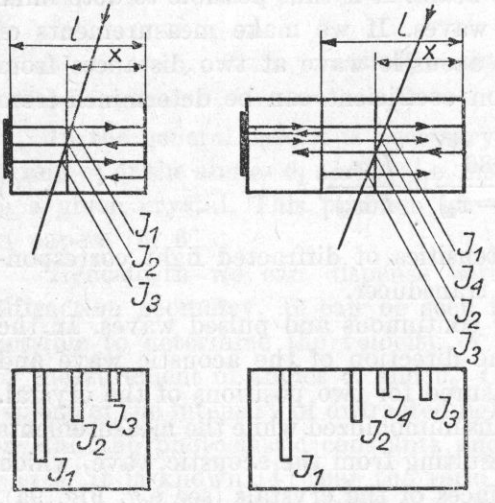

Fig. 4. Diagram of oscillogram patterns for standard sample

Fig. 5. Diagram of oscillogram for investigated substances

In case of the light diffracted in the quartz itself (Fig. 4) the first pulse (I_1) corresponds to the diffraction by the wave incident directly from the transducer, the other pulse (I_2) corresponds to the diffraction by the wave

reflected from the end of the crystal, while the third pulse (I_3) — to the diffraction of the light reflected from the transducer etc. As the laser beam moves towards the end of the crystal, the distance between the pulses I_1 and I_2 decreases, but that between the pulses I_1 and I_3 remains constant at a value corresponding to the time of passing through the double crystal length. When the specimen crystal (Fig. 5) is gived to the quartz reference, the acoustic wave is reflected from the crystal—air surface. Thus for small acoustic wave absorption in a specimen crystal the following pulses can be seen: the first pulse that corresponds to the diffraction by the wave emitted by the transducer and passing directly through the reference pattern-tested crystal surface of separation. This is followed by pulses that correspond to the diffraction of light by acoustic waves reflected from following surfaces: specimen crystal — air, specimen crystal — reference substance, reference substance — transducer, etc. depending on the length of crystal and the velocity of acoustic wave propagation.

Fig. 6 shows the system used for measuring the absorption coefficient of the acoustic waves. The light beam reflected by the acoustic wave is divided into two parts by means of a semi-transparent mirror. One of them, after being reflected from a totally reflecting mirror, is passed through the polarizer

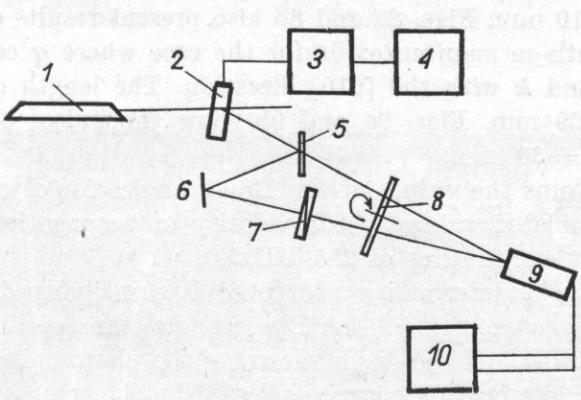

Fig. 6. Diagram of the experimental design used in the measurement of the absorption coefficient of acoustic waves

1 — laser He—Ne, *2* — tested cristall, *3* — high frequency (h. f.) generator, *4* — modulator, *5* — semi—transparent mirror, *6* — mirror, *7* — polarizer, *8* — mechanical modulator, *9* — photomultiplier, *10* — oscilloscope

and the mechanical modulator and is incident on the photomultiplier. The second part of the diffracted beam is passed through the modulator. The signal from the photomultiplier is fed to a double beam oscilloscope. The mechanical modulator, operating at a frequency of about 200 Hz, allows only one light beam to pass at a given moment onto the photomultiplier. In this manner it is possible to observe on the oscilloscope two rows of pulses on each beam. The height of pulses coming from one of the diffracted light beams can be adjusted by the polarizer. Using this facility and that of the oscilloscope for

the mutual displacement of pulses, it is feasible to superimpose two sets of pulses. Knowing the path x_2-x_1 travelled by the acoustic pulse and the ratio $I(x_1)/I(x_2)$, it is possible to evaluate the absorption coefficient of acoustic wave from equation (6).

3. Discussion of experimental results

The diffraction of light by acoustic waves has been investigated in melt quartz, rutile, calcium fluoride, lithium niobate and bismuth-germanium oxide.

Experiments have been aimed at assessing the suitability of the system for measurement of the propagation velocity and the absorption coefficient of acoustic waves, and also in determining the photoelastic constants of certain crystals. The measurement accuracy of each of the above-mentioned physical quantities has also been determined.

Figs. 7-9 show some of oscillograms obtained. In these drawings the distance from the transducer to the laser beam is denoted by x. Figs. 7a and 7b are made from bismuth-germanium oxide with the acoustic wave propagation in the [100] direction and the light wave in the [010] direction, the length of crystal being 10 mm. Figs. 8a and 8b also present results of the diffraction of light in bismuth-germanium oxide for the case where $\boldsymbol{q}$ coincides with the [001] direction and $\boldsymbol{k}$ with the [010] direction. The length of crystal in this direction is $l = 29$ mm. Figs. 9a and 9b show the pulses obtained in rutile with $q \| Z$ and $l = 30$ mm.

Table 1 contains the values of the Bragg angles for crystals investigated and also the calculated values of the velocity of propagation of longitudinal acoustic waves at a frequence of 215 MHz.

The accuracy of determining the speed is principally dependent on the accuracy of the measurement of the Bragg angle, thus of the distance transducer-photomultiplier and the displacement of the photomultiplier. It amounts to about 0.2%. This accuracy may be affected by the error in determining the index of refraction. This method is very accurate and can be used for the determination of photoelastic constants for investigated crystals.

Table 2 states the values of the absorption coefficient of acoustic waves with frequencies 825 MHz measured by the above described method, Table 3 contains the values of some photoelastic constants for investigated crystals.

The accuracy of the determination of the absorption coefficient is about 15% and that of photoelastic constants — 10 to 12%. The error at the measurement of α is affected mainly by irregularities of crystal faces as well as by the divergence of an acoustic beam.

The test results indicate that the described method and used measuring systems can be successfully utilized for testing the acoustic and acoustic-and-optical properties of crystals.

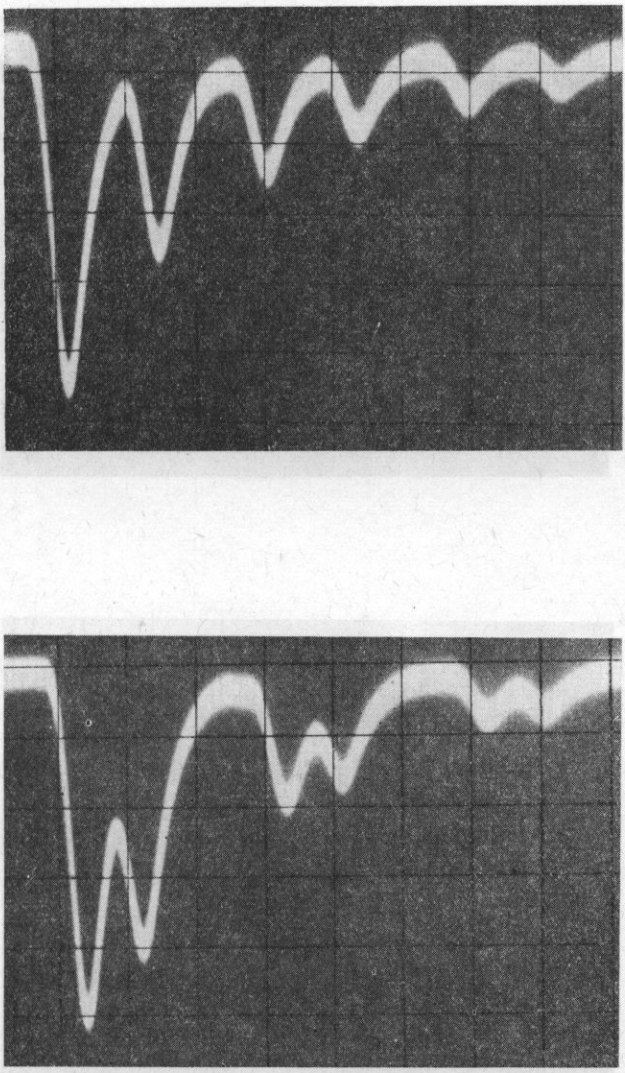

Fig. 7. Oscillogram patterns for bismuth germanium oxide; $\boldsymbol{q} \| X$; $\boldsymbol{k} \| Y$, $l = 10$ mm, time scale 2 μs/cm, a) $x = 7$ mm, b) $x = 4$ mm

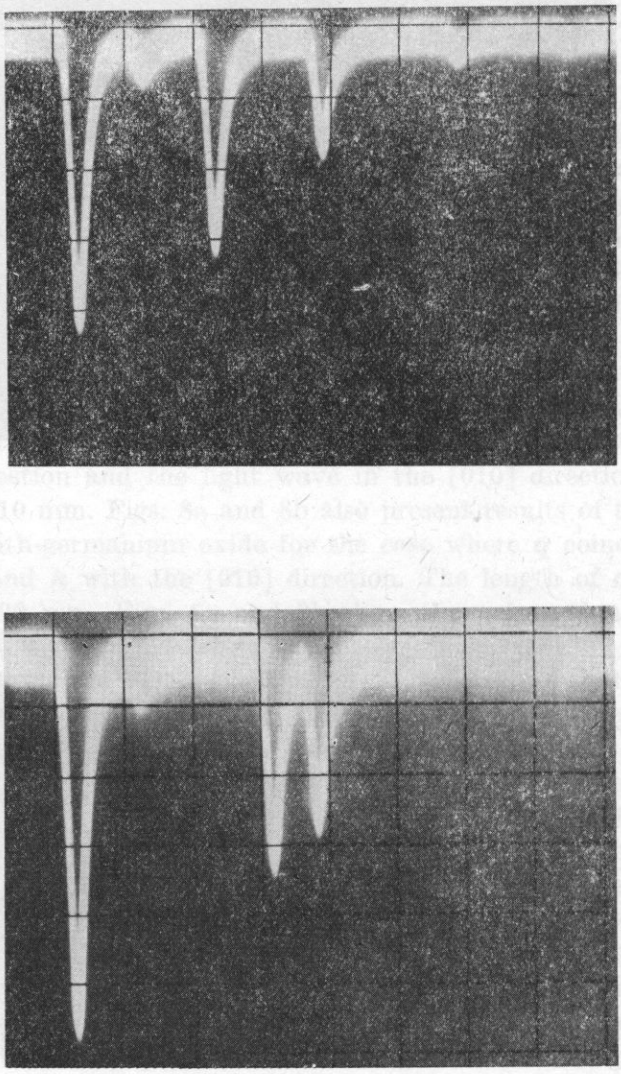

Fig. 8. Oscillogram patterns for bismuth germanium oxide; $q \| Z$, time scale 5 μs/cm, $l = 29$ mm, a) $x = 21$ mm, b) $x = 14$ mm

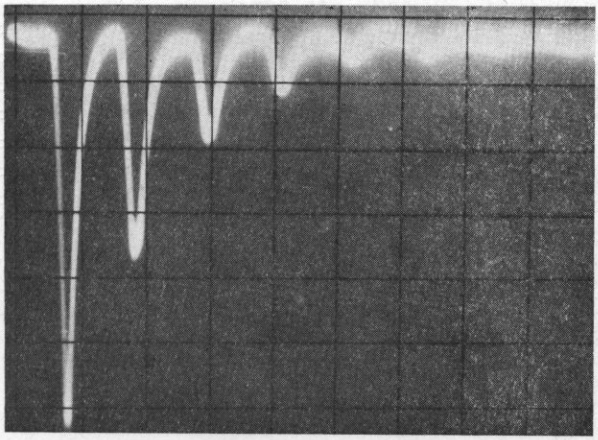

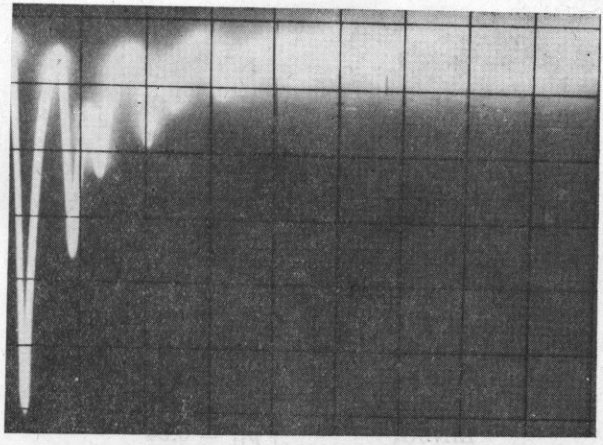

Fig. 9. Oscillograms for rutile; $q \| Z$, time scale 5 μs/cm, $l = 30$ mm, a) $x = 19$ mm, b) $x = 11$

Table 1. Values of the Bragg angle and velocities of longitudinal acoustic waves for the crystals investigated

Substance	n	Direction	θ_B	V [m/s]
Melt quartz	1.45	—	25′50″	5890 ± 15
TiO_2	2.58	[100]	11′20″	7860 ± 20
CaF_2	1.43	[100]	22′00″	7070 ± 20
$Bi_{12}GeO_{20}$	2.55	[101]	25′50″	3300 ± 10
		[001]	26′00″	3210 ± 10
$LiNbO_3$	2.20	[100]	16′50″	6530 ± 15
		[001]	14′00″	7330 ± 12

Table 2. Absorption coefficients of longitudinal acoustic waves for the crystals investigated (f = 825 MHz, T = 293 K)

Substance	α [dB/cm]
Melt quartz	7 ± 1,5
TiO_2	0,9 ± 0,2
CaF_2	4,5 ± 0,7

Table 3. Measured values of the photoelastic constants for the crystals investigated

Substance	p_{ij}
CaF_2	$p_{11} = 0.06$
	$p_{12} = 0.23$
TiO_2	$p_{12} = 0.18$
	$p_{31} = 0.10$
	$p_{13} = 0.17$
$LiNbO_3$	$p_{11} = 0.04$
	$p_{12} = 0.08$
	$p_{31} = 0.18$

References

[1] L. Bergmann, *Der Ultraschall*, Zürich 1954, 312-336.

[2] R. Dixon, M. Cohen, *A new technique for measuring magnitudes of photoelastic tensors and its application to lithium niobiate*, Appl. Phys. Letters, 8, 205-207 (1966).

[3] V. G. Martynov, K. S. Aleksandrov, A. T. Anistratov, *Measurements of elasto-optic effect in ferroelectric by the light diffraction on ultrasound method*, Fizika Tvierdovo Tiela, **15**, 10, 2922-2926 (1973) [in Russian].

[4] W. P. Mason, *Physical Acoustics*, vol. 7, Academic Press, New York 1968.

[5] W. W. Lemanov, O. W. Shakin, *Light scattering on elastic waves in uniaxial crystals*, Fizika Tvierdovo Tiela, **14**, 1, 229-236 (1972) [in Russian].

[6] Yu. V. Pisariev, I. M. Sylvestrova, *Light scattering on elastic waves in biaxial crystals*, Kristallografia, **18**, 1003-1013 (1973) [in Russian].

[7] A. Śliwiński, E. Ozimek, *Laboratory Acoustics*, PWN, tom III, 1973 (in Polish).

Received on 26th May 1975

C H R O N I C L E

22ND OPENED SEMINAR ON ACOUSTICS

Świeradów Zdrój, September 8-13, 1975

The Seminar was held September 8-13, 1975 at Świeradów Zdrój. The promotor of the Seminar was the Wrocław Section of Polish Acoustics Society as well as the Institute of Telecommunication and Acoustics of Wrocław Technical University.

The Organizational Committee was composed of: Chairman Zb. Żyszkowski, Assistant Chairmen: St. Będkowski, W. Jankowski, W. Majewski, Secretary General E. Talarczyk as well as members: Cz. Basztura, T. Ciszewski, A. Gabor, M. Głowacki, R. Godyń, J. Gogolewski, T. Gudra, A. Hołówko, Zb. Jakubek, J. Jaroszyński, J. Kamiński, B. Kulesza, H. Kusek, H. Kustrzycka, K. Łowińska, W. Myślecki, St. Nuckowski, A. Podrez, J. Świerkowski, B. Tokarz, K. Warszawski, T. Wawrykowicz, Z. Wasowicz, J. Zalewski, J. Zarzycki.

The Seminar was attended by over 300 participants, including 18 persons from abroad. Those present were scientists from Great Britain, Czechoslovakia, Denmark, France, the German Democratic Republic, Sweden and Hungary.

Most of participants were PTA members, namely 179.

The participants were lodged in the buildings of Sanatorium Odra at Świeradów and rest-homes.

Four plenary lectures as well as 145 lectures and reports in sections were delivered. Individual sections comprised the following fields of acoustics:

Section A – Cybernetic acoustics, physiological acoustics, speech acoustics, musical acoustics, psychologic acoustics and electroacoustics.

Section B – Physical acoustics, architectural and room acoustics, noise and vibrations.

Section C – Quantum and molecular acoustics, hydroacoustics and ultrasounds.

The time of one lecture in section was 15 min., the discussion following the lecture – 10 min.; a report lasted 10 min., discussion – 5 min.

The lectures submitted to the Organizational Committee at fixed term were printed in Typographic Establishment of Wrocław Technical University in two volumes entitled «The Papers of 22nd Opened Seminar on Acoustics» numbering 650 pages. The lectures of Polish authors are published in Polish. All lectures are preceded with an English summary. According to the opinion of the participants the verification – used for the first time at the 22nd Seminar – of lectures to be delivered has stimulated the authors to a better elaboration of their papers and has contributed to raising the scientific level of the Seminar.

The «Papers» comprise a total of 114 lectures; thereof 13 were not delivered because there authors were absent at the Seminar. Apart from lectures published in the "Papers" eight reports and ten lectures submitted at a later date were delivered.

Lectures delivered by young scientific workers, members of Polish Acoustics Society (PTA), all at the age under 35 have been evaluated within the framework of Marek Kwiek competition. The competition involved 62 lectures.

Besides plenary and section deliberations there were held «round table» sessions on the subject:

1. The use of digital techniques in acoustic metrology.
2. Acoustooptics and holography.

This new form of deliberations in the history of Opened Seminars on Acoustics has aroused a vivid interest amongst their participants.

During the Seminar several organizational meetings were held, of which special mention deserves the Convention of Delegates of Polish Acoustics Society (PTA) at which, among others, the draft of a new statute of the Society has been discussed and new members of Main Board were elected. A special event to the Convention was the conferment upon prof. Wiktor Jankowski of the dignity of honorary member of PTA.

An event of special importance was the Session of Environmental Protection Section at which in addition to the members of Environmental Protection Section also the concerned representatives of industrial establishments of Lower Silesia participated. On the agenda were problems concerning the sources of industrial noise and the methods of noise control.

During the seminar the firm Brüel-Kjaer displayed its present activities in the field of electroacoustic measurement.

An attractive diversification of the laboriously spent days were the evening social get-togethers facilitating the establishment of scientific contacts amongst the members of the Seminar. Doubtless they contributed to the friendly climate prevailing at the Seminar and further integration of the milien of acousticians.

Plenary lectures

1. L. Filipczyński, *Ultrasonar methods of medical diagnostics.*
2. W. Jankowski, Z. Ziemski, *Resistance of hearing organ in experimenting with animals.*
3. L. Pimonow, *A new system of automatic recognition of objects, especially of speech words.*
4. B. Rogala, *The probabilistic characteristics of the signals transmittes in electroacoustical systems.*

Lectures in sections

Section A

1. B. Adamczyk, W. Kuniszyk-Jóźwiak, E. Smółka, P. Pałczyński, *Echo-reverberation correlation by influence on the velocity of speaking.*
2. Cz. Basztura, W. Majewski, *Influence of frequency ranges on speaker identification by means of statistical analysis of zero-crossing rates.*
3. S. P. Brachmański, A. Masny, Z. .Wąsowicz, *Investigation of reverberation time for typical living rooms.*
4. A. E. Brown, *An assessment of differences between players of the horn.*
5. G. Budzyński, A. Kulowski, *Bowed string oscillation analysis.*
6. K. Dekan, *Investigations of brass instruments.*
7. A. Dobrucki, C. Szmal, *The results of objective loudspeaker estimation which takes into consideration some properties of hearing.*

8. M. M. Dobrzański, K. Lenczewska, *Quantum effects in the mechanism of hearing.*
9. M. Drobner, W. Głowacka, *Perception of simultaneity and no-simultaneity of sound.*
10. M. Drobner, I. Romek, *Influence of fundamental note intensity on quality of sound.*
11. R. Dyba, B. Żółtogórski, *Spectral analysis Doppler effect in loudspeakers.*
12. T. Fidecki, *Contactless, unbiased magnetic recording of harmonic signals.*
13. A. Gabor, J. Zarzycki, *Electroacoustical systems nonlinearity and memory analysis using Volterra series.*
14. M. Głowacki, B. Rogala, J. Szymbor, *Acoustical signals and noise in electroacoustical systems.*
15. H. Harajda, *Acoustic research done during the IV International Henryk Wieniawski Competition.*
16. W. Hamer, *The effect of audiomonitoring room upon the location of image sources.*
17. H. Harajda, J. Kluczek, I. Narucka, *Chickens' reaction to acoustic stimuli.*
18. S. Hlibowicki, J. Renowski, *The influence of the outer and middle ear frequency response on the width of the critical bands.*
19. D. Holz, *Investigations on a possible substitution of resonance wood by synthetic materials.*
20. W. Jassem, *Classification of Polish voiceless fricatives.*
21. J. Kacprowski, W. Mikiel, A. Szewczyk, *Acoustical modelling in the physio-pathology of the human vocal system.*
22. T. Kopczewski, T. Fidecki, *Fast recirculating memory as a delay line for low frequency signals.*
23. W. Kraak, G. Fuder, L. Kracht, *Individual variabilities and differences in noise-induced hearing stress.*
24. H. Kubzdela, K. Mytkowski, *The preparation of technical conditions for computerizing the analysis of the speech signal.*
25. B. W. Kulesza, B. Rogala, J. Sobolewski, *Studies of shortterm correlation functions of musical signals.*
26. H. Kusek, *Attempt of determination of speech understanding degree during mental concentration preceding physical effort.*
27. H. Kusek, *Speech understanding during physical effort of static characteristics.*
28. W. Majewski, Cz. Basztura, *Speaker identification based on statistical distributions of F_0 determined by means of zero-crossing rates.*
29. W. Makowski, *Audio motoring room of Musical Acoustic Chair of State College of Music.*
30. W. Mikiel, J. Drzewiecki, J. Jakubowicz, I. Kupczyk, K. Kupczyk, *A logarithmic analog/digital converter.*
31. W. Mikiel R. Gubrynowicz, W. Hagmajer, *A logarithmic A/D conversion of peak value of speech signal and a method of time representation of measurement data.*
32. K. Mlicka, S. Prus, *The formation of loudness sensation for partially masking sounds.*
33. W. Myślecki, J. Zalewski, A. Gos, *Investigation the influence of glottal excitation pulse shape on the quality of polish synthetic vowels.*
34. S. Nuckowski, B. Rogala, J. Szymbor, *Experimental investigations on transfer properties of nonlinear systems with memory.*
35. S. Nuckowski, B. Rogala, M. Walaszek, *Nonlinear distortion measurements using wide-band signal.*
36. S. Nuckowski, B. Rogala, R. Zmonarski, *Acoustic signal distortions in loudspeaker systems.*
37. A. Podrez, J. Renowski, K. Rudno-Rudziński, *Analysis and design of loudspeaker — open back enclosure system.*
38. S. Prus, *The diffluence effect in decision processes.*
39. A. Rakowski, *Acoustic dissonance of a beating tone pair.*

40. H. Rzeczkowska-Sienkiewicz, A. Herman, *Investigation on stability of «High-Energy» magnetic oxides and tapes.*
41. Z. Sołtys, *Programmed device for automatic phonic-signals switching.*
42. J. Sundberg, *Vibrato and vowel identification.*
43. D. Szybista, *Recognition of Polish idiophonemes in continuous speech.*
44. Z. G. Wąsowicz, Z. Sołtys, *The tests for listening loudspeakers evaluation.*
45. J. Zalewski, W. Myślecki, *Investigation the influence of glottal excitation frequency and amplitude changes on the quality of synthetic isolated vowels.*
46. J. Zarzycki, A. Gabor, *Random signals power spectrum deformations due to the electroacoustical system memory and nonlinearity.*
47. Z. Ziemski, H. Kusek, W. Jankowski, H. Rodziewicz, *Understanding of speech at heavy industry working environment.*

Section B

1. B. Albiński, *Investigation results concerning sound level precision meters PDJ-202 in cooperation with octave filters.*
2. D. Augustyńska, *Experiments on the effect of an airflow on the characteristics of absorptive muflers for ventilating systems.*
3. W. Bartelmus, A. Studziński, *The coherence of vibration, acoustic signals in diagnostic of gearbox.*
4. W. Beblo, W. Mrukwa, W. Kochan, J. Desselberger, *Measurement of vibroisolation properties of polyuretan elastomers made in Poland.*
5. St. Będkowski, St. Duda, Zb. Jakubek, M. Staffa, *Prefabricated sound-protecting cabins for industry.*
6. B. Bogusz, H. Idczak, A. Jaroch, *Measurement of room absorption by steady-state method.*
7. V. Chalupova, *The changes of the spectral composition of noise in the course of working cycle of a motor.*
8. W. Cholewa, *The cepstrum analysis — spectrum of acoustic or vibration signal spectrum in the diagnosis of machines.*
9. S. Czarnecki, M. Czechowicz, *Suppressors for exhaust high-pressure installations.*
10. M. Czarny, E. Amarowicz, *Application of Laval nozzle for noise stifling of pulsatory exhaust jets.*
11. M. Czarny, W. Samborski, *The surces of noise in ore dressing plants and some methods of noise reduction.*
12. M. Czarny, L. Szumilas, *Vibration dampers for manual air-operated tools.*
13. Z. Dukiewicz, W. Ziółkowski, A. Śliwiński, *Cross correlation between air and structural sound signals of a bar.*
14. R. Dyba, *Spectrum distortions of acoustical signals produced by a plane wave source.*
15. G. Engler, *Calculation of noise passenger cars and conclusions for construction.*
16. G. Engler, *Nomograms for calculation of noise emitted by motor vehicles.*
17. S. Jaworski, *Methods of the investigation of the efficiency of personal protections against vibrations transmitted through the legs.*
18. J. Kamiński, *The acoustic method of analysing the one working cycle of the motorcycle engine.*
19. N. Kosińska, A. Śliwiński, *Testing of dilatation slots effect of saw blades on decrease of rotation noise level.*
20. T. Kwiek-Walasiak, A. Walasiak, *Tentative determination of usefulness of narrow-band spectral analysis, correlation analysis and power-spectrum analysis methods to estimation of main noise and vibrations sources and transmission ways of them in complicated mechanical system.*

21. T. KWIEK-WALASIAK, A. WALASIAK, A. FREULICH, *The application of a correlation and power spectrum analyses to a settlement of the main sources of the noise and vibrations in the cabin of the lorry Star 200.*
22. T. KWIEK-WALASIAK, A. WALASIAK, B. WIERZCHOWSKI, K. JĘDRZEJCZYK, *The noise and vibrations sources analysis in the cabin of the prototypical lorry Star 200.*
23. R. MAKAREWICZ, *Highway routes in terms of L_{eq} decrease in a given point.*
24. R. MAKAREWICZ, *Determinatioon of sonic boom focus lines.*
25. J. MARCZYK, *Methodology of the investigations of efficient protections against vibrations acting upon the hands.*
26. J. MOTYLEWSKI, D. NITECKI, *Measurement of noise emitted by machines under industrial conditions.*
27. A. MUSZYŃSKI, H. CHODKIEWICZ, *Shock absorbers in transient state.*
28. Z. NICZYPORUK, A. LIPOWCZAN, *The investigation of microphone transmission function for incoherent turbulence interaction on surface of membrane.*
29. B. PLEBAŃSKI, E. IGNASZEWSKI, A. SZKLAREK, *Measurements and evaluation of vibrations which occur on the rail vehicle driver's work stand.*
30. M. RABIEGA, B. RUDNO-RUDZIŃSKA, J. SZYMBOR, *Utilization of the tone-burst method to the investigation the acoustical properties of small resonant filters in the impedance tube.*
31. L. RUTKOWSKI, *Acoustic control and prediction of the technical state of machine.*
32. H. RYFFERT, R. MAKAREWICZ, E. KRASIŃSKA, *Generalized formula for the level of noise penetrating into the room.*
33. M. SANKIEWICZ, A. WITKOWSKI, *Acoustical adaptation of auditory hall into recording studio.*
34. M. TAJCHERT, *A digital method of geometrical analysis of acoustical field within an enclosure.*
35. A. WITKOWSKI, *Optical-acoustical modelling of the room acoustics.*
36. M. ZWIERNIK, R. WYRZYKOWSKI, *Sound velocity in superheated steam in conditions of intermolecular action according to Stockmayer's potential.*
37. B. ŻÓŁTOGÓRSKI, *Finite amplitude effects in plane sound waves.*

Section C

1. M. ALEKSIEJUK, *Acoustic waves velocity near structural phase transition in $KMnF_3$.*
2. J. BERTRAND, E. DRESCHER, J. RANACHOWSKI, *Ultrasonar of the evaluation of the degree of wear of molybdenum electrodes.*
3. J. BEDNAREK, T. CISZEWSKI, J. GOLANOWSKI, T. GUDRA, E. TALARCZYK, *An ultrasonic method of measuring the stress in rocks.*
4. J. BEDNAREK, T. CISZEWSKI, J. GOLANOWSKI, T. GUDRA, E. TALARCZYK, *An ultrasonic method of alarming the discontinuity of stream in belt conveyors.*
5. W. BECZEK, R. GOMUŁA, P. WITORT, *Ultrasonograph USG-10.*
6. J. BERDOWSKI, J. SZUBER, *Investigations of the properties of DADA — crystals by the method of light dispersion on acoustic phonons.*
7. W. BOCH, *Acoustical studies of solvatation in $ZnCl_2$ in methanol solutions.*
8. W. BOCH, *Ultrasonic absorption properties of $ZnCl_2$ in methanol solutions.*
9. M. BRZOZOWSKA, *The comparison of accoustic field scattering on the sinusoidal and saw-form surface.*
10. E. DANICKI, *Velocity dispersion in piezoelectric wavequides.*
11. M. M. DOBRZAŃSKI, *Low temperature acoustoelectrodynamic effect.*
12. A. DRZYMAŁA, M. CIEŚLAK, *Definition of phase transition in liquid crystals with the aid of acoustic methods.*
13. E. EGGERT, J. SCHREIER, *A method for simultaneous measurement of ultrasonic attenuation and velocity in solid polymers.*

14. E. Eggert, J. Schreier, *Investigation of mechanical relaxation in polymers by attenuation of ultrasound.*
15. J. Etienne, L. Filipczyński, A. Firek, J. Groniowski, H. Klawe, J. Kretowicz, *Doppler method with two probes operation mode for placenta location and ultrasonic intensity measurements in vivo.*
16. L. Filipczyński, G. Łypacewicz, J. Sałkowski, T. Waszczuk, *Ultrasonograph UO-4 for eye examination and intensity determination in focused beam by means of electrodynamic method.*
17. J. Finak, Z. Kleszczewski, M. Wojewoda, *Measurements of the acoustooptic properties of the 1 GHz piezoelectric transducers.*
18. J. Finak, Z. Kleszczewski, M. Wojewoda, *Acoustic and acoustooptic properties investigations of crystals by means of light diffraction on acoustic waves method.*
19. J. Górczyński, *Industrial applications of ultrasonics in Poland.*
20. Z. Jagodziński, *Parameters and service characteristic of side sonar.*
21. Z. Kaczkowski, *Alcofers — new piezomagnetic alloys.*
22. Z. Kaczkowski, E. Milewska, S. Różański, *Alfer transducers for the range 55 kHz.*
23. W. Kasprzyk, *The determination of aerosol coagulation time in the acoustic field using Oseen's theory of the flow around a sphere.*
24. Z. Klusek, *Static properties of subaqueous noise in Balticsea.*
25. W. Kołtoński, A. Jaroszewska, *Echo-sounder for the salt mines.*
26. E. Kozaczka, F. Markiewicz, T. Nowak, L. Szluiński, *Propagation of normal mode in shallow water.*
27. M. Kozioł, *Wide-band quartz transducers and their application investigations of highly attenuating liquids.*
28. R. Kubak, M. Nevertal, J. Rozman, G. Dvorsky, *Digital processing of the Doppler velocity meter signal in hemodynamics measurements.*
29. R. Leć, *The interaction of a circularly polarized light and an acoustic waves in a optically active isotropic crystals.*
30. B. Leśniak, *Investigations on an air jet generator by means of the Toepler method.*
31. Cz. Lewa, B. Linde, St. Łętowski, *Piezoelectric properties of polymers as well as attempts of their utilization for electroacoustic conversion.*
32. J. Lewandowski, *The propagation of acoustic waves in viscous suspensions.*
33. M. Łabowski, P. Miecznik, *Intensity ratio of the central line and Mandelshtam-Brillouin line in mixtures.*
34. J. Mamczarek, W. Graczyk, *Determination of the acoustic load impedance of high power piezoceramic transducer in dummy load arrays.*
35. A. Markiewicz, *The influence of the quarter wavelength layer on the transient behavior of the piezoelectric transducer.*
36. J. Morawiec, *Investigation temperature dependence of ultrasonic waves propagation and some solids in $BaTiO_3$ ceramics.*
37. W. Nasalski, *Theory of multiple-liquid acousto-optical transducer in ultrasonar holography.*
38. B. Niemczewski, *Results of measuring cavitation intensity in function of temperature for principal chlorine solvents suitable for use in ultrasonic cleaning.*
39. A. Nowicki, K. Borodziński, T. Powałowski, *In vitro and in vivo blood flow velocity profiles measurements.*
40. J. Olszewski, *Scattering of plane longitudinal waves of different frequencies by a rotary ellipsoid particle.*
41. A. Opilski, *The influence of the surface states upon the propagation of the ultrasound surface waves.*
42. A. Opilski, O. Delekta, D. Dudek, *The influence of admixtures on a propagation of longitudinal ultrasound wave in TGS single crystals doped by Cu^{2+} ions.*

43. B. Peńsko, Z. Toczyski, *The capacitance method of distance measurement and its application in displacement meter up to 40 kHz.*
44. P. Peronneau, J. P. Bournat, W. Sandman, M. Xhaard, *Pulsed Doppler ultrasonic blood flowmetry: Application to the study of tubings and stenotic vessels.*
45. R. Płowiec, *Ultrasonic determination of limiting shear rigidity of some syntetic oils.*
46. E. Soczkiewicz, *Freevolume in solutions of liquids measured by means of acoustical method.*
47. S. Szyma, *An acoustic method of determining the characteristics of the dispersive composition of polymer solutions.*
48. A. Śliwiński, J. Sułocki, P. Czyż, L. Lipiński, *The ultrasonic method and apparatus for measure of concentraction of liquid mixtures.*
49. J. Tabin, *The ultrasonic focusing mirror.*
50. E. Talarczyk, *Sandwich transducer for air-borne pulse ultrasound.*
51. Sz. B. Tőkés, *Digital analysis and filtering of holographic reconstruction.*
52. T. Walecki, *Method of mathematical computation of ΔE — effect in ferrites.*
53. E. M. Walerian, *Explanation of the assymetry of Bordoni peaks.*
54. M. Walewski, P. Rajchert, *Digital measurement of temperature by means of quartz resonator.*
55. L. Werblan, L. Skubiszek, *Attenuation of ultrasonar waves in aqueous mixtures of tetra — hydrofuran and propylene carbonate.*
56. K. Więckiewicz, E. Maciejko, A. Wojnar, *The influence of some construction parameters on properties of ultrasonic piezoelectric transducers.*
57. B. Wiślicki, W. Szachnowski, *Structural analysis of jet fuels hydrocarbon fractions*
58. M. Witkowska, *Problem of elastic constants of liquid crystals.*
59. B. Zapiór, A. Grzegorczyk, A. Juszkiewicz, *Ultrasonic velocity and adiabatic compressibility in molten salt mixtures of $CdCl_2(Na, K)Cl$.*
60. B. Zapiór, A. Łomnicka, *The influence of ultrasonic field on the catalytic activity of the MnO_2, CuO and Ag_2O oxides.*
61. J. K. Zieniuk, *Improved system for ultrasonar holography.*

Zbigniew Żyszkowski (*Wrocław*)